

CZECH TECHNICAL UNIVERSITY IN PRAGUE

FACULTY OF ELECTRICAL ENGINEERING

DEPARTMENT OF CYBERNETICS



**Spike Sorting of Microelectrode
Single-channel Recordings:
Evaluation and Applications**
Doctoral Thesis

Ing. Jiří Wild

Prague, August 2015

PhD. Study Programme: P2612 - Electrotechnics and Informatics
Branch of Study: 3902V035 - Artificial Intelligence and Biocybernetics

Supervisor: **Ing. Daniel Novák, Ph.D.**
Supervisor-Specialist: **prof. RNDr. Olga Štěpánková, CSc.**

Abstract

Until now the experimental research in medical neuroscience has been limited to analyzing summary activity of large neuron populations. However, thanks to recent efforts in using neuroinformatics, artificial intelligence and machine learning methods in neuroscience as well as medical and technological advances, new opportunities to record activity of individual neurons arises. These opportunities allow us to better understand the neural mechanism of complex behavior, as well as identify parts of the brain responsible for specific tasks.

In this thesis, we were focusing on applying such methods to data recorded from patients with Parkinson's disease that were treated with deep brain stimulation, to improve our understanding of the human brain and the mechanism of the deep brain stimulation in particular.

This thesis concentrated mainly on two problems in this field. First, the evaluation of the state-of-the-art methods used to identify and classify neuronal action potentials (i.e spike sorting methods) in microelectrode recordings, which required devising and implementation of signal generator that produced artificial signals with similar properties as the signals recorded from basal ganglia.

Second, to use these methods to discriminate individual neurons from a microelectrode recording and to use this knowledge to identify neurons with specific functions in basal ganglia and better understanding of the human brain in general. Spike sorting methods allowed us to find approx. 20% of basal ganglia neurons with activity related to control of eye movements and 17% of basal ganglia neurons with activity related to processing emotional stimuli or responding to different types of emotional stimuli. We were also able to find several statistically significant relations between severity of Parkinson's disease symptoms (described using Unified Parkinson's Disease Rating Scale subscores) and statistical characteristics of both microelectrode records and by individual neuron firing patterns using linear mixed-effects models.

Keywords: spike sorting, single-neuron recordings, Parkinson's disease, deep brain stimulation, basal ganglia, subthalamic nucleus, linear mixed-effects models, UPDRS, emotion, arousal.

Acknowledgment

I would like to express my sincerest gratitude and warm appreciation to the following persons who had contributed much in helping me shape and reshape this piece of work.

- Daniel Novák and Olga Štěpánková, thesis advisers, for their many suggestions and constant support throughout my whole PhD studies.
- Tomáš Sieger and Eduard Bakštein, fellow PhD students, for being always available to listen and share their opinion, not minding the time I have stolen from them (at least I hope so).
- Jakub Schneider, fellow PhD student, for joining discussion and helping me with some tedious task (UPDRS, artifacts).
- Robert Jech, professor of neurology, for answering a lot of rather naive questions and letting me work in such an interesting field by providing medical expertise and by steering the team towards relevant problems.
- Filip Růžička and Markéta Fialová, for helping me gather necessary research data.
- My whole family for their extensive support during my PhD studies.

Contents

1	Introduction	1
1.1	Goals of the Thesis	2
1.2	Structure of the Thesis	2
2	Medical Background	3
2.1	Parkinson's disease	3
2.2	Parkinson's disease Treatment	3
2.3	Unified Parkinson Disease Rating Scale	4
2.4	Deep brain stimulation	5
2.4.1	Neurosurgery	6
2.4.2	Navigation	7
2.4.3	Microrecording	7
3	Spike sorting	11
3.1	Introduction	11
3.2	Methodology	15
3.2.1	Spike sorting algorithms	16
3.2.2	Preparation of test data	17
3.2.3	Artificial signal generator	20
3.2.4	Noise Level Estimation	20
3.2.5	Performance rating function	22
3.2.6	Spike sorting parameters	22
3.2.7	Dimensional Stacking	25
3.2.8	Statistical methods	26
3.3	Results and Discussion	26
3.3.1	Optimized parameters	26
3.3.2	Spike sorting accuracy	27

3.3.3	Spike sorting time complexity	30
3.4	Conclusion	31
4	Application Results of Spike Sorting	33
4.1	Basal Ganglia Neuronal Activity during Scanning Eye Movements in Parkinson's Disease	33
4.1.1	Introduction	34
4.1.2	Methods	35
4.1.3	Tasks	36
4.1.4	Data analysis	38
4.1.5	Results	40
4.1.6	Discussion	44
4.1.7	Conclusions	47
4.2	Distinct Populations of Neurons Respond to Emotional Valence and Arousal in the Human Subthalamic Nucleus	48
4.2.1	Introduction	48
4.2.2	Methods	50
4.2.3	Results	52
4.2.4	Discussion	55
4.2.5	Conclusion	58
4.3	Relation between UPDRS scores and statistical characteristics of micro-electrode recordings from STN	59
4.3.1	Introduction	59
4.3.2	Methodology	60
4.3.3	Results and Discussion	64
4.3.4	Conclusion	69
5	Summary and perspective	71
5.1	Thesis Achievements	72
5.2	List of Candidate's Publications Related to the Thesis	74
5.2.1	Publications in Impacted Journals	74
5.2.2	Other Publications	75
	References	77
A	List of Candidate's Publications Citations	I

List of Figures

2.1	Deep Brain Stimulation scheme	6
2.2	MRI and X-Ray image showing the DBS electrodes in thalamus	7
2.3	Example of microelectrode signals recorded from different depths of human brain	8
2.4	Sample of operation protocol	9
3.1	Illustration of several neurons measured by microelectrodes	12
3.2	Unsupervised Spike Sorting Diagram	13
3.3	Waveforms of extracted real spikes	18
3.4	Example signal with different noise level	19
3.5	Clustering with different AMI score	23
3.6	Example of dimensional stacking visualization of WaveClus parameter space	25
3.7	Spike sorting evaluation - optimized/default parameters	27
3.8	Spike sorting evaluation - noise level - short signals	28
3.9	Spike sorting evaluation - noise level - long signals	29
3.10	Comparison of spike sorting algorithms speed	31
4.1	EM tasks employed in the study	37
4.2	MER and EOG signal acquisition and processing.	38
4.3	Time lag of neuronal activity with respect to EOG.	40
4.4	Neuronal activity during the scanning movement task.	43
4.5	The relationship of the single-neuron alpha band activity on the valence.	53
4.6	The relationship of the single-neuron alpha band activity on the arousal.	54
4.7	Mean PSD spectrum of 100 MER signals from different patients	62
4.8	Relation between $psd_{rel.beta}$ feature and $depth_{relative}$	64
4.9	Relation between $psd_{rel.beta}$ feature and UPDRS subscores	66
4.10	Relation between neuron spike train features and UPDRS subscores . . .	68

List of Tables

2.1	UPDRS scores of a sample patient	5
3.1	Summary of the properties of each spike sorting algorithm	16
3.2	List of parameters impacting the spike sorting accuracy for each algorithm.	24
4.1	Eye movement-related neurons detected in the scanning eye movement task and/or visual guided saccade tasks.	41
4.2	Number of neurons related to eye movements in the scanning eye movement task.	41
4.3	Eye movement-related neurons detected in the scanning eye movement task and/or visual guided saccade tasks.	42
4.4	Patients' and normative ratings of emotional stimuli used.	55
4.5	P-values of tested mixed-effects models.	65
4.6	Correlation coefficients of analyzed relations between neuron spike train features and UPDRS subscores.	67

List of Abbreviations

ACCEL	Eye Acceleration
ADC	Amplitude Distribution Comparison
AMI	Adjusted Mutual Information
DBS	Deep Brain Stimulation
EM	Eye Movements
EOG	Electrooculography
GP	Globus Pallidus
GPI	Globus Pallidus interna
IAPS	International Affective Picture System IFR Instantaneous Firing Rate
ICA	Independent Component Analysis
IDC	Interval Distribution Comparison
IFR	Instantaneous Firing Rate
IPG	Implantable Pulse Generator
LFP	Local Field Potential
MER	Microelectrode Recording
PCA	Principal Component Analysis
PD	Parkinson's Disease
POS	Eye Position
SEM	Scanning Eye Movement Task
SNr	Substantia Nigra, Pars Reticulata
SPC	Superparamagnetic clustering
STN	Subthalamic Nucleus
UPDRS	Unified Parkinson Disease Rating Scale
VELOC	Eye Velocity
VGS	Visually Guided Saccade Task

Chapter 1

Introduction

Until now the experimental research in medical neuroscience has been limited to analyzing summary activity of large neuron populations. However, thanks to recent efforts to use neuroinformatics, artificial intelligence and machine learning methods in neuroscience as well as medical and technological advances, new opportunities to record activity of individual neurons arises. These opportunities allow us to better understand the neural mechanism of complex behavior, as well as identify parts of the brain responsible.

We are focusing generally on applying such methods to data recorded from patients with Parkinson's disease (PD) that are treated with deep brain stimulation, to improve our understanding of the human brain and the mechanism of the deep brain stimulation in particular. Deep brain stimulation (DBS) has been an effective tool in the treatment of Parkinson's disease as well as other movement disorders. However, the clinical use of DBS is still novel and it has severe side effects like increase rate of depression episodes in post-DBS-treatment. Cause of these side effects is still a matter of debate as the functions of the stimulated region - subthalamic nucleus (STN) - have not yet been fully uncovered.

This thesis concentrates mainly on two problems in this field. First, the evaluation of methods used to identify and classify neuronal action potentials (i.e spike sorting methods) in microelectrode recordings. Second, to use these methods to discriminate individual neurons from a microelectrode recording and use this knowledge to identify neurons with specific functions in basal ganglia.

1.1 Goals of the Thesis

- to evaluate performance of methods for transforming raw data consisting of summary neuronal activity (microelectrode records) into analyzable spiking activity of individual neurons in order to be able to analyze brain activity at neuron level,
- to devise a method for generation of artificial signals similar to those created by summary neuronal activity in basal ganglia that is necessary for objective evaluation of various spike sorting methods,
- to experimentally evaluate that basal ganglia neurons are related to scanning eye movements,
- to analyze firing patterns of neurons in STN to determine its function in the high-level representation of emotions,
- to find objective relation between severity of various PD symptoms and statistical characteristics of microelectrode records and individual neuron firing patterns.

1.2 Structure of the Thesis

This thesis is structured as follows. Chapter 2 serves as an introduction to the Parkinson's disease (Section 2.1), its treatment (Section 2.2) and standardized means of rating severity of the Parkinson's disease symptoms (Section 2.3). Last Section 2.4 looks into problems connected with Deep Brain Stimulation treatment and also discusses where do the data used in this thesis come from.

Chapter 3 looks into the transformation of raw data from extracellular microelectrode into spiking activity of individual neurons (i.e. spike sorting), involving evaluation of state-of-the-art spike sorting methods based on ground truth synthetic data I created by devising an artificial signal generator.

Chapter 4 summarizes the application results in neuroscientific field achieved using spike sorting methods. Section 4.1 describes our finding of basal ganglia neurons related to eye movements. Section 4.2 presents the process of searching for emotion-related neurons in the subthalamic nucleus. Section 4.3 identifies activity in subthalamic nucleus that is directly related to PD symptoms.

Finally, Chapter 5 concludes the thesis and discusses the achievements of the thesis.

Chapter 2

Medical Background

2.1 Parkinson's disease

Parkinson's disease (PD) belongs to a group of conditions called motor system disorders, which are the result of the loss of dopamine-producing brain cells (NINDS Office of Communications and Public Liaison 2006). PD primary symptoms are tremor (trembling of arms, hands, legs, ...); bradykinesia (a movement slowness); rigidity (arm, leg stiffness) and postural instability. Secondary symptoms include depression or another emotional changes, difficulty speaking, sleep problems, urinary problems etc.

PD mainly develops in people over age of 50. At the beginning, PD symptoms are subtle and are usually occurring progressively. The speed of the disease is different among people. As the symptoms become more severe, they might interfere with daily activities - e.g difficulty walking, talking or completing simple tasks.

The diagnosis of PD is based solely on medical history and neurological examination as there are currently no laboratory tests that can ascertain PD. Therefore, the disease can be often difficult to diagnose, so M.D. usually rule out other diseases first (NINDS Office of Communications and Public Liaison 2006).

2.2 Parkinson's disease Treatment

PD is currently not curable, but various medications significantly improve life quality of patients. Usually, levodopa combined with carbidopa is used, because levodopa can be used by cells in brain to make dopamine compensating for the low dopamine levels.

Carbidopa helps delaying the levodopa to dopamine conversion until it reaches the brain.

Levodopa is used as a treatment in at least 75% parkinsonian patients, however, only some symptoms are respond well to the drug. Bradykinesia and rigidity are among those that are most successfully treated with levodopa treatment, but tremor is often only slightly affected and postural instability and several secondary symptoms are not affected at all. Aside from levodopa, anticholinergics are sometimes used for tremor and rigidity control and a group of drugs such as bromocriptine that mimic the role of dopamine in the brain are also successfully used for PD patient treatment.

Before discovery of levodopa, surgery was a common treatment of PD. Nowadays, it is only prescribed to patients with the most severe PD symptoms, that are insensitive to drug therapy (NINDS Office of Communications and Public Liaison 2006).

2.3 Unified Parkinson Disease Rating Scale

The Unified Parkinson Disease Rating Scale (UPDRS) scale is a standardized measure of the effect of the disease on patients' motor skills and mental abilities. The UPDRS is commonly used as a rating tool to follow the progress of Parkinson's Disease.

It is made up of the

1. Mentation, Behavior, and Mood section
2. Activities of daily living section
3. Motor section

Patient's ratings are evaluated by examiner during interview. It is possible to achieve maximum rating of 135 points, which represents the worst (total) disability, while rating of 0 points means no disability. As the disease progresses, UPDRS scores usually increase. The complete list of all UPDRS scores of a sample patient is shown in Table 2.1.

Although being a standardized measure, the UPDRS score is still a subjective measure depending on an experience and skills of the examiner. An objective UPDRS analysis would be a valuable contribution as a decision support tool to help examiners with PD treatment.

18.	Speech	1	23.	Right hand finger tapping	1
19.	Mimicry	2		Left hand finger tapping	0.5
20.	Head rest tremor	0	24.	Right palm movements	1
	Upper-right extremity rest tremor	1		Left palm movement	0.5
	Upper-left extremity rest tremor	1	25.	Right hand pronation	1
	Lower-right extremity rest tremor	0		Left hand pronation	0
	Lower-left extremity rest tremor	0	26.	Right heel taps	2
21.	Upper-right extremity action tremor	1		Left heel taps	2
	Upper-left extremity action tremor	1	27.	Arising from chair	0
22.	Neck rigidity	2	28.	Posture	1
	Upper-right extremity rigidity	3	29.	Gait	0
	Upper-left extremity rigidity	1.5	30.	Postural stability	1
	Lower-right extremity rigidity	2	31.	Body Bradykinesia	0
	Lower-left extremity rigidity	1			

Table 2.1: UPDRS scores of a patient along with the corresponding sequence numbers from the UPDRS III form

2.4 Deep brain stimulation

Deep brain stimulation (DBS) is a surgical procedure used most commonly to treat the symptoms of Parkinson's disease (PD), such as rigidity, bradykinesia and tremor. DBS is also used to treat essential tremor, which is also a common neurological movement disorder. The procedure is currently only used for patients whose symptoms can no longer be controlled with medications (Kringelbach et al. 2007).

High-frequency stimulation of the subthalamic nucleus (STN) suppress motor symptoms in Parkinson disease and is thought to mimic the effects of lesions of the STN (Bergman et al. 1990) or of levodopa (Pollak et al. 1996). However, the mechanism of action of STN stimulation is still a matter of debate (Welter et al. 2004).

As shown in Figure 2.1, the DBS system consists of three parts (1) DBS electrode, or lead, (2) connecting wire and (3) implantable pulse generator (IPG). The electrical pulses generated by the IPG are lead through the connecting wires to the DBS electrodes that are placed in deep brain structures. Mostly subthalamic nucleus (STN) or globus pallidus interna (GPi) is stimulated.

Pulse generator is placed inside a small incision made near the collarbone. The wire

is lead under the scalp and skin. The by far most time consuming and complicated part is the placement of the DBS electrodes (Jahanshahi et al. 2000).

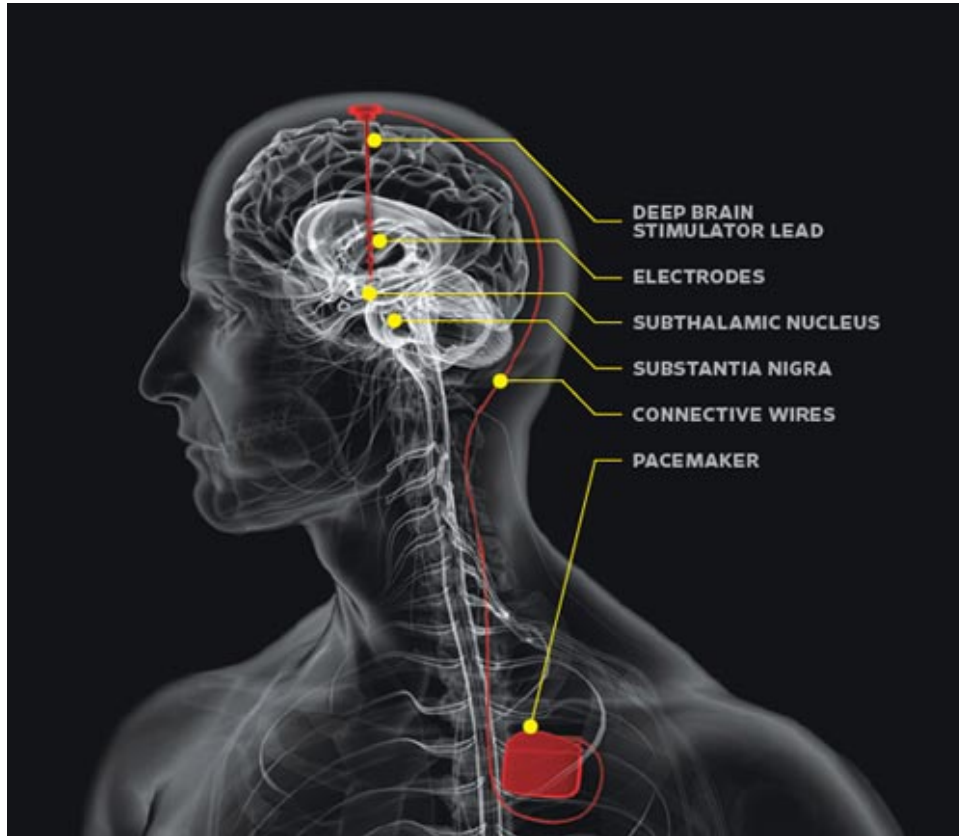


Figure 2.1: Deep Brain Stimulation scheme (Gulie 2007a).

2.4.1 Neurosurgery

The stimulation electrodes are implanted during stereotactic surgery. A neurosurgeon uses a stereotactic head frame and magnetic resonance imaging (MRI) to localize the target within the brain.

Stereotactic head frame is attached to the head of the patient prior to the operation. The frame defines three dimensional coordinate system for the MRI brain mapping. The resulting map becomes the blueprint for planning the least invasive trajectories of the microelectrodes into the deep brain structures. In order to maintain the head in a fixed position through the operation, the head frame is screwed to the operating table. The operation has to be done with patient awake, so that he can report any sensory anomalies. The awoken state is also necessary in order to test the effect of the stimulation at the

end of the surgery (Baltuch et al. 2007). Therefore no global anesthetic is administered – only local ones to avoid the pain caused by the stereotactic frame.

2.4.2 Navigation

As the location of STN is variable and due to the relatively small size of the nucleus itself (approx. 25mm^3), STN targeting is quite challenging. Neurosurgeon uses a combination of MRI calibrated with a stereo-tactic frame, coordinates relative to established anatomic landmarks from brain atlas and intraoperative neurophysiology. Figure 2.2 shows the MRI and X-Ray image of DBS electrodes in thalamus (Slavin et al. 2007).

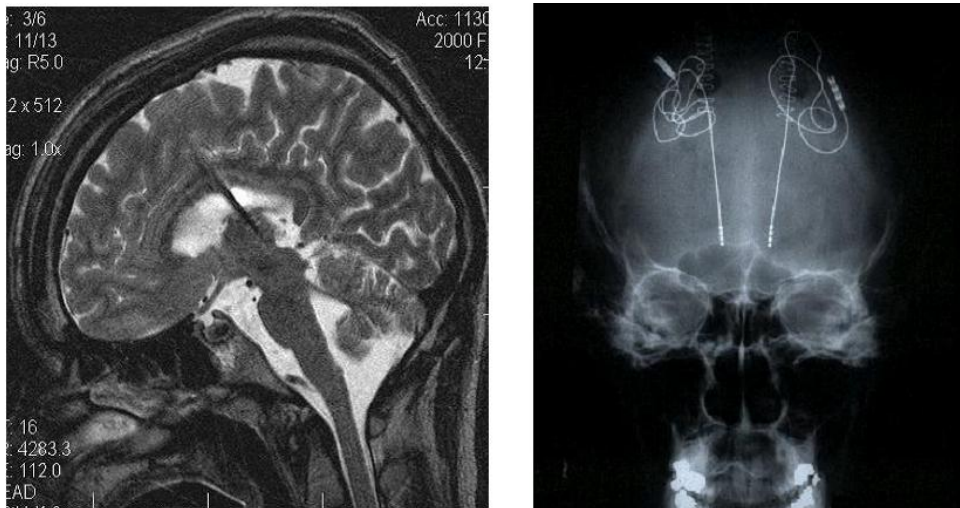


Figure 2.2: MRI and X-Ray image showing the DBS electrodes in thalamus (Hutchison et al. 1998a; Gulie 2007b).

2.4.3 Microrecording

Microelectrode recording (MER) is used by neurosurgeon as an additional means to ensure the accuracy of the surgical probe. This technique uses tungsten microelectrodes that can record summary electrical activity of neurons within the deep brain structures. In order to minimize the damage done, the microelectrodes are much smaller than the stimulation electrode. During the surgery signals recorded using microelectrodes from various depths are amplified and played using earphones to the neurosurgeon, who acoustically analyzes

the summary activity of different brain structures (thalamus, STN, globus pallidus etc.) and help steer the electrodes toward the desired surgical target.

All the data examined in this thesis, was recorded using five parallel parylenecoated tungsten microelectrodes spaced 2-mm apart in a “Ben-gun” configuration with an exposed tip size of 15 – 25 μm . Microelectrode tips were plated with gold and platinum to reduce the impedance to 0.2 $\text{M}\Omega$ at 1 kHz. The five parallel microelectrodes were advanced simultaneously with a motor microdrive in 0.5-mm steps, beginning 10 mm above the target.

Signals were amplified and filtered using the Medtronic Lead Point System with sampling frequency 24kHz. The simultaneous recording of neuron channel was performed using a tetra-electrode setup in which four microelectrodes were inserted as a glued pair separated by a distance of 250 – 300 μm .

Every dataset came along with an operation protocol, that describes what electrodes were used and till what depth and where was the STN found – based on the subjective judgment of the surgeon. Sample of the operation protocol is shown in Figure 2.4.

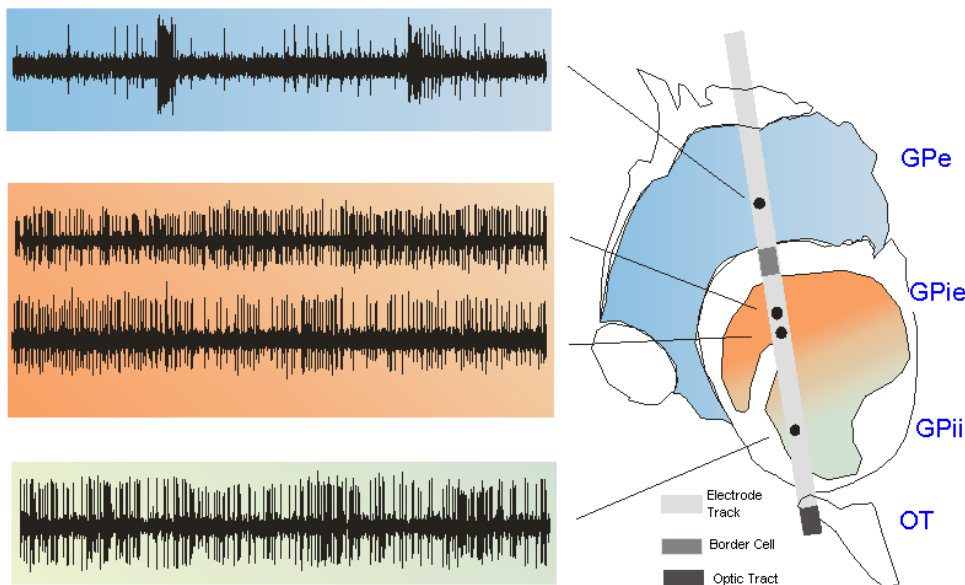


Figure 2.3: Example of microelectrode signals recorded from different depths of human brain (Hutchison et al. 1998a).

STNdex, 20.9.05

	Center EL	Anterior EL	Posterior EL	Medial EL	Lateral EL	DBS Lead Position
T-10						
T-9						
T-8	<i>R</i>					
T-7	<i>R</i>					
T-6						
T-5						
T-4						
T-3						
T-2						
T-1						
Target						
T+1						
T+2						
T+3						
T+4						
T+5						
T+6						
T+7						

STN ok plan

5mm inf (K2-P)
11.5 mm lat (K2-R)
2.5 mm pos (K2-R)

diag. ok
dist. from 0° to all
pos from 3° to -7.5 mm

Figure 2.4: Sample of operation protocol. It clearly describes that only the central microelectrode was used till depth $T + 1$ (24 depths in total) and that the STN was found between $T - 4$ and $T + 1$ (dexter hemisphere). The last column describes the exact placement of leads of the stimulation electrode.

Chapter 3

Spike sorting

Single-channel microelectrode recordings (MER) consist of summed electrical potentials created by individual neurons see Figure 3.1. Depending on how many neurons are close to the recording electrode, recorded signal can contain traces of that many different electrical potentials summed with a contribution of large number of neurons further away from microelectrode (usually referred to as “background noise”). Therefore, in order to study the behavior of individual neurons, we need to unravel the combined neuronal activity and obtain the activity of the individual neurons.

As neuronal activity is discrete (i.e. at any given time neuron is either firing an action potential or being silent), the problem of neuron separation is significantly reduced. All that is needed is to detect all action potentials (also referred to as spikes) in the recording and sort them according to what neuron created them. This process is called spike detection and sorting. It results in a sequence of spikes, called the spike train, for each neuron detected in the microelectrode recording (see Figure 3.2).

The content of the following sections has been published by Wild et al. (2012b).

3.1 Introduction

Classifying neuronal action potentials is a technical challenge that is a prerequisite for studying many types of brain function. Accurate detection of the activity of individual neurons can be difficult to achieve due to the large amount of background noise and the complexity in distinguishing the action potentials of one neuron from others. Even if the activity of several neurons is recorded with only a single electrode as is illustrated in

Figure 3.1, spike sorting allows the researcher to measure the activity of the individual neurons separately. This capability is especially important for experimental investigations of neural codes that use spike timing.

Although there are many spike sorting software packages (including commercial software), we are not aware of any objective comparison of them that discusses adjustments to their parameters and their impact on spike sorting accuracy.

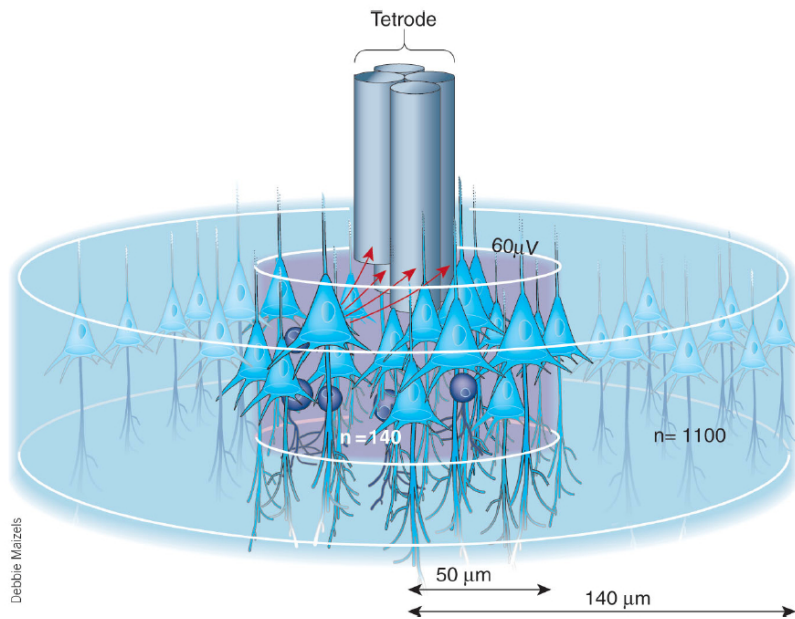


Figure 3.1: Illustration of several neurons measured by microelectrodes (Buzsaki 2004).

Most unsupervised spike sorting algorithms employ three principal steps (Figure 3.2). In the first step, spikes are detected with an automatic spike detection method. In the second step, a set of features is extracted from each spike - principal component analysis (PCA) (Adamos et al. 2008) or the wavelet transform (Quiroga et al. 2004) are usually used in this step. Finally, the spikes represented by their features are assigned to different neurons by an unsupervised learning algorithm (e.g. a clustering algorithm). We should mention that these steps are sometimes combined (Franke et al. 2009; Herbst et al. 2008), but most spike sorting algorithms handle the three steps independently.

We focus on stages 2 and 3, as there are already a number of comparative studies in the field of spike detection (Lewicki 1998; Adamos et al. 2008; Gibson et al. 2008), and because the studied spike sorting algorithms are modular, thus allowing the researcher to choose freely which spike detection algorithm to use. The spike detection part was

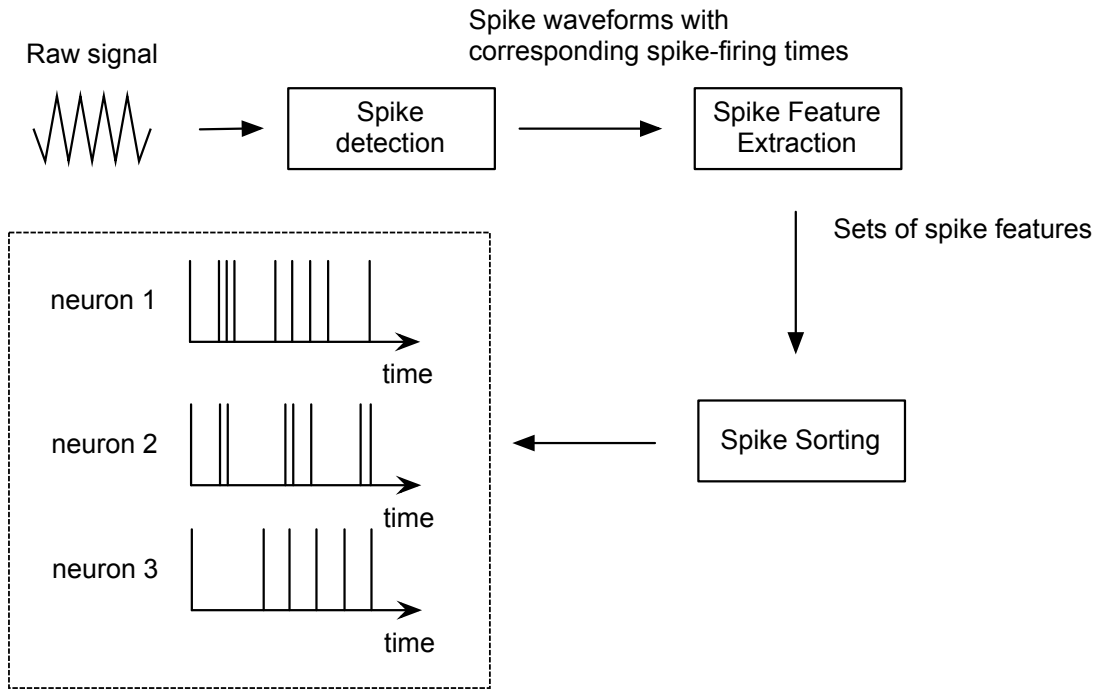


Figure 3.2: Three principal stages of unsupervised spike sorting algorithms.

omitted by providing the algorithms with reference spike times.

The idea of recording multiple neurons and then grouping the action potentials by the source neuron is not new. It was first proposed in the 1960s (Gerstein et al. 1964), and since then numerous approaches to the problem have been developed.

Given a lower-dimensional representation of the spikes and disregarding the times at which the spikes occurred, the spike sorting problem reduces to a clustering problem. Therefore, most of the better known clustering algorithms have been applied to spike sorting: k-means clustering (Salganicoff et al. 1998), hierarchical clustering (Fee et al. 1996), superparamagnetic clustering (Quiroga et al. 2004), as well as mixtures of Gaussians (Sahani 1999) and mixtures of t-distributions (Shoham et al. 2003). The method used in (Fee et al. 1996) grouped multiple classes according to whether the interspike interval histogram of the group showed a significant number of spikes in the refractory period.

Takahashi et al. (2003b) and Takahashi et al. (2003a) combined independent component analysis (ICA) and the efficiency of an ordinary spike sorting technique (k-means clustering) to solve spike overlapping and nonstationarity problems of tetrode recordings with no limitation on the number of single neurons to be separated. Adamos et al. (2010)

attempted to resolve overlapping spikes by introducing a hybrid scheme that combines the robust representation of spike waveforms to facilitate the reliable identification of contributing neurons with efficient data learning to enable the precise decomposition of coactivations.

Fee et al. (1997) described a procedure for efficiently sorting spikes in the presence of noise that is anisotropic, i.e., dominated by particular frequencies, and whose amplitude distribution may be non-Gaussian, such as occurs when spike waveforms are a function of the interspike interval. Support vector machines were used in Ding et al. (2008) to solve the superposition spike problem.

Herbst et al. (2008) combined the spike detection and classification steps into a single computational procedure using a Hidden Markov Model framework. Detection and classification was also merged in Franke et al. (2009), where a method of linear filters was inspected to find a new representation of the data and to optimally enhance the signal-to-noise ratio. By incorporating direct feedback, the algorithm adapted to non-stationary data. Delescluse et al. (2006) used Markov chain Monte Carlo in order to estimate and make use of the firing statistics as well as the spike amplitude dynamics of the Purkinje cells. Online spike sorting approaches suitable for HW implementation were addressed in Gibson et al. (2010) and Rutishauser (2006). (Adamos et al. 2008) performed a comparative study focused on PCA using synthetic data on which correlated and white Gaussian noise processes are superimposed, and the KlustaKwik (Harris 2000) clustering approach was used. Wang et al. (2006) proposed a robust approach employing an automatic overlap decomposition technique based on the relaxation algorithm that required simple fast Fourier transforms. Hulata et al. (2002) used a simple k-means technique for spike sorting while applying the wavelet packets decomposition framework in an extraction step.

The following approaches dealt with the quality of the spike sorting process. Schmitzer-Torbert et al. (2005) introduced two measures: L-ratio and Isolation Distance. The two measures quantified how well separated the spikes of one cluster were from other spikes. Joshua et al. (2007) described the isolation score, which measured the overlap between the noise (non-spike) and the spike clusters. The measure of Tankus et al. (2009) was based on visual features of the spike waveform and an automatic adaptive algorithm that learned the classification by a given human and could apply similar visual characteristics for classifying new data.

This chapter describes a comparative analysis of the three most popular spike sorting approaches with a publicly available source-code: WaveClus (Quiroga et al. 2004), OSort (Rutishauser 2006) and KlustaKwik (Harris 2000). Emphasis was put on involving the

algorithm that can be used for real-time analysis (Rutishauser 2006).

The papers on WaveClus and KlustaKwik did not make direct comparisons with any other spike sorting method. They merely made comparisons between different versions of the same algorithm. OSort was compared with both methods, but from the perspective of online spike sorting (Rutishauser 2006). We are convinced there is a need to evaluate them within a common framework, in order to determine which one to use for a specific task.

Lewicki (1998) presented an extensive review on spike sorting in 1998, but did not include any quantitative experiments, and dozens of new algorithms have been proposed since that review appeared. Gibson et al. (2008) compared several spike detection and feature extraction methods, but they did not include a comparison of the clustering algorithm, because the goal of the paper was only to reduce the data for hardware implementation.

In summary, very few quantitative comparisons of spike sorting methods have been made, and there are no standard criteria for evaluating them. We propose in this chapter an evaluation framework aimed at providing a fair comparison of spike sorting methods on optimal terms.

3.2 Methodology

The objective of the study is to compare the three most widely-used publicly-available spike sorting algorithms (WaveClus, KlustaKwik, OSort) with regard to their parameter settings. We observed that even a small change in the parameters of a spike sorting algorithm may have a dramatic impact on their accuracy. Therefore a comparison between spike sorting algorithms and non-optimal parameters could be biased. To overcome this weakness, we employ an optimization technique on artificial signals to find near-optimal parameter settings. Using these settings, we compared the algorithms on various types of artificial signals, focusing on single-channel recordings (similar to extracellular signals recorded using a single microelectrode).

3.2.1 Spike sorting algorithms

The most important properties of all three spike sorting algorithms selected in the previous section are summarized in Table 3.1. A more detailed description of the algorithms that have been used follows.

Table 3.1: Summary of the properties of each spike sorting algorithm.

	WaveClus	KlustaKwik	OSort
Features	wavelet transform	PCA	Raw data points
Clustering method	superparamagnetic clustering	AutoClass	template matching
User-tunable parameters	20	10	2
Real-time use	no	no	yes
Open source	yes	yes	yes
GUI available	yes	yes	yes (Mclust)
Version tested	2.0	1.6	2.1

WaveClus

WaveClus is an unsupervised spike detection and sorting algorithm that combines the wavelet transform (localizing distinctive spike features) with superparamagnetic clustering (SPC), which is a method used in statistical mechanics (Quiroga et al. 2004). It enables clustering of the data without assumptions such as low variance or Gaussian distributions. In the first step, spikes are detected with an automatic amplitude threshold on the high-pass filtered data. In the second step, a small set of wavelet coefficients from each spike is chosen as the input for the clustering algorithm. Finally, SPC classifies the spikes according to the selected set of wavelet coefficients (Quiroga et al. 2004). WaveClus is one of the most widely-used spike sorting algorithms, and it has a large number of parameters for fine-tuning the method (see Table 3.2 for details). WaveClus version 2.0 was used for the comparison.

OSort

OSort is an implementation of a template-based, unsupervised online spike sorting algorithm. The estimation of the number of neurons present, as well as the assignment of each spike to a neuron, is based on a distance metric between two spikes (Rutishauser 2006). Based on this distance, a threshold is used: (i) to decide how many neurons are present and (ii) to assign each spike uniquely to a neuron cluster, or to a noise cluster

if unsortable. The threshold is calculated from the noise properties of the signal and is equal to the squared average standard deviation of the signal, calculated with a sliding window. The main advantage of OSort over its competitors is that it can be used online, thus enabling real-time spike sorting during an experiment (Rutishauser 2006). OSort version 2.1 was used for the comparison.

KlustaKwik

KlustaKwik is a software for unsupervised classification of multidimensional data. It is employed in the MClust toolbox, which enables both manual and automatic spike sorting on single-electrode, stereotrode and tetrode recordings. KlustaKwik fits a mixture of Gaussians with unconstrained covariance matrices and automatically chooses the number of mixture components. PCA is used to extract spike features for the clustering and a penalty term for selecting the number of clusters is implemented. The penalty is based on the ability to specify Bayesian information content (Cheeseman et al. 1996). KlustaKwik allows a variable number of clusters to be fitted. The program periodically checks if splitting any cluster would improve the overall score. KlustaKwik also checks to see if deleting any cluster and reallocating its points would improve the overall score. The splitting and deletion features often allow the program to escape from local minima, reducing sensitivity to the initial number of clusters, and reducing the total number of starts needed for a data set (Harris 2000). KlustaKwik version 1.6 was used for the comparison.

3.2.2 Preparation of test data

For the purposes of comparison we used two sets of artificial data: previously published data (Quiroga et al. 2004), referred to as QQ (after Quiroga Quiroga), and data generated by our own method, referred to as JW, publicly available online - <http://neuro.felk.cvut.cz/supplementary/spikesorting-comparison/>). Both of these data sets were obtained simulating extracellular signals recorded using a single microelectrode.

Our artificial data was generated by superimposing real spikes at random times onto a noise background – see Section 3.2.3 for details about the generator. Since several aspects of signals affect spike sorting, we used a wide range of signals of different characteristics (signal noise level, number of neurons) to maximize the objectivity and discriminability of our results.

A total of 9 real spikes (64 samples) shown in Figure 3.3 were picked manually from extracellular tungsten microelectrode recordings during a Deep Brain Stimulation operation from the STN of 5 patients. Each spike was deduced from a different position in the STN, thus eliminating the possibility of extracting two separate spikes of the same neuron.

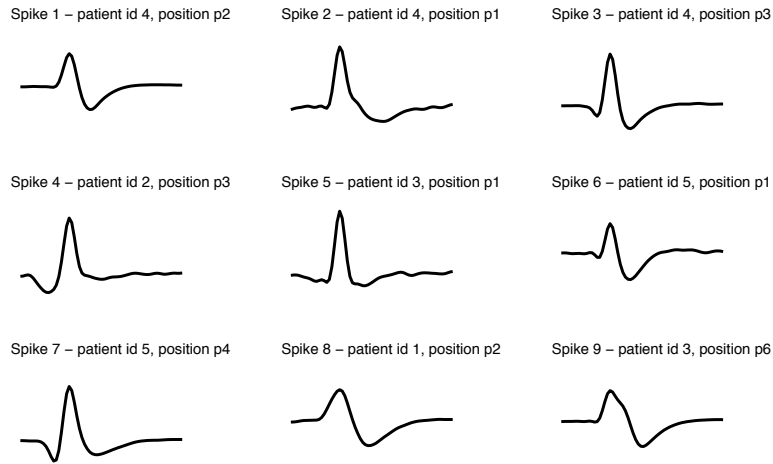


Figure 3.3: Waveforms of 9 real spikes, used for artificial signal generation. Each spike represents a different neuron.

The noise background for longer signals (60, 960 seconds) was generated in the same way as for the QQ data (Quiroga et al. 2004) using over 2 000 different spikes (some of which might be from the same neuron), thus simulating the activity of many distant neurons in the brain. For shorter signals (20 seconds), a spike-less part of a raw signal recorded from STN was used as a noise background to approximate real signals more closely. The noise was then scaled, so that its standard deviation σ lies within the range $\langle 0.05; 0.3 \rangle$, and was then superimposed on the previously generated signal to get the final artificial record.

Twenty two QQ signals (60 seconds) and another 90 JW signals with 2 – 9 neurons generated using the described procedure were used to evaluate the spike sorting algorithms on a large variety of signals with different properties. The JW signals were split into three groups according to their length - 40 short JW signals (20 seconds), 40 long JW signals (60 seconds) and 10 very long JW signals (960 seconds). The signals with the same number of neurons differed in the standard deviation of the noise that was superimposed

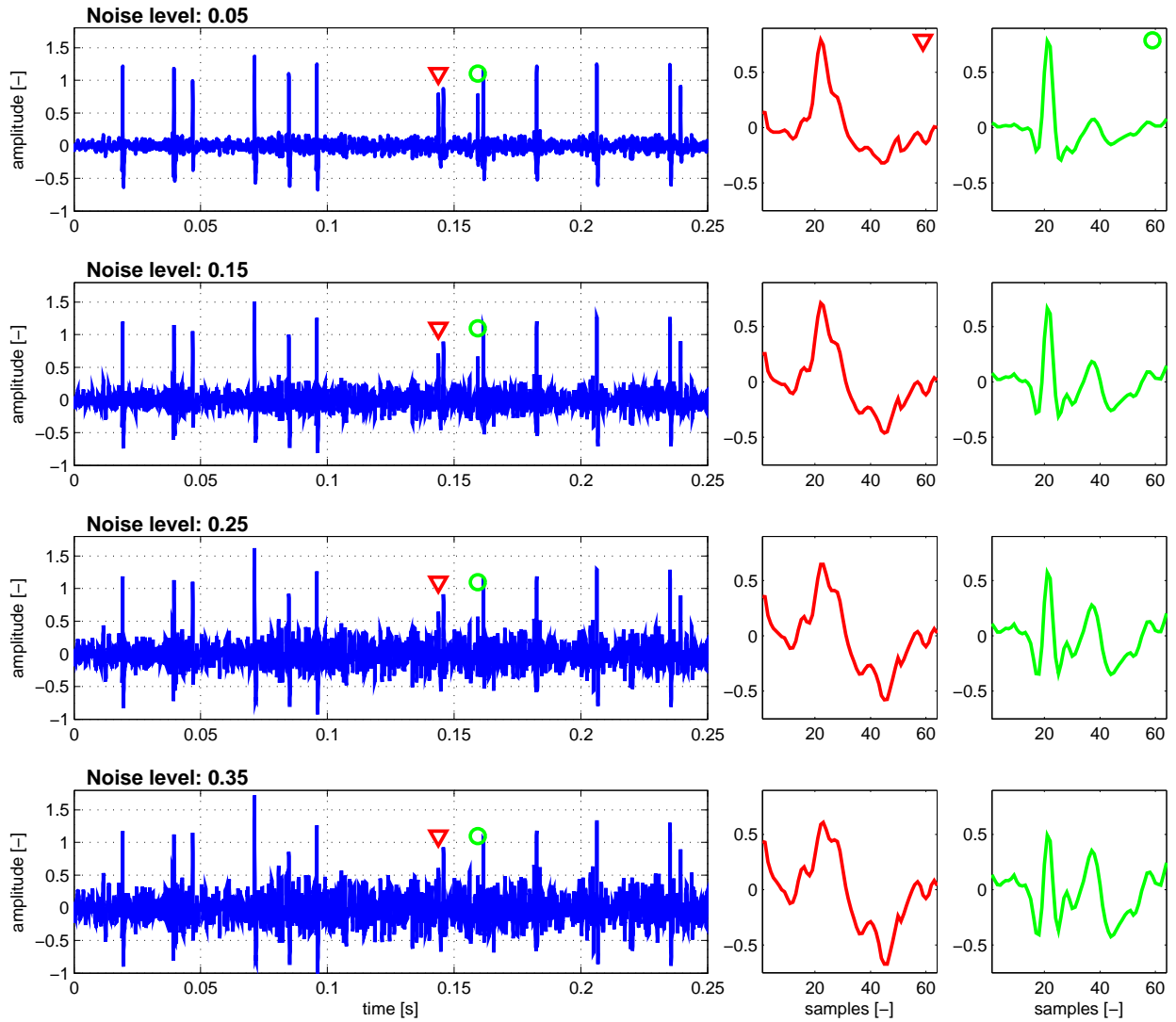


Figure 3.4: Example of the same 250 ms long signal with different noise levels ranging from 0.05 to 0.35. The spikes marked in the signal by a triangle and a circle each belonged to a different neuron and are shown in greater detail on the right side - in the case of a higher noise level at 0.25 and 0.35, a new noisy spike could be misleadingly detected.

on the signal element. However, as it was very difficult to estimate (and compare) the standard deviation of the noise component in the case of real signals, all the JW and QQ data was labeled using a straightforward noise estimation method (see Section 3.2.4).

3.2.3 Artificial signal generator

To generate an artificial signal with n neurons, spikes $1..n$ were used as a template for each neuron. Each template was first scaled to 75%-125% (uniform distribution) of its maximal amplitude to mimic the different spatial distance from each neuron to the electrode and was placed at random positions in the signal, while maintaining a neuronal refractory period of 3ms. The contribution of different neurons was independent, such that spikes of different neurons might have coincided with each other in the signal, simulating the situation of several neurons firing at the same time.

After placing all the spikes, noise should be added to the signal. Our generator used two types of noise. An artificial one that was generated in the same way as the signal itself but with much larger set of neurons (e.g. thousands of neurons). This procedure was selected as it should closely mimic the origin of noise in recorded MER signals. As the other type of noise a spike-less part of real recorded signal from STN was used (repeating as needed). Both types of noises had to be normalized first and then multiplied by the wanted *noise_level*.

See Algorithm 1 for Matlab pseudocode of the artificial generator used.

3.2.4 Noise Level Estimation

The noise level n_l was defined as the reciprocal value to the signal-to-noise ratio SNR (Smith 1999)

$$n_l = \frac{1}{SNR} = \left(\frac{A_{noise}}{A_{signal}} \right)^2 \quad (3.1)$$

where A_{signal} represents the root mean square (RMS) amplitude calculated from all the spikes extracted using spike detection, and A_{noise} accounts for RMS computed from the rest of the signal. As the estimated noise level was normalized, it was easier for comparison across signals with different amplitude ranges, as opposed to standard deviation. An inevitable drawback of the method described here was that the estimation was slightly biased as, in theory, A_{signal} had to be calculated only from the useful signal (spikes), whereas in the real case the spikes themselves were corrupted by noise.

Algorithm 1 Artificial signal generator

```

signal = zeros(1, signal_length)
for each spike in spike_templates do
    % randomly increase/decrease spike size
    nspike = spike · ((rand()/2) + 0.75)/max(spike)

    % calculate interspike intervals (ISI) histogram
    % from Poisson distribution given lambda (1..4)
    lambda = rand() · 4
    histogram = poissrnd(lambda)

    % transform histogram into ISIs, adhering to refractory_period
    % so that each ISI is uniformly spread among the histogram bin
    isi = refractory_period + (histogram - rand()) · bin_width

    % calculate firing indexes from ISIs
    idx = cumsum(isi)

    % place spike according to idx (i.e. neuron spiketrain)
    for i = 1 : length(idx) do
        signal(idx) = signal(idx) + nspike
    end for
end for

    % Add normalized noise with a given noise_level to the signal
    % (noise can be prepared using the same procedure)
    signal = signal + noise · noise_level

```

For illustration purposes, Figure 3.4 depicts the same 250 ms long signal with four different noise levels (0.05, 0.15, 0.25, 0.35). On the right side of each signal there is a detail of two spikes (marked in the signal by a triangle and a circle), each belonging to a different neuron. This is an example to illustrate of how much the noise affected the shape of the spikes.

3.2.5 Performance rating function

In order to assess the accuracy of different spike sorting algorithms and to provide an objective function for optimization, a performance measure was needed. As the experiments were performed using artificial data, the true clustering of the spikes was available. In machine learning research, many measures have been proposed for this type of clustering evaluation task (Warrens 2008; Vinh et al. 2009; Vinh et al. 2010), and some of them have already been used for spike sorting evaluation (Kretzberg et al. 2009; Gasthaus 2008). Recently, Vinh et al. (2010) showed that Adjusted Mutual Information (AMI) had the best properties among all these clustering evaluation measures, so this measure was selected for the evaluation.

AMI is an information theoretic measure which usually provides a value between 0 and 1. The value is 0 if the clustering provides information about the true clustering just by chance, and it is 1 if all information is revealed, meaning that the two clusterings are the same. Hence, AMI can be considered as the ratio of true information in a spike sorting result. Several AMI values and their corresponding clustering are shown in Figure 3.5.

3.2.6 Spike sorting parameters

All of the spike sorting algorithms discussed have a number of parameters (OSort - 2 parameters; KlustaKwik - 9 parameters; WaveClus - 13 parameters) that can be adjusted in order to improve the spike sorting accuracy. However, it was very difficult to set these parameters correctly using manual methods.

Although all the parameters were documented, it was an almost impossible task to find out how to operate them so that the algorithm would perform better on a given signal.

First a visualization of the parameter space was performed using high dimensional stacking (see Section 3.2.7). The visualization did not uncover any specific pattern in

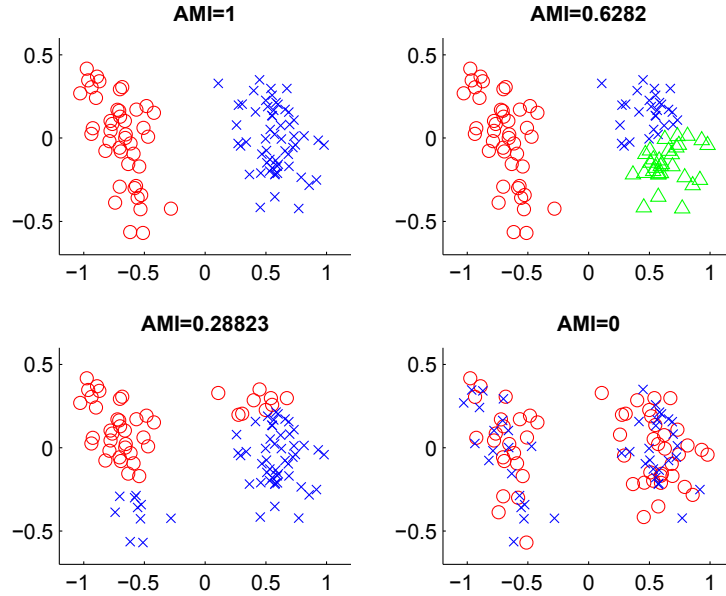


Figure 3.5: Several clustering results with their corresponding AMI values. The correct clustering is presented in the top-left corner with different shapes for each cluster. In the top-right corner, one cluster is further split, so AMI is reduced. In the bottom-left corner, the number of clusters is correct, but there is a wrong split. In the bottom-right corner is a random clustering (AMI=0).

the parameters space, but it did help us find reasonable parameter space boundaries for optimal parameter search.

Second, the parameter search was formulated as an optimization problem: given a set of algorithm parameters

$$\mathbf{x} = \{x_1, x_2, \dots, x_n\}, \quad (3.2)$$

find a solution for

$$\underset{\mathbf{x}}{\text{maximize}} f(\mathbf{x}), \quad (3.3)$$

where the $f(\mathbf{x})$ objective function is the value of the performance rating function (the AMI score) for the spike sorting results obtained with parameter vector \mathbf{x} . As artificial signals were used in this study, the AMI could be calculated for the parameter space and the optimal solution could be identified by an exhaustive search. Gradient descent and genetic algorithms were also considered, but the objective function changed significantly with only a small change in the parameters, so only an exhaustive search guaranteed finding the global optima.

While employing the exhaustive search, only some of the algorithm parameters proved to have an impact on the spike sorting accuracy. The Table 3.2 summarizes the names

of these parameters for all three algorithms. A complete annotated list of all parameters is available online at <http://nit.felk.cvut.cz/~wildj1/ssc> or at each algorithm author's website.

Table 3.2: List of parameters impacting the spike sorting accuracy for each algorithm. The parameter names were taken directly from the original source code of each algorithm author.

WaveClus

force_auto	Automatically force membership of spikes assigned to noise cluster using template matching.
inputs	Number of wavelet coefficients to use as features for clustering.
KNearNeighb	Number of data points used for the nearest neighbors interactions in the SPC.
min_clus_stop	Minimum size of a cluster (cluster will be deleted if the number of spikes it contains is lower than this value).
mintemp	SPC minimum temperature - a lower temperature value groups all data into a single cluster, while higher values allow the data to split into more clusters
scales	Number of wavelet decomposition levels used.
SWCycles	Number of Monte Carlo iterations used by SPC.
template.type	Type of template matching method used - template matching is used for spike sorting speed up in the case of large number of spikes or for assigning spikes in the noise cluster to the existing clusters (if force_auto is set).

KlustaKwik

noDim	Number of PCA dimensions used for clustering.
MinClusters	The random initial assignment will have no less than <i>MinClusters</i> clusters. The final number may be different, since clusters can be split or deleted during the course of the algorithm.
PenaltyMix	Amount of Bayesian information content (BIC) or Akaike information content (AIC) to use as a penalty for more clusters. Default of 0 sets to use all AIC. Use 1.0 to use all BIC (this generally produces fewer clusters).

OSort

minNrSpikes	Minimum size of a cluster (cluster will be deleted if the number of spikes it contains is lower than this value).
correctionFactorThreshold	Value correcting a signal noise estimate used as a clustering threshold.

In order to make a fair comparison between algorithms with different numbers of parameters, all signals were split into two parts. The first part was used for optimization to find the ideal parameters, and the second part was utilized to evaluate the spike sorting accuracy with these parameters.

3.2.7 Dimensional Stacking

In order to use dimensional stacking a two-dimensional grid was divided into embedded rectangles representing the individual parameters (i.e. categorical dimensions). Starting with two outer dimensions along the X and Y-axis, each additional pair of dimensions was embedded into the outer level rectangles. This process was repeated until all parameters were used.

According to Hoffman et al. (1997), the outer dimensions had a different effect than the inner dimensions. Therefore, it is significant in which order to choose the parameters for the stacking, because a specific order of parameters stacking might reveal something another order would not (Hoffman et al. 1997). As there was no exact clue on how to choose the outer and inner dimensions, these were picked manually in order to subjectively reveal the most information.

In order to overcome the limitation of dimensional stacking (necessity of categorical dimensions), we binned (discretized) each noncategorical dimension (algorithm parameter). The color of each point was defined by the AMI value of algorithm performance using the parameter set. Example of dimensional stacking visualization of WaveClus parameter space was shown in Figure 3.6.

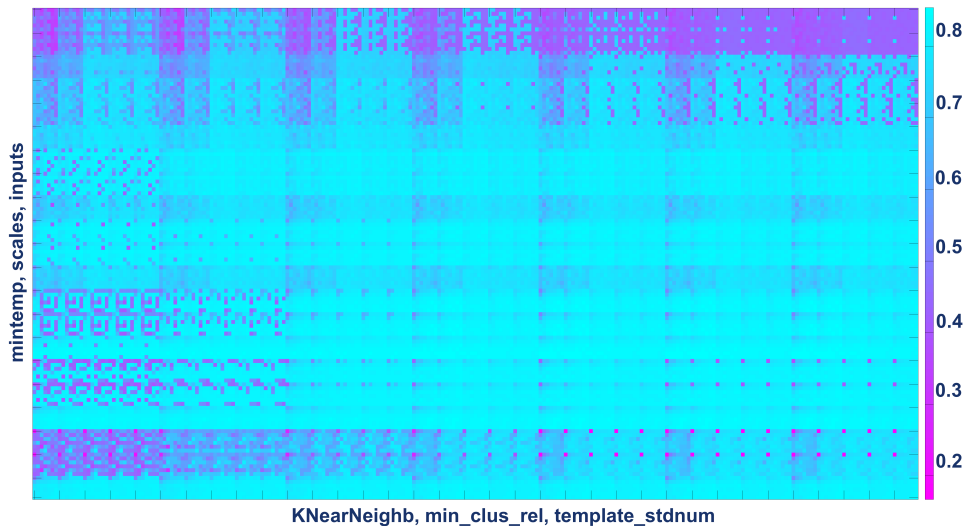


Figure 3.6: Example of dimensional stacking visualization of WaveClus parameter space (six parameters used) for signal QQ_Difficult1_noise015. The cyan color represents better performance (higher AMI), the magenta color means worse performance (lower AMI).

3.2.8 Statistical methods

For each artificial signal the AMI scores were calculated for each spike sorting algorithm, using either optimized or default parameters. For the spike sorting evaluation, the signals and their corresponding AMI scores were grouped according to the algorithm used and the signal noise level. Each group was visualized as a simplified boxplot showing the median and the lower and upper quartiles. The range between these quartiles is referred to as the spread. Differences between group medians were assessed using the two-sided Wilcoxon signed-rank test. Bonferroni corrections for multiple comparisons were applied whenever appropriate.

For the comparison between the optimized parameters, and the default parameters the AMI scores were grouped according to the algorithm and parameters that were used (either optimized or default). For visualization, the simplified boxplots were used as described above. Significant differences between the medians of the groups were assessed in the same way as for the spike sorting evaluation, using the two-sided Wilcoxon signed rank test.

All calculations and statistical analyses were performed using MatLab (Mathworks, Natick, MA). The spike sorting results for the different algorithms were calculated using a Dell Precision workstation running 32-bit Linux Mint with a 2.13GHz Intel Core 2 Duo E6400 2.13GHz and 2 GB of DDR2 RAM.

3.3 Results and Discussion

The algorithms were compared in two main aspects. First, the spike sorting accuracy was measured with AMI (one AMI score for each signal and algorithm). The results correspond to the evaluation part of the signals, unless otherwise stated. Second, the speeds of these algorithms were compared to give some impression of the number of spikes that can be processed within a reasonable time.

3.3.1 Optimized parameters

As was already discussed in Section 3.2.6, the parameters were optimized on one part of the signal and evaluated on the other half. It was important to see whether this optimization really yielded better results than the default parameters of the algorithm.

Figure 3.7 shows the spike sorting accuracy results using near-optimal parameters in comparison with the results employing the default parameters. JW short, long and QQ signals with noise levels ranging from 0.0 to 0.6 were used for this comparison. Although the spread of the AMI values was quite high, mainly due to the noise level diversity of signals used, it could be clearly seen that the optimization improved all three algorithms ($p < 0.01$).

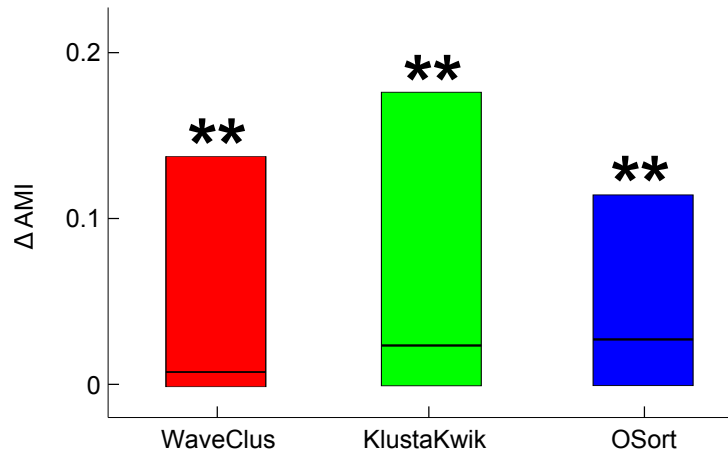


Figure 3.7: Comparison of the accuracy of the algorithms when used with default and optimized parameters. The y-axis represents the difference between the achieved AMI score while using optimized parameters and while using default parameters). Symbol ** indicates that the medians of the marked boxplots are significantly different from zero ($p < 0.01$).

3.3.2 Spike sorting accuracy

Our main assumption was that increasing noise levels have a negative effect on spike sorting accuracy. We therefore present our results depending on noise levels. Figure 3.8 shows the spike sorting accuracy of WaveClus, KlustaKwik and OSort on short (10s) JW signals with noise levels ranging from 0.0 to 0.6. For signals with noise level between 0.00 – 0.15, WaveClus was the most accurate algorithm, with a median AMI of 0.7. However, because of its large spread the difference between WaveClus and KlustaKwik or OSort was not significant.

With added noise, the median AMI of all respective algorithms decreased, with both WaveClus and KlustaKwik proving to be significantly better than OSort ($p < 0.05$ and

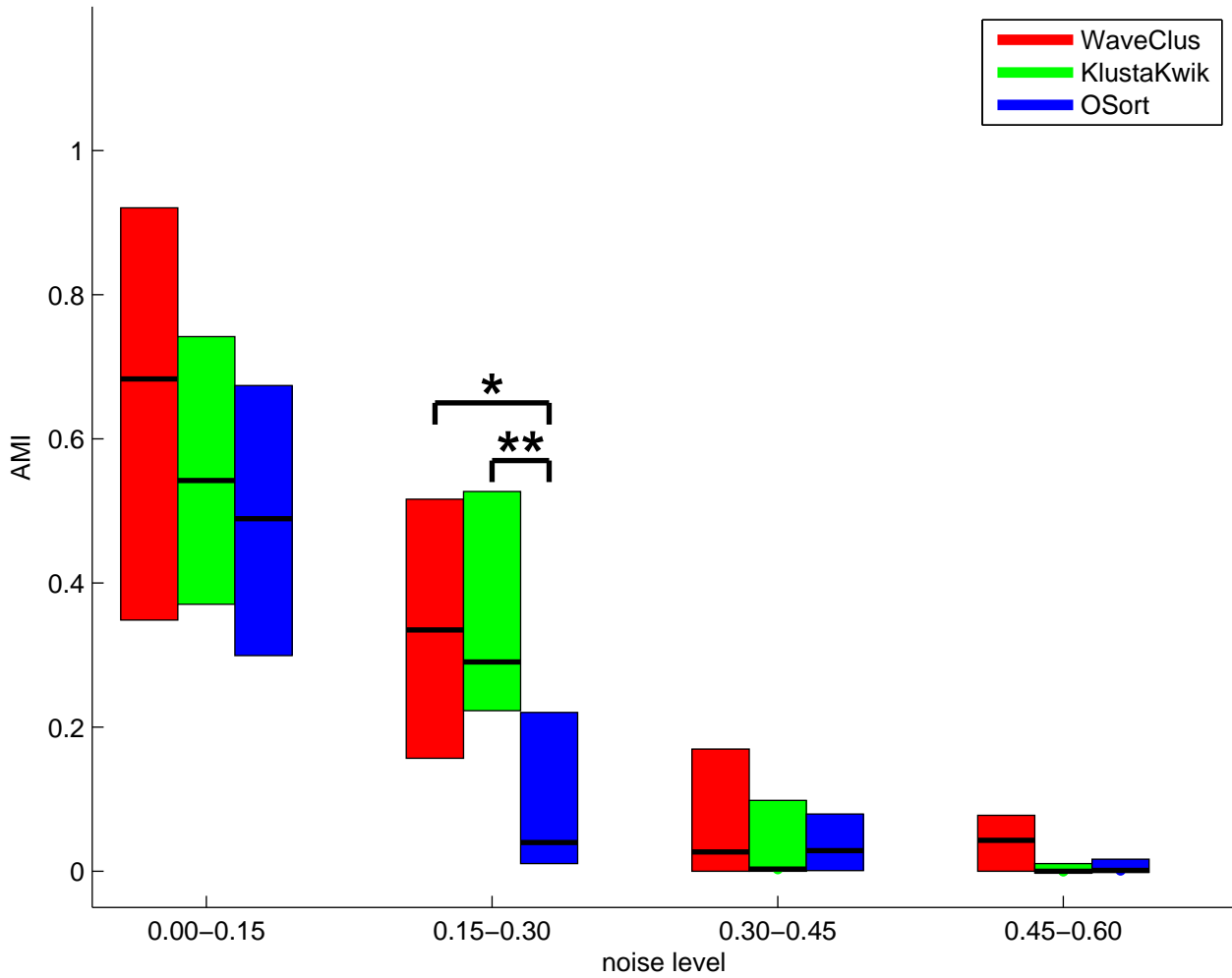


Figure 3.8: Performance of spike sorting algorithms using short (10s) artificial JW signals with noise levels binned and optimized parameters. The y-axis represents the AMI score of each algorithm along with its spread. Symbols * and ** indicate that the medians of the marked boxplots are significantly different ($p < 0.05$ and $p < 0.01$, corrected for 3 comparisons).

$p < 0.01$ at noise level 0.15 – 0.30), both having a better AMI score than OSort for 80% of 10s signals within the respective noise level range. For signals with noise levels above 0.30 all three algorithms had very poor accuracy, indicating that signals with such a high noise level were beyond their capabilities.

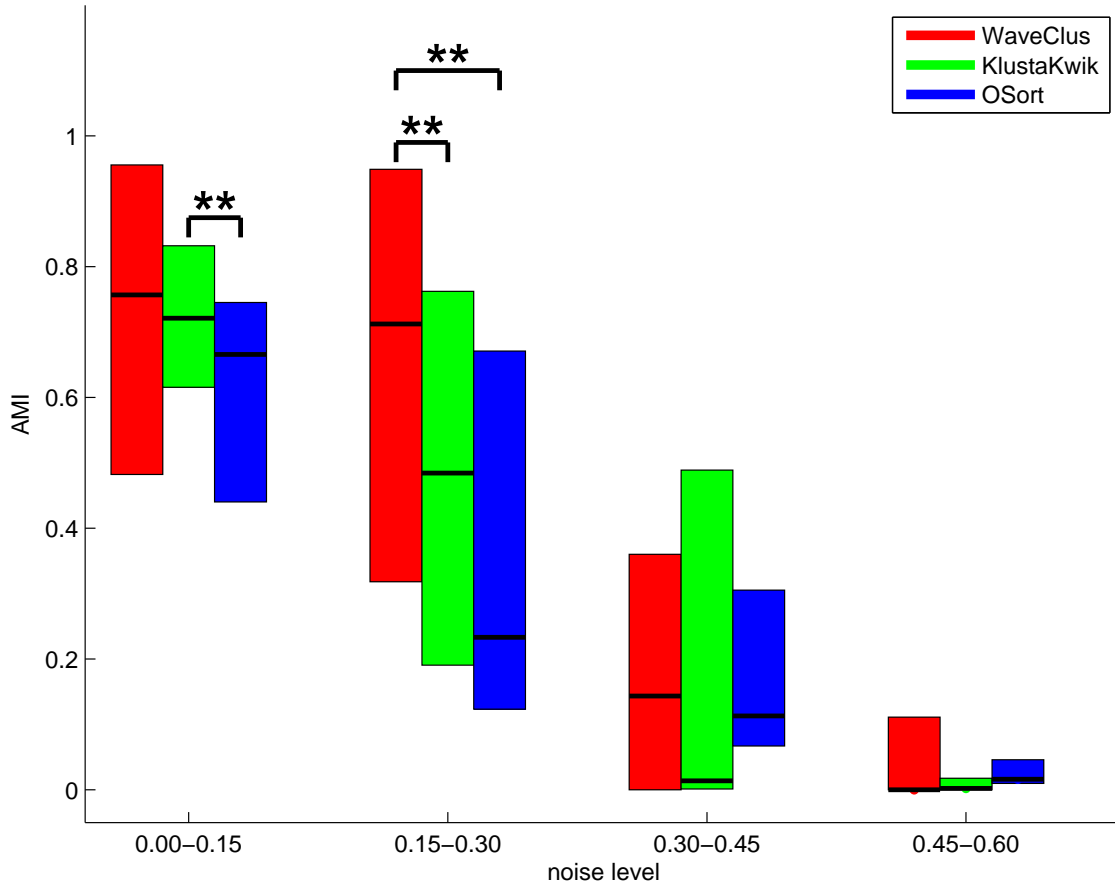


Figure 3.9: Performance of spike sorting algorithms using long (30s) artificial JW and QQ signals with noise levels binned and optimized parameters. The y-axis represents the AMI score of each algorithm along with its spread. Symbol ** indicates that the medians of the marked boxplots are significantly different ($p < 0.01$ corrected for 3 comparisons).

Figure 3.9, which depicts the same experiment as Figure 3.8, only with longer JW and QQ signals (30s), gave us somewhat similar results for WaveClus and OSort. WaveClus performed best in all cases, though it was significantly better ($p < 0.01$) than both of its competitors only for noise level 0.15 – 0.30 (it had a better AMI score for 89% of

the respective signals). KlustaKwik was significantly better than OSort for noise level 0.00 – 0.15, though with higher noise levels KlustaKwik had a larger spread than OSort. Again, noise level above 0.30 was too high for the algorithms to give reasonable results.

Some spikes were visually investigated in order to explain the effect of the noise levels. Judging from Figure 3.4, the spike shape (in this case) remained almost unchanged for noise levels 0.05 and 0.15, but at 0.25 and 0.35 the spike shape did not seem like the shape at 0.05. This had a direct negative effect on the spike sorting accuracy of OSort, as shown in Figure 3.8 and 3.9, in comparison with WaveClus, because OSort used raw spike shapes (without any filtering) and a simple distance measure for sorting.

3.3.3 Spike sorting time complexity

In a real world scenario, the speed of an algorithm may be of considerable importance. For example, if a certain algorithm can be run online, it will help researchers to gather sorted spiking data from microelectrodes in real time. Of these three algorithms, only OSort is online, which means that it processes spikes one-by-one as they come. For the other two algorithms, the whole spike sorting process needs to be re-run with all previous data to cluster the new spikes, so they are more targeted for offline analysis when new spikes are not coming in. Even for large-scale offline analysis, it would be good to know the computational demand of the algorithms.

Ten very long signals (960 s) with noise level 0.15 were used for evaluating the time complexity of each algorithm. The 960 s signals were cut into shorter signals, with the number of spikes varying from 100 to 19460. The parameters for each spike sorting algorithm were optimized on the first part (1400 spikes) of each 960 s signal, and remained unchanged for all the other parts originating from this signal. As only the speed of the algorithms was measured and not their actual accuracy, parameter optimization of each individual signal part was unnecessary.

The results of the speed test are shown in Figure 3.10. OSort was the fastest algorithm, with an average speed of 1100 spikes/s, whereas the average speed for KlustaKwik and WaveClus was 200 and 100 spikes/s respectively.

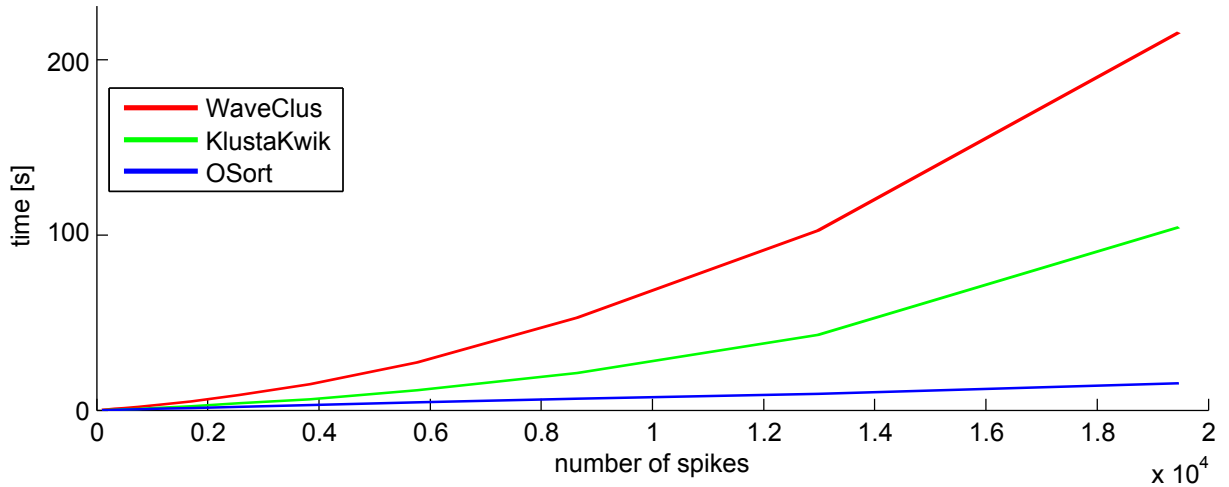


Figure 3.10: Relation between number of spikes and time needed for the spike sorting algorithms to run. Long JW signals (960 s, noise level 0.15) cut into several parts were used. The parameters were optimized using the first signal segment with 1400 spikes and remained the same for all other segments.

3.4 Conclusion

Three widely-used publicly-available spike sorting algorithms were compared (WaveClus, KlustaKwik, OSort) with regard to their parameter settings, using single-channel artificial data with different noise levels and different number of neurons. To avoid biased results, an optimization technique was employed based on Adjusted Mutual Information to find near-optimal parameter settings for our artificial signals. When using the near-optimal parameters, each algorithm improved its spike sorting accuracy as opposed to when only the default parameters were used ($p < 0.01$). Using these settings, an objective comparison of the three algorithms was made.

WaveClus was the best performing spike sorting algorithm. The accuracy of KlustaKwik was comparable to that of WaveClus at a lower noise level (0.00 – 0.15), and worse otherwise (see Figure 3.4 for visual comparison of signals with different noise levels). Although OSort performed less well than both WaveClus and KlustaKwik, it sorted spikes at more than five times faster, and can thus be recommended for real-time signal processing with a low amount of noise present (below noise level 0.15). Where there is high noise (noise level greater than 0.3), none of the three algorithms provided reasonable results.

As our artificial data is publicly available online, we believe that our framework can

be extended to further spike sorting algorithms, thus providing an objective comparison platform for neuroscience researchers – as of 17.8.2015 this work was cited 14 times on Web of Science (see Appendix A).

Chapter 4

Application Results of Spike Sorting

This chapter summarizes the application results in neuroscientific field which built upon the spike sorting methods described in Chapter 3 and could not be realized otherwise. Section 4.1 describes our finding of basal ganglia neurons related to eye movements. Section 4.2 presents the process of searching for emotion-related neurons in the subthalamic nucleus. Section 4.3 identifies activity in subthalamic nucleus that is directly related to PD symptoms.

4.1 Basal Ganglia Neuronal Activity during Scanning Eye Movements in Parkinson's Disease

This section describes the way of searching for basal ganglia neurons whose activity was related to eye movements, employing the results of spike sorting evaluation.

Note: The content of this section has been published by Sieger et al. (2013b). This work was a joint activity of several authors, including the author of this thesis. However, the dominant contributor was Tomáš Sieger. We briefly sketch the work here for completeness. Details can be found in the original article.

4.1.1 Introduction

In everyday life we scan the environment with a series of eye movements, pointing the fovea towards objects of interest and the most salient areas of the scene. The pattern of such eye movements (EM) carried out while exploring an image, also called scanning EM, is composed of a succession of small saccades and fixations, corresponding to successive re-allocation of attention from one detail to another (Araujo et al. 2001). Therefore, scanning EM can be considered as internally triggered EM, as the subject moves the gaze around a complex visual image actively searching for information relevant to current motivations and goals. Scanning EM have mostly been the domain of psychiatric research which has focused on the behavioral aspects of the eye scanning path rather than to pathophysiological origin and scanning EM control (Toh et al. 2011).

The structures and mechanisms involved in scanning EM are still poorly understood. At the subcortical level, an involvement of the basal ganglia during scanning EM was suggested by early research using regional cerebral blood flow in healthy controls and schizophrenic patients (Tsunoda et al. 1992). However, subcortical neuronal activity during scanning EM is still unknown and has never been studied in animals or in humans before. The only evidence of human EM-related neurons was obtained from the subthalamic nucleus during saccade tasks and smooth pursuit movements in patients with Parkinson's disease (Fawcett et al. 2004).

In our study, we systematically searched for basal ganglia neurons participating in scanning EM. We took advantage of intraoperative microelectrode recordings of single neuronal activity routinely used to identify the basal ganglia based on specific electrophysiological pattern (Hutchison et al. 1998b). We have focused on the subthalamic nucleus (STN), substantia nigra pars reticulata (SNr) and globus pallidus (GP) – i.e. nuclei in which EM-related activity was previously reported (Shin et al. 2010) and which are easily accessible during the implantation procedure for deep brain stimulation in Parkinsons disease (PD).

Besides EM-related neurons firing selectively when a specific position, velocity or acceleration of the eyeballs is reached, we expected to find less specialized neurons with activity depending on two or more kinematic features simultaneously (Selemon et al. 1990). On the other hand, there is a segregation hypothesis which expects different neuronal populations to selectively respond to specific kinematic parameters or to fire only during a specific kind of the EM. Therefore, in a subgroup of patients, we additionally studied the basal ganglia neurons during externally triggered EM using a visually guided

saccade task. To further elucidate the function of neurons related to EM, we explored temporal relations of EM kinematic parameters with respect to their preceding and following activity, which may suggest their involvement in execution or control processes.

4.1.2 Methods

Patients

Nineteen PD patients were enrolled consecutively from 2008 to 2011 (15 men, 4 women; mean age: 54.5, SD 9.8, range 28–69 years; mean PD duration: 13.8, SD 6.1, range 3–30 years; Hoehn-Yahr stage 2-4; mean motor score of the Unified Parkinsons Disease Rating scale – UPDRS III in OFF condition: mean 36.5, SD 13.6, range 10–65). All of them were suffering from motor fluctuations and/or disabling dyskinesias and were indicated for treatment with deep brain stimulation due to motor fluctuations and dyskinesias. Four days before surgery, dopamine agonists were substituted by equivalent doses of levodopa. Other anti-PD medication (amantadine, anticholinergics) was suspended earlier for the surgery preparation. Levodopa was withdrawn at least 12 hours before the surgery.

Surgery and intraoperative microrecording

Implantation of the deep brain stimulation system was performed according to the previously mentioned procedure (see Section 2.4.1). The central trajectory was intentionally focused on the STN center near the anterior part of the red nucleus (15 patients) or to the posteroventrolateral portion of the GP interna (4 patients). The extracellular neuronal activity was mapped by conventional microelectrode recordings (MER) using parallel insertion of five tungsten microelectrodes in a "Ben-gun" configuration (see Section 2.4.3). Up to six recording positions in the STN, SNr or GP were used for the EM tasks in each patient. The number of positions depended on the time course of the surgery, patients' clinical conditions and compliance.

Eye movement recording

Eye movements during scanning and visually guided EM tasks were recorded using electrooculography (EOG), a technique measuring the position of the eye in terms of the electric potential induced by the eye dipole. Technical constraints during surgery (limited space around the stereotactic frame and a limited number of recording channels) did not allow for more elaborate recordings than the use of one single-channel EOG. The

signal was band-pass filtered in the range of 0.1–20 Hz and recorded using the Lead-point recording system simultaneously with MER acquisition through a pair of surface electrodes attached near the outer canthus and the lower lid of the left eye. This setup enabled the orthogonal projection of the eye position on the axis connecting the two EOG electrodes. All eye movements except those which were orthogonal to the axis could be recorded with this technique.

4.1.3 Tasks

The EM tasks were presented on a 17"-computer screen placed approximately 55 cm in front of the eyes of patients lying in supine position.

The scanning EM task The goal of this task was to induce self-initiated free-direction scanning EM. The task consisted of a presentation of a series of photographs selected from the International Affective Picture System (IAPS, Figure 4.1A) (Lang et al. 1999), depicting objects, persons, animals and landscapes. To avoid showing the same picture more than once, six unique variants of the test, each containing 24 pictures, were prepared. Each picture was presented for a period of 2 s and was preceded by a black screen for various durations (3500–5500 ms) with a white cross in the center. Patients were asked to fix their eyes on the cross on the black screen and then to simply watch the pictures presented. The MER and EOG signals were acquired in 2 s epoch intervals recorded both during the picture presentation and the black screen. The task lasted approximately for 2.5 minutes.

The visually guided saccade task The goal of the task was to induce externally generated horizontal saccades (Figure 4.1B). Initially, a black screen with a central white cross was shown for a pseudorandom period of 2, 2.25, or 2.5 seconds. Subsequently, a peripheral target, a small white square, was presented for 1 s, 17 degrees laterally from the central fixation cross, pseudorandomly to the left (5 trials) or right (5 trials). Patients were instructed to initially fixate on the central cross and then to track the lateral target as fast as possible. The MER and EOG signals of 2 s durations were recorded during all 10 trials. The task lasted for 32.5 seconds.

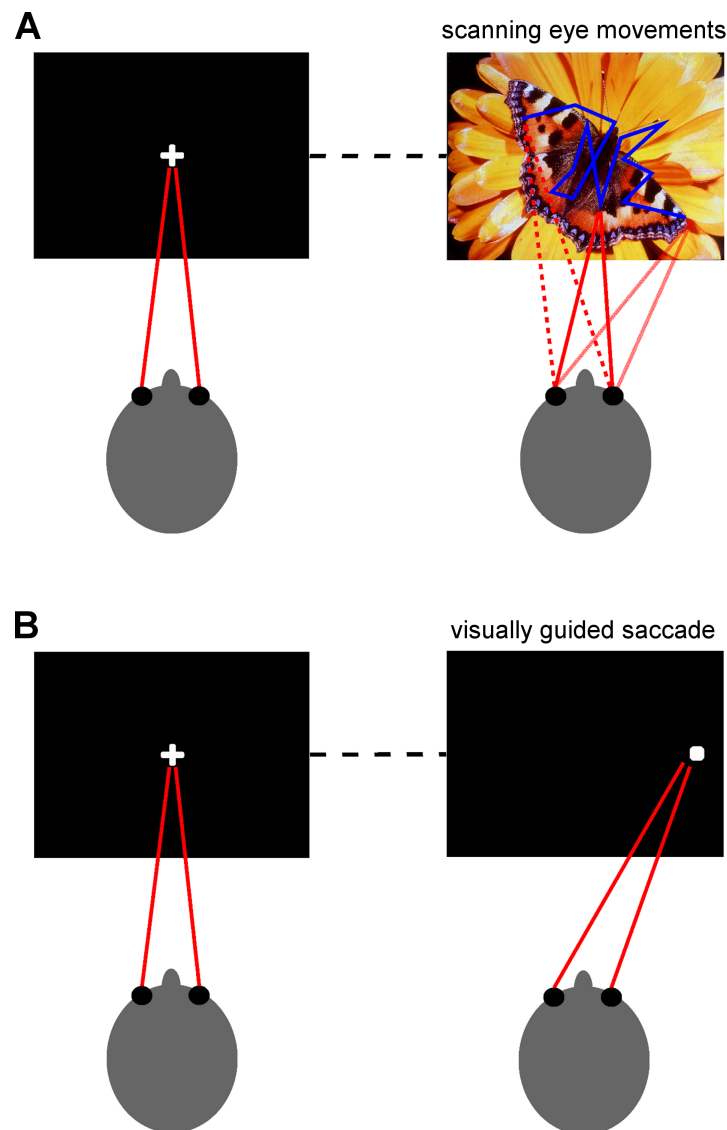


Figure 4.1: EM tasks employed in the study.

A - The scanning EM task. After the presentation of the black screen with a central cross, a photograph chosen from the International Affective Picture System was presented for 2 s. Patients were asked to initially fix their eyes on the cross (left picture) and then simply watch the photograph (right picture). In total, 24 pictures were consecutively used during the task. The blue line highlights a possible eye scanpath.

B - The visually guided saccade task consisted of a presentation of 10 pairs of indifferent central (left picture) and lateral GO (right picture) targets positioned pseudorandomly on the left/right side of the screen. Patients were instructed to initially fixate the central cross and then track to the lateral targets as fast as possible.

4.1.4 Data analysis

Microelectrode recordings WaveClus (Quiroga et al. 2004), an unsupervised spike detection and sorting tool, which performed reasonably well on the single channel MER (Wild et al. 2012b), was used to extract the series of action potentials of individual neurons from MER signals (Figure 4.2). Instantaneous firing rate (IFR) of each neuron was estimated by convolving the series of action potentials with the causal kernel function:

$$f(t) = \alpha^2 \cdot t \cdot \exp(-\alpha * t), \quad (4.1)$$

defined for positive time t , where $\frac{1}{\alpha}$ was empirically set to 20 ms.

Each neuron was then mapped relative to the border of the STN, GPi and SNr identified by intraoperative MER. Onedimensional positions along the dorso-ventral microelectrode trajectory were determined using this technique.

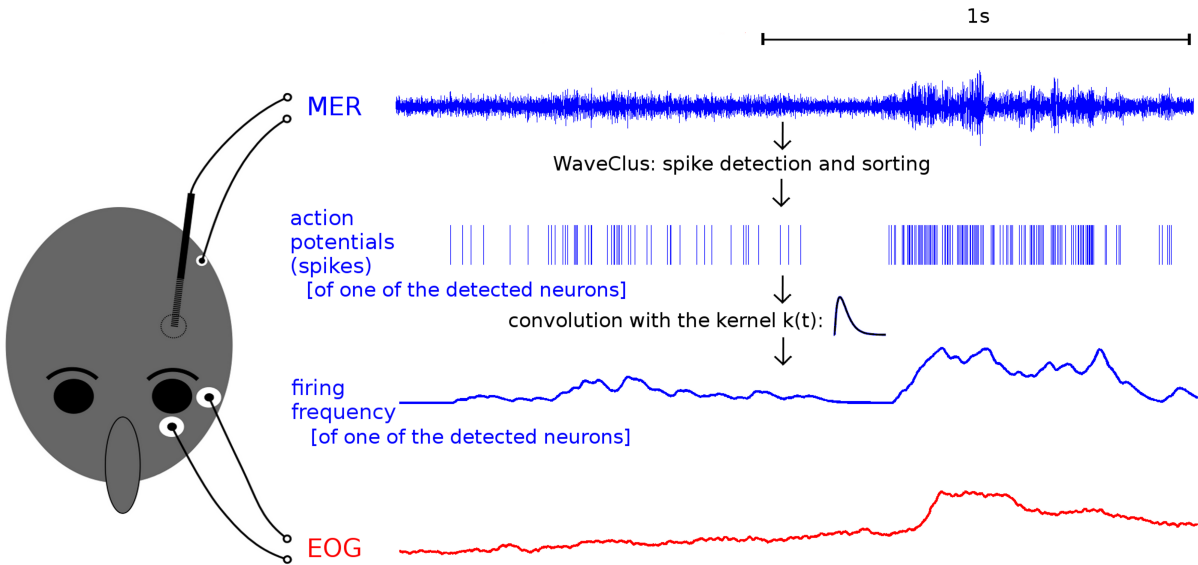


Figure 4.2: MER and EOG signal acquisition and processing. Action potentials of individual neurons were identified using the WaveClus algorithm in the MER signal. The instantaneous firing rate (IFR) was then estimated by convolving a series of extracted action potentials generated by a single neuron with a causal kernel function. Finally, the IFR was correlated with the eye movement kinematic parameters derived from the EOG.

EM recordings EOG signals were rated manually and those contaminated with technical or major blinking artifacts, usually represented by large amplitude changes oversaturating the recording channel, were excluded from further analyses. As we presumed that neuronal activity could be related not only to the position of the eye, but also to its motion and the dynamics of the motion (Fawcett et al. 2004) we characterized EM by: i) the eye position (POS), defined by the EOG signal itself, ii) the eye velocity (VELOC), defined as the derivative of POS, and iii) the acceleration of the eye (ACCEL), defined as the derivative of VELOC. The derivative of the signal was defined in terms of the differences between successive samples in a low-pass filtered signal computed using a sliding rectangular window with the cutoff frequency of 12.5 Hz. The maximum and typical amplitude of the EM was extracted in each recording position in each task for each patient. While the maximum amplitude was defined as the extreme value in VELOC, the typical amplitude was defined as the median peak exceeding ± 1 SD of the VELOC.

To identify neurons whose activity was associated with EM, the relationships between IFR and POS, IFR and VELOC, and IFR and ACCEL were assessed. A neuron was considered connected to EM if its IFR was related to at least one of POS, VELOC, and ACCEL at the Bonferroni-corrected significance level of $p < 0.05$. The relationships between IFR and the EM characteristics were analyzed using cross-correlation, which could reveal not only the link between concurrent IFR and EM, but also the link of IFR to preceding and following EM (Figure 4.3). The maximal crosscorrelation lag considered was ± 500 ms with steps of 2.5 ms.

Biased estimates of correlation coefficients were computed to diminish uncertainty in estimates of correlation coefficients over longer lags. The cross-correlation coefficient between two signals was defined as the extreme correlation coefficient between the signals over all the lags considered. The lag in which the extreme cross-correlation was reached was called the optimal EM-to-IFR cross-correlation lag. The statistical significance of the cross-correlation coefficient between two signals was assessed with Monte-Carlo simulations (Simpson et al. 2001) using original and surrogate signals generated by randomly changing the phases of the spectral representation of the original signal.

The binomial test, Pearson's correlation coefficient test, Fisher exact test, two-sample proportion test, likelihood ratio test comparing Poisson regression models of dependence and independence in a 2-by-2-by-2 contingency table and paired t-test were used for statistical analysis. Data processing and analyses were performed in MATLAB (R2007b, The MathWorks, Natick, MA) and "R" software (R Core Team 2015).

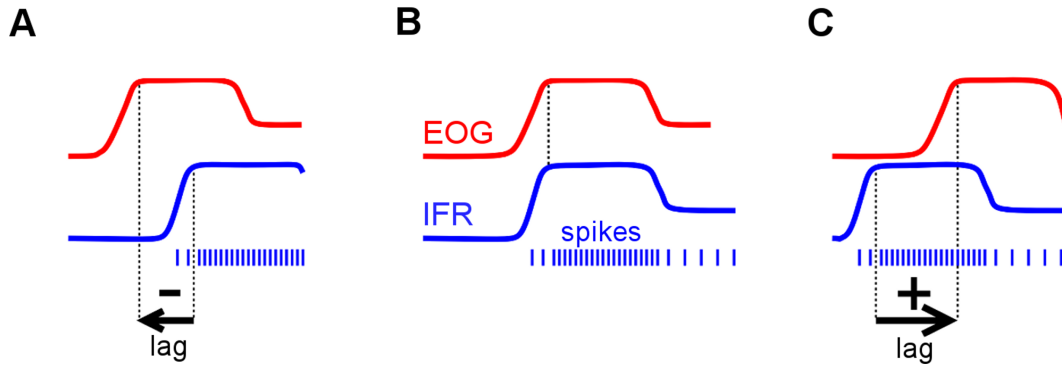


Figure 4.3: Time lag of neuronal activity with respect to EOG. A, B, C - Explanation of the cross-correlation procedure in three examples. Action potentials of three hypothetical neurons along with corresponding IFR were correlated with the theoretical EOG signal. Figure A – the IFR correlates with the past EOG signal suggesting a sensory function of the neuron. Figure B – the IFR correlates with the concurrent EOG signal suggesting an executive function of the neuron. Figure C – the IFR correlates with the future EOG signal suggesting a preparatory function of the neuron.

4.1.5 Results

We acquired 137 pairs of MER and EOG signals from 91 recording positions: 97 MERs were assigned to the STN, 21 to the GP and 19 to the SNr according to their firing pattern. In total, 183 neurons were detected using the spike sorting procedure, out of which 130 were located in the STN, 23 in the GP and 30 in the SNr (Table 4.1).

Neuronal activity related to scanning eye movements

Thirty seven (20%) out of 183 neurons identified in the basal ganglia during the scanning EM task were related to at least one of the EM kinematic parameters (POS, VELOC, ACCEL) (Table 3). Their proportion was higher than the expected false positive rate in each of the analyzed nuclei (binomial test, $p < 0.001$): 26/130 neurons (20%) in the STN, 5/23 neurons (22%) in the GP and 6/30 neurons (20%) in the SNr. In the STN, the ratio of the EM-related neurons was higher in the ventral part (0 to 1 mm from the ventral STN border) compared to the rest of the nucleus (proportion test, $\chi^2 = 2.722$, $df = 1$, $p < 0.05$).

The firing rate of the neurons relating to eye position (POS) significantly correlated with fluctuations of the EOG (Pearson's $r = 0.89$ (STN), 0.91 (GP), 0.86 (SNr); $df = 18$, $p < 0.001$) (Figure 4.4). A relatively large number of neurons were related to more than

Table 4.1: Eye movement-related neurons detected in the scanning eye movement task and/or visual guided saccade tasks.

	STN	GP	SNR	Total
MER count	97	21	19	137
neuron count (SEM task)	130	23	30	183
neuron count (SEM & VGS task)	46	2	5	53

MER count – number of microelectrode recordings obtained in each nucleus; SEM – scanning eye movement task; VGS – visually guided saccade task; neuron count – number of neurons identified in each nucleus during the SEM task (patients 1-19) and during both the SEM and VGS tasks (patients 16-19); STN – subthalamic nucleus; GP – globus pallidus; SNr – substantia nigra pars reticulata.

Table 4.2: Number of neurons related to eye movements in the scanning eye movement task.

	STN	GP	SNr	Total
EM-related neurons†	26 (20%)***	5 (22%)***	6 (20%)***	37 (20%)***
POS	15 (12%)**	6 (26%)***	5 (17%)*	26 (14%)***
VELOC	21 (16%)***	7 (30%)***	7 (23%)***	35 (19%)***
ACCEL	19 (15%)***	3 (13%)	5 (17%)*	27 (15%)***
POS, VELOC	10 (8%)	4 (17%)*	5 (17%)*	19 (10%)**
POS, ACCEL	7 (5%)	3 (13%)	3 (10%)	13 (7%)
VELOC, ACCEL	10 (8%)	3 (13%)	4 (13%)	17 (9%)*
POS, VELOC, ACCEL	7 (5%)	3 (13%)	3 (10%)	13 (7%)

EM-related neurons – the number of eye movement-related neurons associated with at least one kinematic parameter (†Bonferroni-corrected number of neurons for three kinematic parameters). Neurons functionally associated with one or more kinematic parameters (POS – eye position; VELOC – eye velocity; ACCEL – eye acceleration) are reported for each nucleus separately (STN, GP, SNr). Number of neurons significantly greater than expected 5% false positivity rate is denoted: *($p < 0.05$), **($p < 0.01$) ***($p < 0.001$).

one kinematic parameter (likelihood ratio test, $D = 42.2$ (STN), 19.8 (GP), 28.0 (SNr); $df = 3$, $p < 0.001$).

As follows from cross-correlation analysis, the firing rate of the neurons was related either to concurrent, previous, or future EM (Figure 4.3). However, none of the nuclei predominantly contained any kind of the time-related neurons.

Neuronal activity related to visually guided saccades

There were 10/46 neurons (22%) whose activity was related to visually guided saccades in the STN, 1/2 of the neurons were in the GP and 2/5 were in the SNr. A description of neurons related to all EM kinematic parameters (POS, VELOC, ACCEL) is shown in Table 4.3.

Table 4.3: Eye movement-related neurons detected in the scanning eye movement task and/or visual guided saccade tasks.

	STN (46 neurons)			GP (2 neurons)			SNr (5 neurons)		
	SEM	VGS	Both	SEM	VGS	Both	SEM	VGS	Both
EM-related neurons [†]	10	10	2	0	1	0	1	2	0
POS	4	9	0	0	0	0	0	2	0
VELOC	9	4	1	0	0	0	1	0	0
ACCEL	8	11	3	0	1	0	2	0	0
POS, VELOC	3	4	0	0	0	0	0	0	0
POS, ACCEL	2	4	0	0	0	0	0	0	0
VELOC, ACCEL	4	2	0	0	0	0	1	0	0
POS, VELOC, ACCEL	2	2	0	0	0	0	0	0	0

EM-related neurons – the number of eye movement-related neurons associated with at least one kinematic parameter ([†]Bonferroni-corrected number of neurons for three kinematic parameters) identified from patients 16-19 which performed both the scanning eye movement task (SEM) and visual guided saccade task (VGS) in the STN, GP and SNr. Neurons functionally associated with one or more kinematic parameters (POS, VELOC, ACCEL) are reported for each nucleus separately.

Eye movements in the scanning and saccadic tasks

As both the scanning EM and visually guided saccades tasks were executed by only four patients, 19 relevant recording positions were analyzed. Neurons related to scanning

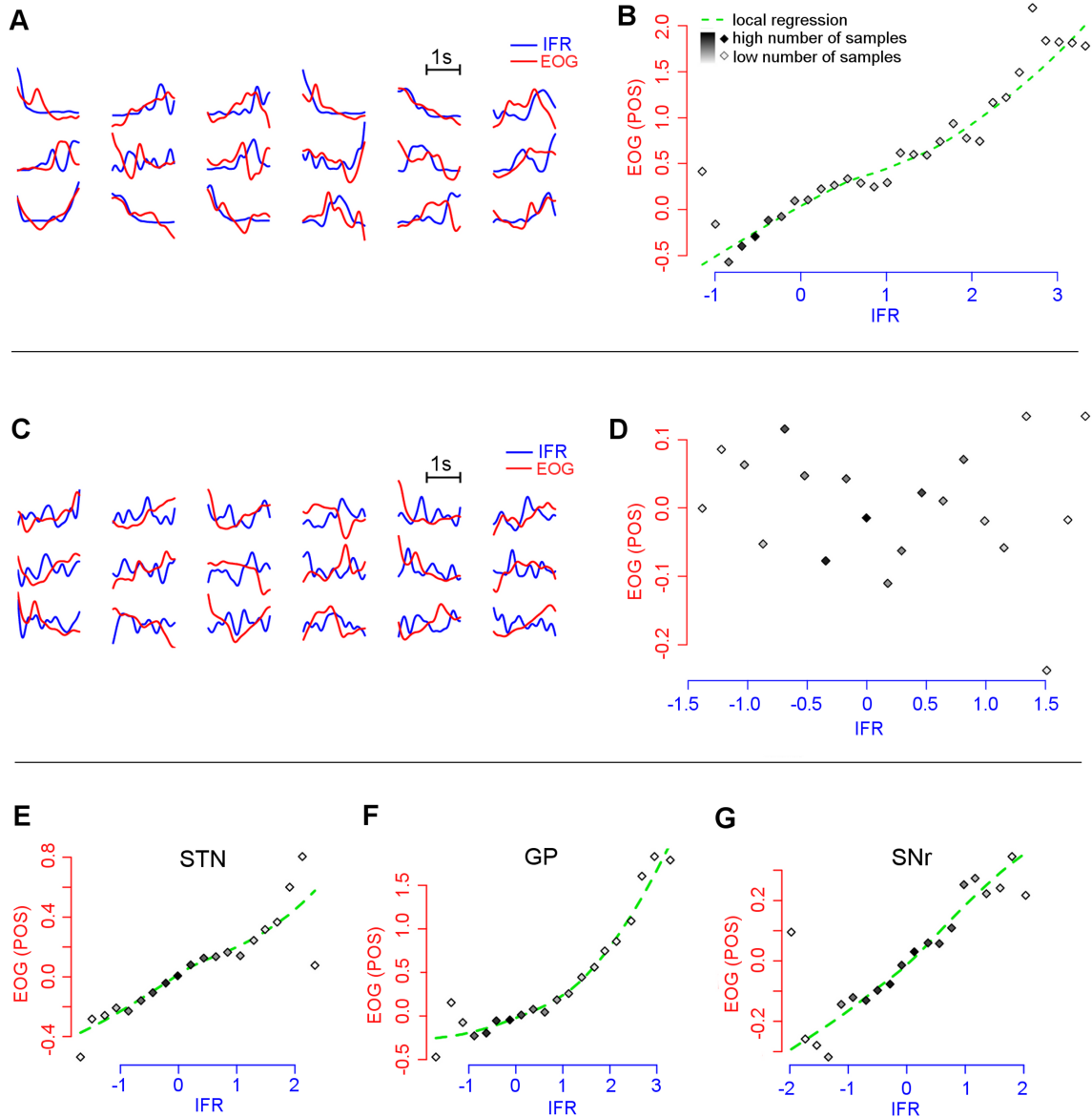


Figure 4.4: Neuronal activity during the scanning movement task. Example of neuron related (A, B) and unrelated (C, D) to eye movements based on correlation analysis of the IFR and POS derived from the EOG. All eye movement-related neuronal populations in the STN, GP and SNr are plotted in figures E, F, and G. Figures A, C show the IFR (blue) and EOG (red) pairs recorded during epochs of the task involving both the black screen and pictures presentations. Figures B, D, E, F, G show the dependency of the normalized POS derived from the EOG on the normalized, sorted and binned amplitude of the IFR. While the IFR from a single neuron was used on figures B and D; the IFR from all eye sensitive neurons were used on figures E, F, and G for each nucleus separately. The amplitudes of the POS signals which correlated negatively with the IFR signal were reversed. The number of signal samples in each bin is expressed by different shades of grey in the diamond glyphs.

EM were usually not activated in the visually guided saccades task and vice versa. Out of 46 STN neurons found in these patients, ten neurons related to scanning EM, ten neurons related to visually guided saccades and only two were activated during both tasks. These neuronal populations seemed to be independent in each of the two tasks as no evidence against the null hypothesis of independence was found (Fisher exact test, $p = 1.0$) although the test had enough power to reject the null hypothesis had the number of co-activated neurons been higher. In the GP and SNr, an insufficient number of neurons were detected for proper assessment of independence in neuronal activity between the two tasks. However, no GP or SNr neurons were co-activated during both tasks. Descriptive analyses of the EM amplitude revealed that the maximal amplitude of the scanning EM and visually guided saccades were nearly identical. As requested by the visually guided task, patients executed large saccades, while small EM predominated in the scanning task where large EM occurred only rarely. The amplitude of the typical EM made during the visually guided saccades task was greater than during the scanning task ($t = 5.7$, $df = 18$, $p < 0.001$). On average, the median saccade amplitude was 2.6 times larger in the visually guided task than in the scanning EM task.

4.1.6 Discussion

We showed that nuclei of the basal ganglia (namely, STN, GP and SNr) contain neurons whose firing rates correlated with eye movements during the scanning EM task. The proportion of EM-related neurons was relatively high reaching 20-22% in each of those nuclei (Table 4.2). Despite technical limitations due to the single-channel EOG recording we found relationships between different kinematic parameters of the EM and the firing rate in many neurons (Table 4.2, Figure 4.4). These findings point to the role of the basal ganglia in the static and dynamic representation of the EM, a role of importance for the maintenance of accuracy in goaldirected movements.

Eye movement activity in basal ganglia

Our single unit records from the STN showed that the proportion of EM-related neurons was higher in its ventral part. A 20% share of oculomotor neurons in the ventral part of the STN has already been noted in monkeys (Matsumura et al. 1991) and in humans (Fawcett et al. 2004). However, those were solely neurons involved in saccadic EM. As suggested by our results, the SNr and GP are probably as equally important for control

of voluntary scanning EM as the STN. We consider this as one of the major outcomes of our study because in both of these nuclei, the oculomotor activity had previously been noted during EM only in animals (Basso et al. 2005).

Segregation and convergence in eye movement control

Scanning EM are an important tool in the exploration of complex visual stimuli (Toh et al. 2011; Noton et al. 1971). Their trajectory is made up of a sequence of variably large saccades and fixations with the visual field maintained for tens to hundreds of milliseconds. As a result, a certain detail is steadily projected on the fovea. This is followed by a saccade, a rapid voluntary movement, by means of which the fovea moves on to a new point of interest while information from the other parts of the retina is being concurrently assessed in search of another point of fixation. This distributed parallel processing has been recently confirmed by the sequential scanning task (Trukenbrod et al. 2012). As expected, in four patients where both tasks were used, the median amplitude of scanning EM was smaller than that of the saccades in the visually guided task. At the same time, the amplitudes of largest EM executed in both tasks were similar. This is in agreement with previous studies (Wartburg et al. 2007).

From what structures and in which way the scanning movements are controlled is still poorly understood. Since they are under voluntary control, they can be seen as a model with internally generated movements – unlike reflexive saccades which are initiated by external stimuli. Internally and externally triggered movements are generally subject to different control and executive mechanisms (Jahanshahi et al. 1995; Wiese et al. 2004). Hence, we assumed that both oculomotor systems are functionally segregated even at basal ganglia level. This hypothesis proved to be correct because in a subgroup of patients engaged in tasks which involved scanning as well as visually guided saccades, we observed that different EM-related neurons were involved in each of the tasks (Table 4.3). The principle of functional segregation in the control of voluntary and automatic EM had already been previously implied in connection with the interpretation of deep brain stimulation effects (Fawcett et al. 2009). Our results go even further in terms of this specialization hierarchy. Apart from the segregation of populations of EM neurons for scanning movements and visually guided saccades, we identified a higher degree of segregation in all three nuclei neurons. In fact, some neurons responded exclusively to a specific kinematic parameter of the EM associated with an increasing or decreasing firing rate depending on whether or not the eye had reached a particular position, velocity or

acceleration of movement (Figure 4.3).

Some of our results conform to the opposite principle – functional overlap of neurons. A small percentage of the STN neurons showed the same neuronal activity in both types of tasks (Table 4.3). The convergence theory is supported by our observation of 5–8% of STN neurons, whose activity correlated with several kinematic parameters simultaneously (Table 4.2, 4.3) suggesting the presence of universal oculomotor neurons. This is in agreement with previous findings of STN neurons which become activated by switching from automatic to voluntary controlled EM (Isoda et al. 2008). The functional convergence is further supported by the STN deep brain stimulation joint effect on the oculomotor and motor system of the neck and trunk in Parkinson’s disease, marked by simultaneously improved orienting eye-head movements (Sauleau et al. 2008).

Time relation between EOG and neuronal activity

In our study, the eye-movement neurons in the STN, SNr or GP were not firing solely in a particular phase of the scanning EM task. In all three nuclei, these neurons became active 200–400 ms before EM, in its course and also 200–400 ms after its onset. While STN neuronal activity expressed in saccaderelated potentials already began 0.8–1.8 s before the saccade, suggesting the involvement of nonspecific readiness non-motor mechanisms (Fawcett et al. 2007), single unit neuronal STN and SNr activity culminated within 250 ms after the saccade onset suggesting monitoring or sensory function. Our results are more in agreement with observations of the STN showing modified neuronal activity before, during and after the saccade (Matsumura et al. 1991). This means that scanning EM-related neurons of the STN could be involved in all the preparatory, executive and monitoring phases of EM. This cannot be concluded for GP and SNr due to a relatively low amount of data.

Limitations

As there were several limitations we should interpret our results with caution. The main problem arose from the impossibility of using infra-red oculography or two-channel EOG during surgery. While their use would definitely have improved the accuracy of the kinematic parameters during EM, they would also have interfered with the established implantation procedure. The use of singlechannel EOG, which failed to capture the full extent of free-direction EM and yielded no more than EM projection into a onedimensional space, is clearly a limitation which to some extent compromised the sensitivity

of our study. Another limitation is connected with the assessment of neuronal activity during the oculomotor tasks based on just correlation analysis. Neuronal firing does not have to relate to EM activity alone but it may also reflect visual perception, planning, visuo-spatial attention or other cognitive processing which coincide with oculomotor activity. In addition, our results could be affected by the fact that our data was obtained from patients with Parkinson's disease in whom abnormal saccadic EM were repeatedly reported (Pinkhardt et al. 2012; Antoniadou et al. 2012). Whether any abnormalities exist in Parkinson's disease during scanning EM also is not clearly known since, with the exception of one study which showed a deficit in trans-saccadic working memory (Hodgson 2002), no-one has systematically focused on scanpath or other parameters of complex exploratory EM in these patients.

4.1.7 Conclusions

Employing spike sorting methods in our study was vital for showing that the STN, SNr and GP contain neuronal populations related to scanning EM. Their representation reached about 20% in each of the three nuclei. Basal ganglia are thus not limited to previously described saccade control and perhaps play a more general role in EM circuitry. Oculomotor systems responsible for the execution and monitoring of scanning EM and visually guided saccades are mostly segregated as suggested by neurons involved exclusively in one of two EM tasks or by neurons selectively co-activated in association with a specific kinematic parameter. However, some functional overlap of the two oculomotor systems does exist, albeit confined to small groups of neurons conforming to the complementary convergence principle. Further studies combining clinical and electrophysiological approaches are needed to clarify the role of the basal ganglia in automatic and voluntary oculomotor behavior. We should emphasize that the large representation of basal ganglia neurons showing activity during all phases of the EM is also an argument for taking them into account when designing new tasks using single unit microrecording. Many visual, ocular or motor experiments are potentially oculomotor in their nature which may compromise results if the EM-related neuronal activity was not considered.

4.2 Distinct Populations of Neurons Respond to Emotional Valence and Arousal in the Human Subthalamic Nucleus

This section describes the way of searching for basal ganglia neurons whose activity was related to emotional valence and arousal. Spike sorting was vital to this work as it allowed us an analysis of firing pattern of individual neurons necessary for confirming our hypothesis.

Note: The content of this section has been published by Sieger et al. (2015b). This work was a joint activity of a few authors, including the author of this thesis. However, the dominant contributor was Tomáš Sieger. We briefly sketch the work here for completeness. Details can be found in the original article.

4.2.1 Introduction

Once the subthalamic nucleus was considered as an important regulator of motor function (Okun 2012; Alexander et al. 1991). However, the occurrence of postoperative neuropsychiatric complications has expanded interest in the non-motor function of the STN (Voon et al. 2006; Castrioto et al. 2014). Animal and human studies have already demonstrated the additional functional role of the STN in emotional and motivational processes (Schneider et al. 2003). In addition, recent fMRI studies found STN activation in response to emotional stimuli in healthy subjects (Karama et al. 2011; Fruhholz et al. 2012). Therefore we hypothesized that emotional activity related neurons should exist in the STN. However, participation of this nucleus in processing emotion has not been investigated directly at the single-neuron level in humans before.

Single-neuron activity related to a priori defined emotional categories (e.g. positive vs. negative) has already been detected in humans in a few brain regions such as in the hippocampus, amygdala and in the prefrontal and subcallosal cortex (Kawasaki et al. 2005; Laxton et al. 2013; Wang et al. 2014).

It has been proposed that emotional behavior is organized along two psycho-physiological dimensions: emotional valence, varying from negative to positive, and arousal, varying from low to high (Russell 2003). The individual assessment of these dimensions is well correlated with somatic and autonomic measures of emotions (Lang et al. 1998). Contrary to a priori categories they can better reflect emotional characteristics of the stimulus

in an individual context and they take into account inter-individual differences based on specific behavioral determinants, such as affective disposition and personality traits (Hamann 2004).

We aimed to detect single-neuron firing pattern changes in the STN that were related to emotional arousal and valence from the individual ratings of emotionally charged and neutral pictures presented to PD patients undergoing DBS electrode implantation. It has been shown that different features of tasks are linked to neuronal activity in different frequency bands. While beta band oscillations (13-30Hz) restricted to the dorsolateral (sensorimotor) part of the STN are linked mainly to motor functions and their alteration in PD Degas et al. (2008) and Jenkinson et al. (2011), the gamma band oscillations (30-100Hz) have perhaps more general meaning. Besides motor functions, they are modulated by picture perception and early emotional arousal (Huebl et al. 2014). As we were interested in affective content of visual processing, we focused on the alpha oscillations (8-12Hz) because they repeatedly showed emotion-related behavior in local field potentials (LFP) recordings (Kuhn et al. 2005; Brucke et al. 2007; Huebl et al. 2011). We used the power spectra bands, which are well known in description of continuous LFP and EEG signal that we adopted for analysis of the discrete single-neuron signal from the STN during the task with affective pictures presentation.

In our study, we compared the individual alpha firing activity of single-neurons with specific affective experience expressed in subjective ratings of the emotional valence and arousal of each presented picture and we mapped these neurons into the STN model (Morel 2007). A neuron was classified as affective, if its history-adjusted (and category-adjusted) activity in the alpha band correlated with these ratings.

Studies on spatiotemporal dynamics of emotions (affective picture or facial emotion processing) have observed early and late changes that have been attributed to different stages of emotional processing (Bradley et al. 2006). Therefore for the analysis we split arbitrarily the picture observation period lasting 2s in two time-windows. Within the early one (0-500 ms) which may contain early emotional image confounded more by perceptual and attentional processes (Guillory et al. 2014) we searched for activity related to the affective picture presentation with contrast to the black screen periods preceding each picture. For emotional activity we searched in the late window, starting 500 ms after the visual stimulus onset, because it can be better related to emotional processing after the conceptual knowledge of the presented emotion (represented here in individual ratings of the emotional valence and arousal) is built (Adolphs 2002).

4.2.2 Methods

Subjects

Thirteen PD patients (11 men, 2 women; mean (SD) age 55.5 (8.7), range 42-69 years; mean PD duration 14.2 (5.6), range 9-30; mean motor score of the Unified Parkinson's Disease Rating Scale (UPDRS-III) in off-medication condition was 38.7 (11.4) range 18-65) undergoing bilateral electrode implantation for the STN DBS due to motor fluctuations and/or disabling dyskinesias were enrolled. Additionally, we included another four patients undergoing bilateral electrode implantation for the globus pallidus interna DBS due to PD to study the neuronal activity outside of the STN.

Affective task

Emotionally charged pictures of three categories were selected from the International Affective Picture System (IAPS) (Lang et al. 1999). The pleasant category involved pictures with erotic themes (people, romantic couples) and adventure (exotic landscapes, animals, sports), the unpleasant category involved pictures of victims (mutilations) and threats (human or animal attacks, aimed guns) and the neutral category comprised of pictures of household objects, buildings, plants, neutral faces and scenes. Out of 144 unique pictures six different variants of the task containing 24 pictures were compiled involving 8 pictures from each category. Pleasant and unpleasant pictures were selected in a way so they represented emotional stimuli scaled from weak to strong according to normative emotional valence and arousal. Additionally, the pictures were pseudo-randomly organized so that no more than two pictures from one category followed. Each picture was presented for 2 s and preceded by a black screen with a white cross in the center for various durations (3500-5500 ms). Patients were instructed to fix their eyes on the cross on the black screen and to simply watch the pictures presented and stay motionless until the end of the task.

Surgery and intraoperative microrecording

DBS electrodes (model 3389, Medtronic, Minneapolis, MN) were implanted bilaterally under local anesthesia as described in Section 2.4.

The central trajectory of the exploratory microelectrode was aimed at the STN center near the anterior part of the red nucleus. The extracellular single-neuron activity was mapped by the MER as described in Section 2.4.3. For analyses of eye movement-related

neuronal activity a single-channel electrooculography was recorded (Sieger et al. 2013b). In up to six regions with easily classifiable neuronal pattern specific for STN, the neuronal activity was recorded during the affective task presentation with a unique variant of affective pictures in each position. The number of positions depended on the time course of the surgery and patient’s decision, clinical condition and compliance. Patients were observed during the affective task and if there appeared to be any distracting discomfort or sleepiness during surgery the experimental part was shortened or not performed. The affective task was presented on a 17“-computer screen placed approximately 55 cm in front of patient’s eyes who were lying motionless in the supine position as is customary for this surgical procedure. The MER signals were acquired in 2 s epoch intervals recorded both during the picture presentation (PIC epoch) and the black screen (FIX epoch), producing a sequence of 48 MER epochs (FIX1, PIC1, ..., FIX24, PIC24) for a total duration of 96s.

Data analysis

WaveClus (Quiroga et al. 2004), an unsupervised spike detection and sorting tool, which performed reasonably well on the single-channel MER (see Chapter 3), was used to extract the series of action potentials of single-neurons from MER signals. Neurons related to eye movements were excluded from further analysis (see Section 4.1). For other neurons, the alpha band activity expressing the magnitude of 8-12Hz periodic increases and decreases in the intensity of neuronal firing was computed as described below. The number of action potentials in 5 ms segments was calculated and concatenated to form a discrete signal representing the instantaneous intensity of firing. The signal was standardized to zero mean and the fast Fourier transform was carried out applying the Hann window of length 100 with 75% overlap. The alpha band (8-12 Hz) spectral component of the signal was then extracted and the alpha band activity was defined as the mean power of the alpha band spectral component, subjected to the square root transform to stabilize variance.

To detect neurons with emotion-related activity, linear models of the alpha band activity obtained during PIC epochs in the 500-2000 ms interval after the picture onset were built. To find valence-related neurons, a model of the alpha band activity during PIC epochs was built for each neuron in terms of the valence ratings. To find arousal-related neurons, another model of the alpha band activity during PIC epochs was created in terms of the arousal ratings including additional covariates to adjust for each apriori

IAPS picture category (neutral, positive, negative). As strong serial correlation was observed in the alpha band (see supplementary material), each model also included two covariates representing the alpha band activity in the last FIX and PIC epoch preceding the analyzed PIC epoch. A neuron was considered to be related to valence (arousal), if the valence (arousal) covariate in the respective model was significant.

To detect neurons sensitive to visual stimuli, differences in the alpha band activity between the FIX epoch and the 0-500 ms interval of the following PIC epoch were analyzed using the paired t-test.

Data processing and analyses were performed in MATLAB (R2007b, The MathWorks, Natick, MA) and R statistical software (84).

4.2.3 Results

We recorded single-neuron activity in the STN from 14 PD patients intraoperatively performing an affective task consisting of a presentation with pleasant, unpleasant and neutral pictures displayed for 2000ms preceded by a black screen with a white fixating cross presented for 3500-5500 ms. We acquired 97 microelectrode recordings obtained from 47 sites in the STN where 125 neurons were totally detected. The activity of 35 neurons was related to eye movements and were excluded from further analysis. The remaining 90 neurons (69 in the left hemisphere) were searched for early perceptual and emotional characteristics. Normative and postoperatively recorded individual valence and arousal ratings for each picture category are presented in Table 4.4.

The alpha band activity of 15 (17%) out of 90 neurons during late period of picture presentation (500-2000 ms post-stimulus-onset) epochs was related to the emotional content of the presented pictures expressed in individual valence or arousal ratings ($p < 0.05$, uncorrected): the activity of 6 (7%) neurons correlated with the valence ratings (4 neurons negatively, 2 neurons positively – Figure 4.5); the activity of other 9 (10%) neurons correlated with the arousal ratings (7 neurons positively, 2 neurons negatively – Figure 4.6). The number of these 15 emotion-related neurons was greater than expected by chance - (test in binomial distribution with false positive rate of 0.1, $P < 0.05$). Figure S1 shows an explanation on how the alpha band activity was derived in one selected neuron associated with the arousal rating.

In addition, 13 (14%) neurons significantly changed the alpha band activity between the black screen (duration 2000 ms) and the early picture presentation (window 0-500 ms post-stimulus-onset)($p < 0.05$). Only 1 neuron demonstrated an alpha band activity change

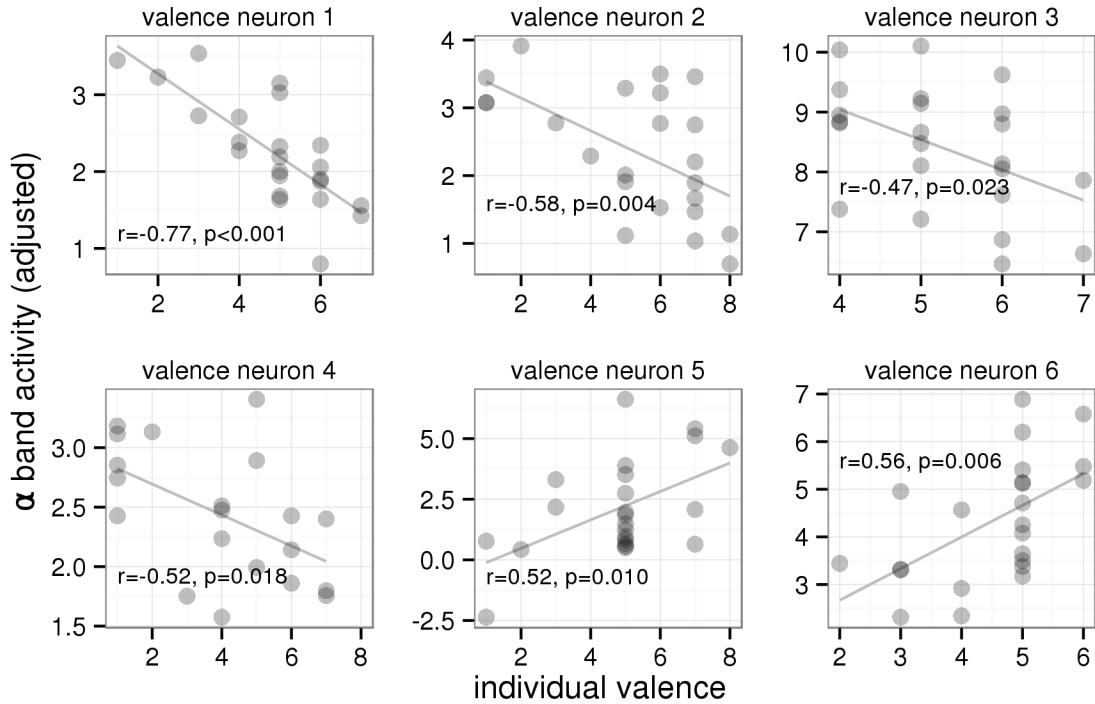


Figure 4.5: The relationship of the single-neuron alpha band activity during emotional picture presentation (in the interval of 500-2000 ms after picture onset) on the individual valence ratings of the presented pictures in 6 neurons of the subthalamic nucleus in patients with Parkinson's disease, for which the relationship was significant (as identified by linear models, see Section 4.2.2). The horizontal axis shows the individual ratings of the pictures' valence varying from 1 (negative) to 9 (positive). The vertical axis shows the alpha band neuronal activity adjusted for the past activity. For visualization purposes, correlation coefficients and their significances were included.

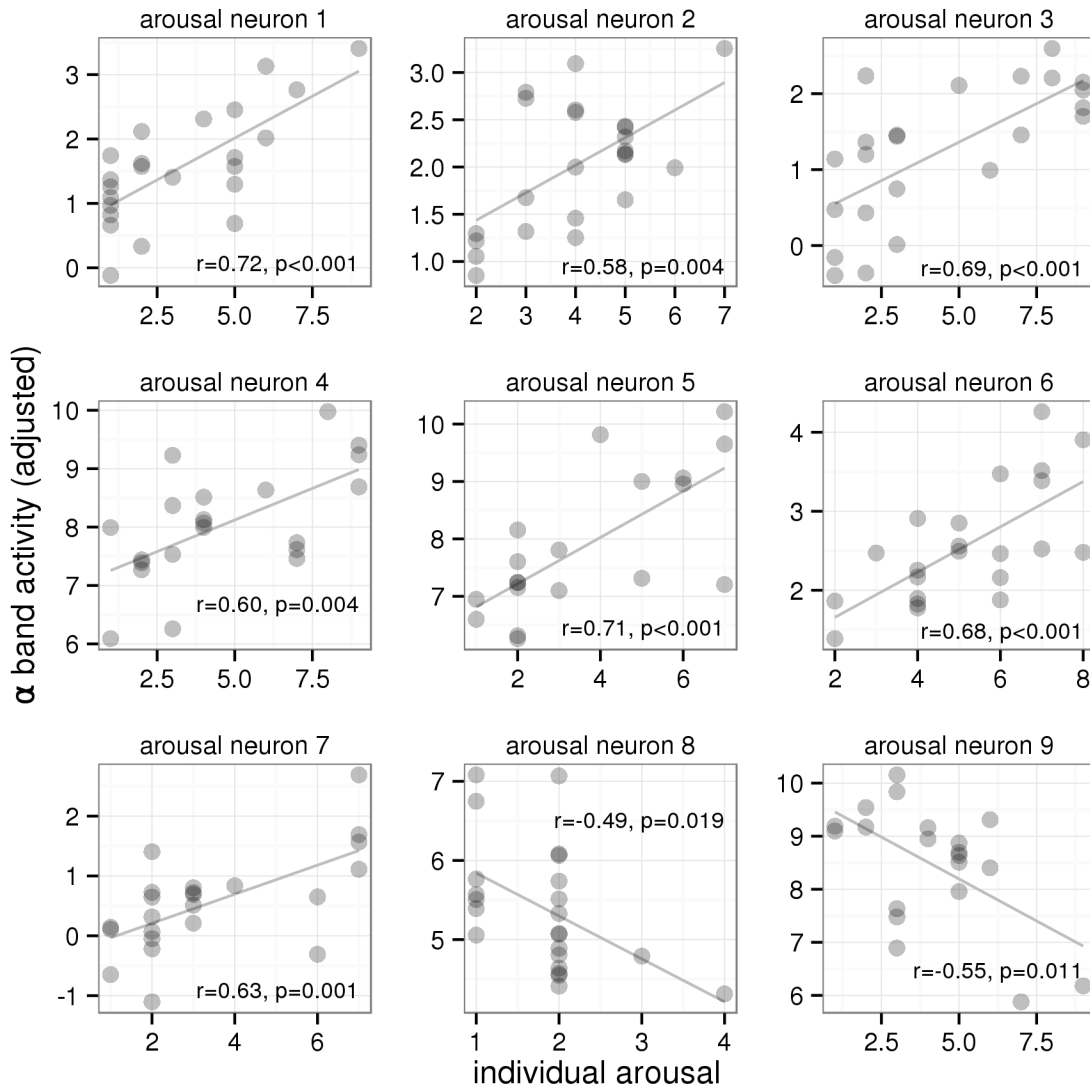


Figure 4.6: The relationship of the single-neuron alpha band activity during emotional picture presentation (in the interval of 500-2000 ms after picture onset) on the individual arousal ratings of the presented pictures in 9 neurons of the subthalamic nucleus in patients with Parkinson's disease, for which the dependency was significant (as identified by linear models, see Section 4.2.2). The horizontal axis shows the individual ratings of the pictures' arousal varying from 1 (low) to 9 (high). The vertical axis shows the alpha band neuronal activity adjusted for the past activity and picture categories. For visualization purposes, correlation coefficients and their significances were included.

Table 4.4: Patients' and normative ratings of emotional stimuli used.

Category	Patients' rating		Normative rating	
	Mean (SD) valence	Mean (SD) intensity	Mean (SD) valence	Mean (SD) intensity
Negative	3.1 (1.6)	5.1 (2.6)	3.4 (0.7)	5.2 (1.1)
Neutral	5.2 (1.0)	2.6 (1.7)	5.0 (0.2)	2.8 (0.3)
Positive	6.0 (1.3)	4.0 (2.1)	6.6 (0.8)	5.2 (1.1)

Patients' ratings represent subjective ratings assessed one month after bilateral insertion of the permanent electrode into subthalamic nucleus after overnight withdrawal of levodopa in DBS OFF condition. Normative ratings are those available from International Affective Picture System (IAPS) (Lang et al. 1999).

in both the early and late time windows.

In post-hoc analyses, we searched for emotion-related neuronal activity in other frequency bands. Four neurons were related to arousal in the beta band, but their number was insignificant (binomial test $P=0.98$). In the gamma band, seven neurons were found to be related to arousal. This number was not significant (binomial test $P = 0.81$). No overlaps of beta and gamma emotion-related neurons with alpha emotion-related neurons were observed.

To support specificity of emotion-related neurons located in the STN, we analyzed the activity of 32 other eye movement-unrelated neurons in other basal ganglia: 18 neurons from the substantia nigra pars reticulata and 14 neurons from the globus pallidus. None of these neurons were found to be related to individual valence or arousal ratings of the presented pictures.

4.2.4 Discussion

Using perioperative microrecordings from the subthalamic nucleus of patients with Parkinson's disease, we analyzed changes in the firing pattern of single-neurons in relationship to visually presented emotional material and found a relatively large proportion of neurons with activity related to emotional and early perceptual processing. In addition, we showed how easy it is to transform the single-neuron action potentials to a pseudo-continuous

signal to perform spectral analysis typical for conventional electroencephalography. Using this approach we documented the impact of a visual emotional task on single-neuron activity in the alpha band similar to those previously shown with local field potentials (Kuhn et al. 2005).

Affective neurons in the STN

Seventeen percent of the STN neurons whose activity in the alpha band was analyzed in our study responded to emotional stimuli. We found different neurons responding to changes in emotional valence or in arousal ratings. As for the character of changes in neuronal activity, both the increase or decrease were observed in either population of neurons suggesting a further level of specialization within each emotional dimension. There is a large body of evidence suggesting that behavioral responses to emotional valence and arousal are mediated by different brain circuits. The independence of valence and arousal have already been demonstrated for a variety of physiological reactions (Cacioppo et al. 1986; Vrana et al. 1988), or in affect-related cognitive processing (Kuhbandner et al. 2011). Functional imaging and animal studies have also showed their functional segregation as several brain regions have been associated with affective valence (the orbitofrontal cortex, the mesolimbic dopamine system) while the others were associated with affective arousal (the amygdala, the mesencephalic reticular activating system) (Faure et al. 2008). However there is also evidence that the two emotional dimensions are not fully independent (Bradley et al. 2006) and that some subcortical regions may code the overall emotional value of a stimulus (Winston 2005).

The neuronal activity in the STN that we observed during the late window (500-2000 ms) may reflect the formation of conceptual knowledge related to emotional valence and arousal as this is in line with the late neuronal response (625-1500 ms) related to different valence of stimuli described already in amygdala (Wang et al. 2014). We may speculate that the information represented in ratings of emotional valence and arousal in the late time window depends on processes that involve the orbitofrontal and ventromedial prefrontal cortex which provide significant input to the STN and plays a major role in stimulus subjective valuation, representation of hedonic pleasure and value-based decision making (Roy et al. 2012). Moreover, the previous passage of the emotional information from the ventral basal ganglia involving input from amygdala to the dorsal basal ganglia including the dorsal portion of the STN can also be a reason for late emotional activity (Humphries et al. 2010).

As expected, we did not find a statistically sufficient number of neurons responding to the emotional valence and arousal in the beta and gamma frequency bands. This corresponds to negative results of previous LFP studies (Huebl et al. 2011) and further corroborate functional specialization of different frequencies within the STN. In addition, no neurons responding to emotional content were found in the globus pallidus interna and substantia nigra pars reticulata, suggesting that finding affective neurons was specific to the STN, and can be explained by its central position in the in the cortico-basal ganglia circuit (Peron et al. 2013) and its connections to both the cortical and the subcortical components of the reward and limbic circuits (Ghashghaei et al. 2007; Winter et al. 2007).

Perceptual neurons in the STN

Fourteen percent of the subthalamic neurons responded in the alpha band firing activity during the early-time window (0-500 ms) suggesting their connection with perceptual processing. Neuronal short-latency activity changes related to visual perception have already been found in animal STN (Matsumura et al. 1991) and confirmed in humans by distortion of visual evoked potentials due to STN DBS (Jech et al. 2006). However, the difference in neural activity between fixation and picture viewing periods is not necessary evidence of visual processing since it may also reflect other processes such as an engagement of selective attention, a shift from gaze fixation to scanning eye movements or other cognitive functions intervening between vision and action – memory involvement, target selection, saccade choice or content valuation (Shires et al. 2010). On the other hand, the neuronal activity in the early time-window could also be affected by early emotional and motivational activity. The STN is anatomically connected to subcortical centres that contain visually responsive neurons (superior colliculus, pulvinar, amygdala, substantia innominate, nucleus accumbens) involved in the visual encoding of emotional stimuli (Tamietto et al. 2010). As the visual, attentional and emotional systems are intensively interconnected, one might expect that some proportion of the affective neurons would also respond in the early time window. Nevertheless, here only a one of the neurons was activated during both early and late-time window. Therefore, we can speculate that distinct populations of neurons are involved at different stages of processing of the visual emotional material within the dorsolateral part of the STN.

Limitations

There are several factors that could affect our results and reduce the inferences that can be drawn with regards to physiology of emotional processing and the role of the STN in the limbic circuits. One limitation is that the study was conducted with PD patients, who are known to have a widespread central nervous system pathology (Braak et al. 2002) and experience problems in emotional processing (Peron et al. 2013). Therefore the number of neurons responding to emotional stimuli in the STN might be different than in healthy subjects. Their number is rather low but comparable to former relevant single-neuron studies on emotion in humans (15, 18). Another fact that might have contributed to the relatively low number of neurons is that our study was limited to the routine trajectory of intraoperative microrecording exploration targeting the lateral sensorimotor part the STN that has shown less reactivity to emotional stimuli than the ventromedial part (Eitan et al. 2013). Moreover, emotional pictures were selected according to normative ratings that were acquired in a healthy, younger population with a culturally different background. Finally, some our PD patients rated the stimuli less variable along the dimensions of emotional valence and arousal making the mathematical model less sensitive (Lang et al. 1999).

4.2.5 Conclusion

Early-perceptual and late-emotional single-neuron activity in the human STN corroborates its participation in non-motor circuits. The STN was previously shown to participate in different components of emotional processing such as emotion recognition and subjective feelings (Castrìoto et al. 2014). We confirm the importance of the STN as a hub within the limbic circuitry involved in both emotional valence and arousal processing as in two functionally and spatially segregated systems. This together with finding several neurons involved separately in perceptual and emotional processing supports the complex role of the STN, previously only known using local field potentials recording. Usage of spike sorting methods was thus vital to uncover results extending our knowledge on the STN role in limbic circuits and contributing to understanding of affective disturbances seen in Parkinson's disease patients treated with subthalamic stimulation.

4.3 Relation between UPDRS scores and statistical characteristics of microelectrode recordings from STN

4.3.1 Introduction

The UPDRS (see Section 2.3) is a standardized measure of patients' abilities to perform basic motor skills, as well as the effect of the disease on activities of daily living and mental abilities. Although the UPDRS is standardized, it is still only a subjective measure depending on the experience and skills of the examiner.

An objective UPDRS analysis would be a valuable contribution as a decision support tool to help examiners. Additionally, it might reveal which parts of STN are responsible for which symptoms of PD and thus help creating a function map of STN and its surroundings. Another possible outcome is to aid examiners to quickly adapt the implanted DBS device parameters to its bearer, saving the patient's and examiner's time and suppressing majority of the PD symptoms shortly after the DBS surgery.

Several studies has already succeeded in finding relations between synchronization of basal ganglia neurons and motor disorders (Gatev et al. 2006; Hammond et al. 2007). Analysis of local field potentials (LFP) recorded from stimulation macroelectrode inserted into STN inferred that oscillatory synchronization in patients with PD tends to occur at frequencies of a *beta* band (13-35Hz) (Hammond et al. 2007). According to Kühn et al. (2008), *beta* synchronization of STN is significantly reduced during high-frequency DBS, resulting in major improvement in PD symptoms. Therefore the LFP *beta* activity in STN seems to be tightly related to the severity of motor PD symptoms (Little et al. 2012). As LFP originates locally in synchronized local neuronal activity in STN (Brown et al. 2005), we were interested in looking for a relation between oscillatory activity of STN neurons and PD symptoms (characterized by UPDRS scores).

However the processing of single-unit recordings conveys many challenges itself as it is not known whether all of the neurons in STN have influence on UPDRS score or only some of them – as discussed in Section 4.1 and 4.2 where activity of few neurons in STN actually related to eye scanning movements and emotions.

4.3.2 Methodology

We used microelectrode recordings from deep brain stimulation surgery of 53 Parkinson’s disease patients (21 men, 32 women; mean age: 56.8, SD 4.2, range 42–64 years; mean PD duration: 13.45, SD 2.7, range 7–23 years; Hoehn-Yahr stage 2-4; mean motor score of the Unified Parkinsons Disease Rating scale – UPDRS III in OFF condition: mean 25.37, SD 8.3, range 10–46). All of them were suffering from motor fluctuations and/or disabling dyskinesias and were indicated for treatment with deep brain stimulation due to motor fluctuations and dyskinesias.

Before the surgery, UPDRS evaluation form (see Section 2.3) was filled for each patient by an experience examiner. During the examination (as well as surgery) patients were in an OFF condition (i.e. abstaining from PD medications). Using the UPDRS evaluation, for each patient a set of UPDRS subscores were calculated according to Sharott et al. (2014):

- $rigidity_{ipsi}$ – Limb rigidity calculated as a sum of UPDRS III sub-item 22 (only arm and leg ipsilateral to the side of recording).
- $rigidity_{contra}$ – Limb rigidity calculated as a sum of UPDRS III sub-item 22 (only arm and leg contralateral to the side of recording).
- $bradykinesia_{ipsi}$ – Bradykinesia calculated as a sum of UPDRS III sub-items 23-26 (arm and leg ipsilateral to the side of recording).
- $bradykinesia_{contra}$ – Bradykinesia calculated as a sum of UPDRS III sub-items 23-26 (arm and leg contralateral to the side of recording).
- $tremor_{ipsi}$ – Tremor calculated as a sum of UPDRS III sub-items 20-21 (only arm and leg ipsilateral to to side of recording).
- $tremor_{contra}$ – Tremor calculated as a sum of UPDRS III sub-items 20-21 (only arm and leg contralateral to to side of recording).

Microelectrode recordings were acquired and preprocessed using five parylenecoated tungsten microelectrodes in a “Ben-gun” configuration as described in Section 2.4.3. Only signals from regions annotated by a surgeon as STN were used, as these recordings should contain signals from neurons that were then stimulated by DBS and thus should be partly responsible for the patient’s state. All signals were visually inspected for artificial artifacts. Artifacts were remove by either shortening the recorded signal (to minimum of

5 seconds) or removing it altogether – up to 21 artifact-free signals per patient (912 in total) were recorded; each signal 5-10 seconds long (mean duration: 9.1s, SD 1.6s).

As our signals were much shorter than those used by Sharott et al. (2014), we extracted and analyzed features from the raw MER signals (i.e. the aggregated neuronal activity, omitting the spike sorting step) first. Subsequently, spike detection and sorting was employed to discern individual neurons extracting features from their activity, thus possibly revealing the relation even if the affecting neurons were sparse in the STN.

Only features that were manually selected during data exploration stage, were used as noted in Section 4.3.2 and 4.3.2.

Raw MER signal features

Features extracted from the 24kHz sampled signal are referred to as *raw MER signal features*. Spectral parameters of recordings were evaluated using fast Fourier transform as described previously (Halliday et al., 1995) using 0.5 Hz frequency bins. Following power spectra features were selected for analysis:

- $psd_{subbeta}$ – sum of power spectral density (PSD) of the signal in range 4–13Hz
- psd_{beta} – sum of PSD of the signal in range 13–35Hz
- psd_{gamma} – sum of PSD of the signal in range 35–70Hz

As the PSD spectra vary a lot between individual recording positions not to mention patients (see Figure 4.7), Kühn et al. (2005) encouraged use of a normalized version of the features:

- $psd_{rel.subbeta}$ – sum of PSD of the signal in range 4–13Hz divided by sum of PSD in range 4–45Hz
- $psd_{rel.beta}$ – sum of PSD of the signal in range 13-35Hz divided by sum of PSD in range 4–45Hz
- $psd_{rel.gamma}$ – sum of PSD of the signal in range 35-70Hz divided by sum of PSD in range 4–100Hz

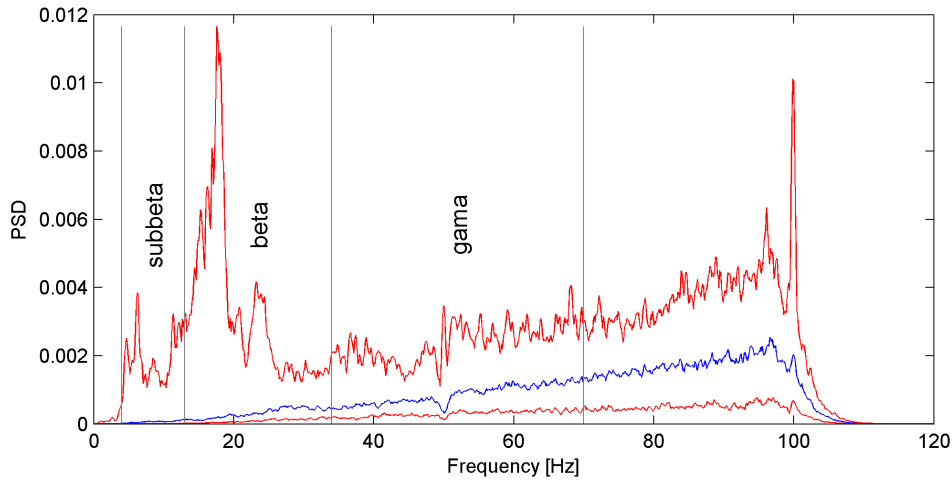


Figure 4.7: Mean PSD spectrum of 100 MER signals from different patients (blue line) with bootstrapped confidence interval (red line, 5%-95%).

Neuronal spike train features

As the recorded signals are a sum of coordinated discharge of neurons in the area, an assumption is made that by analyzing neuronal firing pattern one can identify a neuron involved in a specific motor function (as shown in Figure 4.1). To analyze behavior of single neurons, WaveClus (Quiroga et al. 2004) a reasonably well performing spike detection and sorting tool (see Chapter 3) was used to extract firing patterns from the recordings.

Section 4.1 and 4.2 confirmed that there are neurons in STN related to eye movement and emotion processing. We wanted to remove such neurons from this study. However, that would lead to omitting a large amount of data recorded from patients that did not participate in the beforementioned trials. We decided to use all the data recorded and in order to cope with the possible bias caused by neurons not related to PD symptoms, a grouping characteristic was used.

Neurons were assigned into four groups (*none*, *subbeta*, *beta* and *gamma*) based on the PSD spectrum of their firing pattern as described in Sharott et al. (2014). Each neuronal spike train was converted to zero-one signal and PSD spectrum with bin size of 0.5Hz was calculated. Then the spike train was randomly reshuffled 1000 times creating a bootstrap set to estimate 5%-95% confidence interval for the PSD spectrum. If three consecutive bins exceeded the 95% quantile, neuron was assigned to the group according

to the frequency of beforementioned bins (i.e. 4-13Hz for *subbeta*, 13-35Hz for *beta*, 35-70Hz for *gamma* and *none* for no bins) indicating in which frequency range they oscillate.

For each patient a percentage of neurons belonging to each individual oscillatory group divided by total number of neurons for that patient was calculated and used as features:

- $neuron_{subbeta\%}$ – sum of neurons in *subbeta* oscillation group divided by total number of neurons of the patient
- $neuron_{beta\%}$ – sum of neurons in *beta* oscillation group divided by total number of neurons of the patient
- $neuron_{gamma\%}$ – sum of neurons in *gamma* oscillation group divided by total number of neurons of the patient

Assuming that the percentage of neurons that were not related to PD symptoms would be approximately the same for all patients the variation of $neuron_{subbeta\%}$, $neuron_{beta\%}$ and $neuron_{gamma\%}$ should be only attributed to variation in PD symptoms.

Statistical methods

For each MER, both raw MER signal and neuronal spike train features were calculated. As several (up to 21) signals were recorded for each patient (and thus UPDRS subscores), conventional correlation and linear regression models cannot be used to analyze relationship between the calculated features and UPDRS subscores. Instead linear mixed-effects models (McLean et al. 1991) were employed, to compensate for multiple recordings per patient. Visual inspection of residual plots was done for each linear mixed-effects model to detect any obvious deviations from homoscedasticity or normality. P-values were obtained by likelihood ratio tests of the full model with the effect in question against the model without the effect in question.

As oscillatory percentage group features ($neuron_{subbeta\%}$, $neuron_{beta\%}$, $neuron_{gamma\%}$) had already the same magnitude as number of patients, mixed-effect models were not needed to determine their relation to UPDRS subscores. In that case the relations were examined using Pearson's correlation (if both variables were normally distributed) – in the same way as in Sharott et al. (2014).

All calculations were performed using Matlab R2013b (Mathworks, Natick, MA) software. All statistical hypotheses and linear mixed-effects analysis were tested at significance level 0.05 using R software (2.14.1, R Foundation for Statistical Computing, Vienna, Austria) with corrections for multiple comparisons.

4.3.3 Results and Discussion

Firstly we tested a hypothesis that overall *beta* activity in STN is dependent on a position in STN, as Weinberger et al. (2006) shown that e.g. the dorsal part of the STN has more *beta* activity than the rest of STN. Therefore, we performed a linear mixed effects analysis of the relationship between $psd_{rel.beta}$ feature and $depth_{relative}$ (indicated distance in millimeters of recorded position from the bottom of STN). As fixed effects, we entered the $depth_{relative}$ into the model. As a random effect, we had intercepts for subjects, as well as by-subject random slopes for the effect of $depth_{relative}$. Visual inspection of residual plots did not reveal any obvious deviations from homoscedasticity or normality. The found model showed that $depth_{relative}$ affected $psd_{rel.beta}$ ($\chi^2 = 15.29$, $Df = 1$, $p < 0.0001$), increasing it by 0.008 ± 0.002 (standard error), confirming that $psd_{rel.beta}$ is highest in the dorsal of STN. Data points along with linear regression model (i.e. omitting the random effect) are shown on Figure 4.8.

Based on the findings, we decided to add $depth_{relative}$ as a fixed effect to the rest of the mixed-effects models.

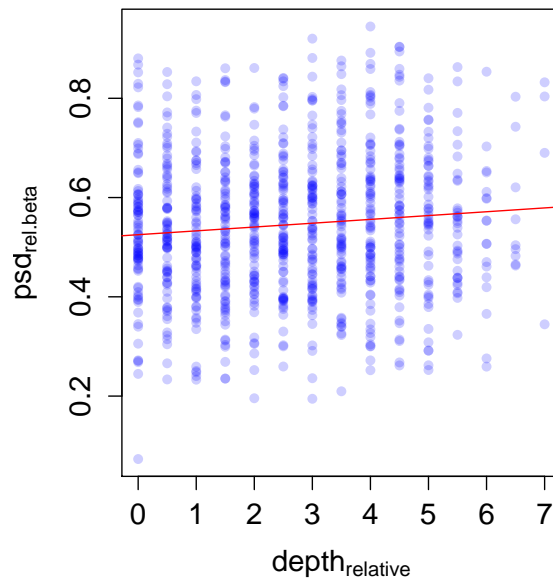


Figure 4.8: Relation between $psd_{rel.beta}$ feature and $depth_{relative}$ with linear regression line fitted.

UPDRS subscores in relation to raw MER signal features

We performed a linear mixed effects analysis of the relationship between one of the three raw MER signal features ($psd_{rel.subbeta}$, $psd_{rel.beta}$ and $psd_{rel.gamma}$) and one of the six UPDRS subscores ($rigidity_{ipsi}$, $rigidity_{contra}$, $bradykinesia_{ipsi}$, $bradykinesia_{contra}$, $tremor_{ipsi}$, $tremor_{contra}$). As fixed effects, we entered the appropriate UPDRS subscore and $depth_{relative}$ (without interaction term) into the model. As random effects, we had intercepts for subjects, as well as by-subject random slopes for the effect of $depth_{relative}$. Visual inspection of residual plots did not reveal any obvious deviations from homoscedasticity or normality.

Table 4.5 summarizes the results. We found that $psd_{rel.beta}$ was affected by both $tremor_{contra}$ ($\chi^2 = 34.09$, $Df = 1$, $p < 0.0001$; decrease of 0.028 ± 0.005), and $tremor_{ipsi}$ ($\chi^2 = 28.81$, $Df = 1$, $p < 0.0001$; increase of 0.026 ± 0.005). The analysis further showed that $psd_{rel.beta}$ was also affected by both $bradykinesia_{contra}$ ($\chi^2 = 34.21$, $Df = 1$, $p < 0.0001$; increase of 0.021 ± 0.003) and $bradykinesia_{ipsi}$ ($\chi^2 = 32.89$, $Df = 1$, $p < 0.0001$; decrease of 0.020 ± 0.003). P-values were corrected using Bonferroni corrections for 18 comparisons. Figure 4.9 shows data points along with linear regression model of the three beforementioned mixed-effects models.

Table 4.5: P-values of tested mixed-effects models.

UPDRS subscore	$psd_{rel.subbeta}$	$psd_{rel.beta}$	$psd_{rel.gamma}$
$rigidity_{ipsi}$	0.135	0.042	0.455
$rigidity_{contra}$	0.135	0.319	0.858
$tremor_{ipsi}$	0.045	<0.001	0.957
$tremor_{contra}$	0.025	<0.001	0.621
$bradykinesia_{ipsi}$	0.363	<0.001	0.320
$bradykinesia_{contra}$	0.729	<0.001	0.680

Highlighted relations were significant at level 0.05 after performing Bonferroni corrections for 18 trials ($p < 0.0027$).

Positive $bradykinesia_{contra}$ subscore effect on $psd_{rel.beta}$ is in agreement with findings in Kühn et al. (2008), as according to our results $beta$ activity increases for patients with worse bradykinesia symptoms. Slightly weaker but the same effect of $bradykinesia_{ipsi}$ subscore on $psd_{rel.beta}$ is not surprising as Tabbal et al. (2008) confirmed both ipsilateral and contralateral effects of DBS on bradykinesia and rigidity symptoms in patients with

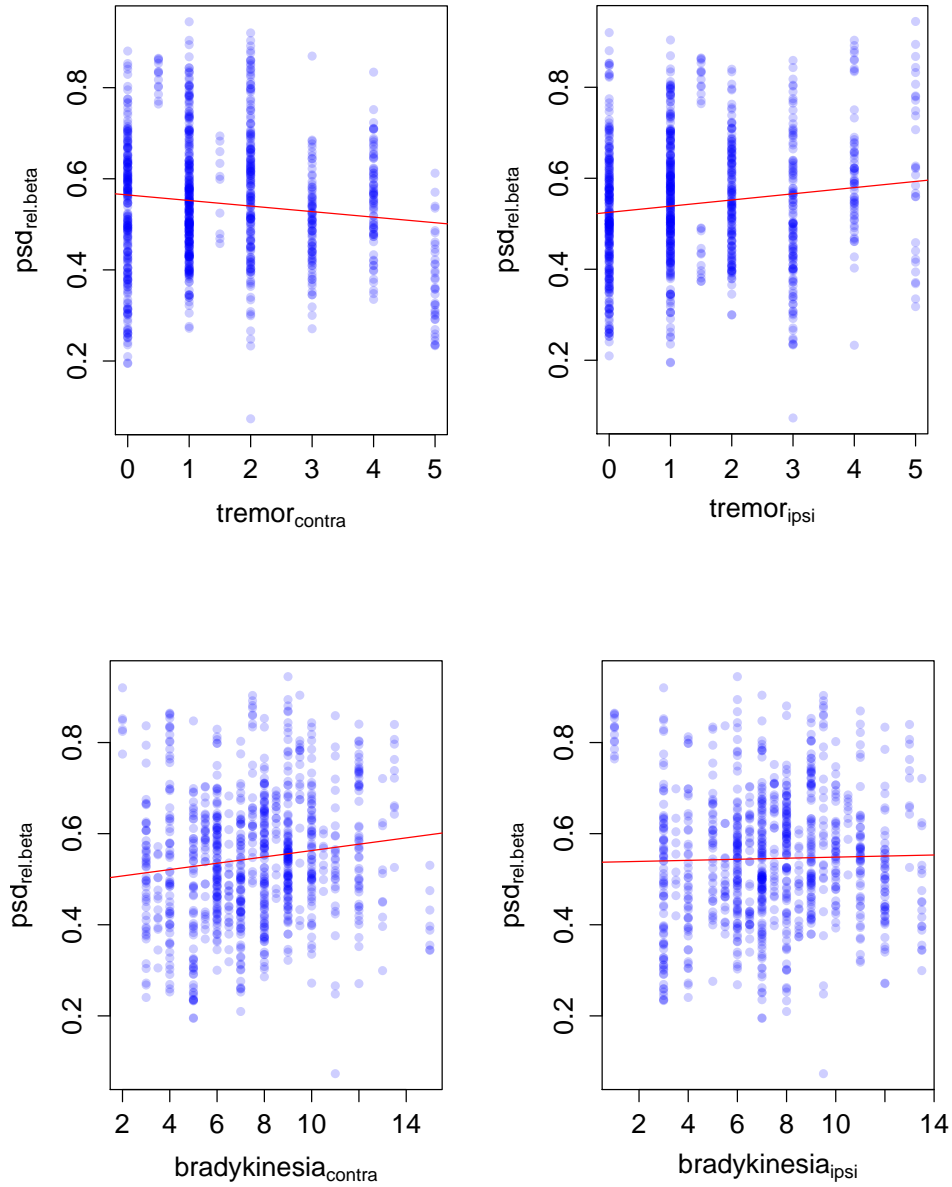


Figure 4.9: Relation between $psd_{rel.beta}$ feature and $tremor_{contra}$, $tremor_{ipsi}$, $bradykinesia_{contra}$, $bradykinesia_{ipsi}$ with linear regression line fitted

PD.

Unfortunately, no significant relations with UPDRS subscores were found in *subbeta* band, although according to Contarino et al. (2012) *subbeta* band should be correlated with tremor. However, $tremor_{contra}$ negative effect on $psd_{rel.beta}$ might be an indication of such relation, as PSD of patients with more severe tremor symptoms should have more power in *subbeta* band, which effectively lowers power in *beta* band.

Gamma band also did not show any significant relations with any of UPDRS subscores, although Weinberger et al. (2009) stated that *gamma* oscillatory activity in STN is pronounced in tremor patients with PD to the detriment of *beta* activity.

UPDRS subscores in relation to neuronal spike train features

Previous section confirmed that our data were coherent with at least two PD symptoms. In order to find such relations also by employing features extracted from neurons, we calculated correlations between the feature/subscore pairs. As we wanted to verify the formed finding of Sharott et al. (2014), while using shorter signals we did not correct for the multiple comparisons performed.

As shown in Table 4.6, only correlations between $neuron_{beta\%}$ and $rigidity_{ipsi}$ ($r = 0.22$, $p < 0.05$), $neuron_{gamma\%}$ and $bradykin_{ipsi}$ ($r = -0.26$, $p < 0.05$) and $neuron_{gamma\%}$ and $bradykin_{contra}$ ($r = -0.23$, $p < 0.05$) were found significant (see also Figure 4.10).

Table 4.6: Correlation coefficients of analyzed relations between neuron spike train features and UPDRS subscores.

UPDRS subscore	$neuron_{subbeta\%}$	$neuron_{beta\%}$	$neuron_{gamma\%}$
$rigidity_{ipsi}$	0.04	0.22*	-0.11
$rigidity_{contra}$	0.03	0.07	-0.21
$bradykinesia_{ipsi}$	-0.05	0.05	-0.26*
$bradykinesia_{contra}$	-0.05	0.11	-0.23*
$tremor_{ipsi}$	0.05	-0.11	-0.05
$tremor_{contra}$	0.00	-0.04	-0.14

* denotes correlation significant at level 0.05.

Positive correlation between $neuron_{beta\%}$ and $rigidity_{ipsi}$ (along with the relation between *beta* band and *bradykinesia* in previous section) matches our understanding of how neuron *beta* oscillation (and synchronization of similarly oscillating neuron) affects motor

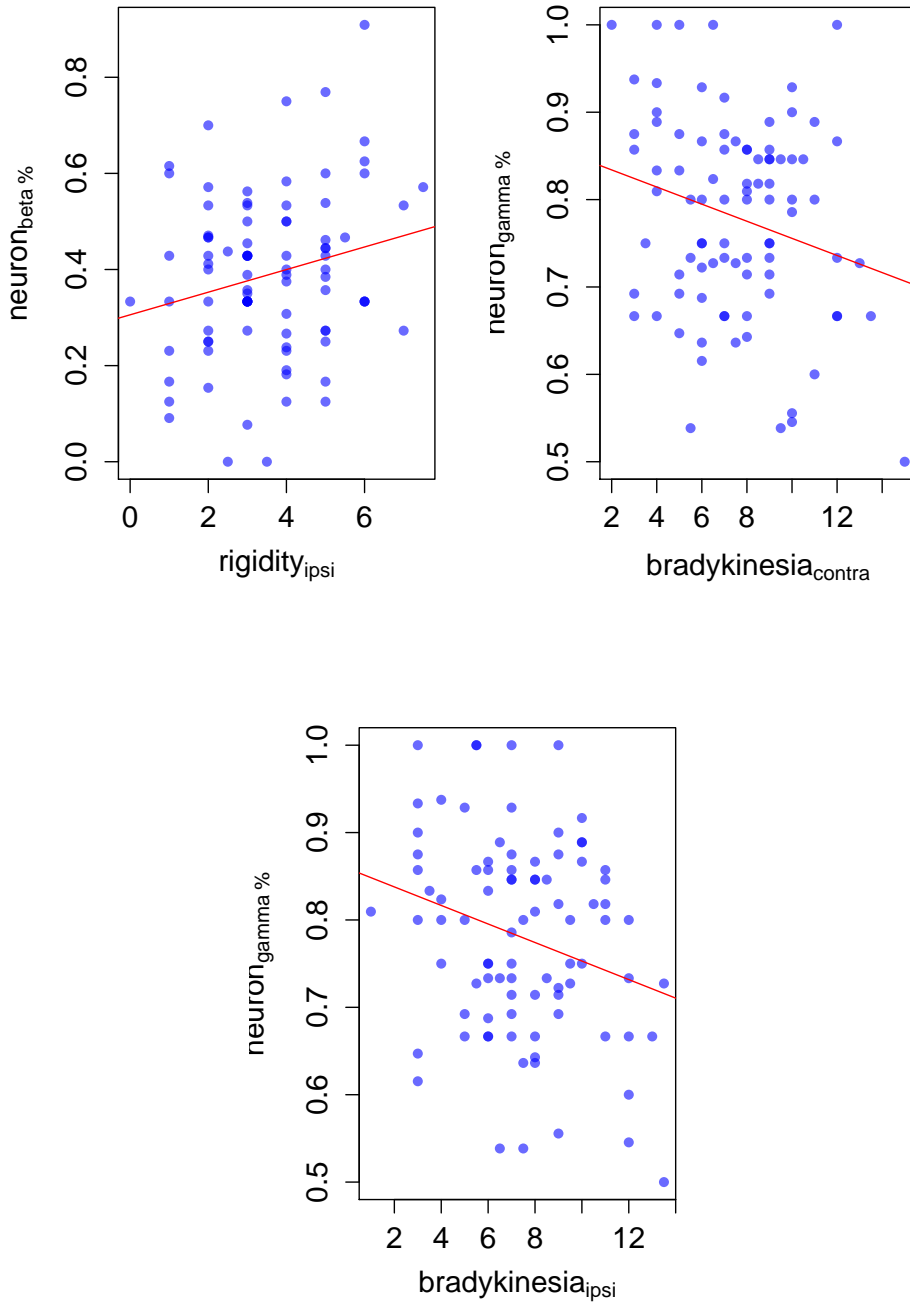


Figure 4.10: Relations between $neuron_{beta\%}$ feature and $rigidity_{ipsi}$ ($r = 0.22, p = 0.05$); $neuron_{gamma\%}$ and $bradykinesia_{contra}$ ($r = 0.23, p = 0.027$) and $bradykinesia_{ipsi}$ ($r = 0.26, p = 0.015$) with linear regression line fitted.

functions of patients with PD. Interestingly, relation between *beta* band and *rigidity_{ipsi}* was not significant when using raw MER signal features, while neuronal features did discern it. This demonstrates the need for transforming the neuronal recording using spike sorting methods in order to unveil the relevant information hidden in the aggregated neuronal activity.

On the other hand, relation between *tremor* and raw MER signal features was not detected when using neuronal features, which supports our theory that this link was only indirect due to increase in *beta* band at the same time. Furthermore, correlation between *bradykinesia* and *neuron_{beta%}* was not found as well.

Finding a negative correlation between *bradykinesia* and *neuron_{gamma%}* was consistent with hypothesis of Schoffelen et al. (2005) that *gamma* oscillations facilitate a readiness to move and thus higher number of *gamma* oscillating neurons should lead to lower *bradykinesia* score.

Considering the other correlations described in Sharott et al. (2014) were insignificant, we assumed that the length and possibly signal-to-noise ratio of our MER data was the culprit. Sharott et al. (2014) was using at least 45 second long signals and discarded initial 5–15 s part, which was not possible in our case as our signals were only 5–10 s long. This could have an adverse effect on spike sorting as well as assigning neurons to oscillatory groups.

4.3.4 Conclusion

In pursuit of objectivization the UPDRS in patients with PD, we analyzed 912 signals recorded using microelectrodes during DBS surgery from STN and compared them with UPDRS scores of the patients undergoing the implantation.

Two sets of features were extracted from the recorded signals – one set was calculated from summary neuronal activity recorded on the microelectrode (raw MER signal features) and the other set was computed from activity of individual neurons (neuronal spike train features) employing WaveClus (Quiroga et al. 2004) spike detection and sorting.

Raw MER signal feature *psd_{rel.beta}* was positively correlated to bradykinesia subscore, confirming findings of Kühn et al. (2008) that power of *beta* activity increases with worsening of rigidity and bradykinesia symptoms. This hypothesis was further affirmed by finding a significant positive correlation between neuronal feature *neuron_{beta%}* and rigidity subscore.

Bradykinesia was also significantly negatively correlated with *neuron_{gamma%}* neuronal

feature, supporting conclusion of Schoffelen et al. (2005) that higher *gamma* activity in STN indicates weaker rigidity and bradykinesia symptoms.

Contrary to our expectations and findings of Contarino et al. (2012), $psd_{rel.subbeta}$ activity was not directly linked to severity of tremor symptoms, but $tremor_{contra}$ negative relation to $psd_{rel.beta}$ lead us to a hypothesis that $psd_{rel.subbeta}$ is linked to tremor indirectly (i.e. by lowering $psd_{rel.beta}$).

We thus confirmed that severity of PD symptoms (i.e. UPDRS scores) has its reflection in firing pattern of neurons (individual or summed together). However further research needs to be done in order to ascertain whether the neuronal activity in STN is the cause of PD symptoms or if it is the other way around.

Chapter 5

Summary and perspective

We focused on applying spike sorting methods to data recorded from patients with Parkinson's disease that are treated with deep brain stimulation, to improve our understanding of the human brain in general and the mechanism of the deep brain stimulation in particular.

In Chapter 3, we dealt with problem of the transformation of raw data from extracellular microelectrode into spiking activity of individual neurons (i.e. spike sorting). Classifying neuronal action potentials is a technical challenge that is a prerequisite for studying many types of brain function. Accurate detection of the activity of individual neurons can be difficult to achieve due to the large amount of background noise and the complexity in distinguishing the action potentials of one neuron from others. This capability is especially important for experimental investigations of neural codes that use spike timing.

We have performed a performance evaluation of three widely-used publicly-available spike sorting algorithms (WaveClus, KlustaKwik, OSort) with regard to their parameter settings, using custom generated single-channel artificial data (available online) with different noise levels and different number of neurons. The best spike sorting method (WaveClus) was used throughout the thesis for discerning individual neurons from our MER data.

Sections in Chapter 4 built on top of that we performed various tasks in neuroscientific field that involved statistical analyzes of microelectrode data and individual neuronal activity and resulted in our better understanding of basal ganglia function.

In Section 4.1, we experimentally verified that there are neurons in basal ganglia participating in scanning EM. We took advantage of intraoperative microelectrode recordings of single neuronal activity routinely used to identify the basal ganglia based on specific

electrophysiological pattern. Approx. 20% of neurons with activity related to eye movements were identified.

Section 4.2 presented the process of searching for emotion-related neurons in the subthalamic nucleus. 17% of neurons with activity related to processing emotional stimuli or responding to different types of emotional stimuli were found in basal ganglia, confirming the importance of the STN as a hub within the limbic circuitry involved in both emotional valence and arousal processing. This together with finding several neurons involved separately in perceptual and emotional processing supports the complex role of the STN. Our results thus extended our knowledge on the STN role in limbic circuits and contribute to understanding of affective disturbances seen in Parkinson's disease patients treated with DBS.

In Section 4.3, we found relations among severity of PD symptoms (described as UPDRS scores) and statistical characteristics of MER data and individual neuronal activity in STN. This objective analysis of UPDRS is welcomed by examiners to support their decision process as well as it contributes to specification of particular STN regions and specific PD symptoms and thus help creating a function map of STN and its surroundings. We have found several significant relations between severity of Parkinson's disease symptoms and both raw signal and neuronal features. Namely the relation between *beta* band and bradykinesia and between neuronal beta oscillations and rigidity.

5.1 Thesis Achievements

Scientific contribution of this Thesis is represented by the following achievements:

- Performance of the state-of-the-art spike sorting methods was evaluated, finding the best performing method and its parameters set that is used for transforming all microelectrode signals used in this thesis to spike trains of individual neurons. This evaluation was published (Wild et al. 2012b) in the Journal of Neuroscience Methods (2012 IF 2.484), WoS 14 citations (as of 17.8.2015).
- A new method for generation of artificial signals was devised to produce data with ground truth with similar properties as the signals recorded from basal ganglia. The method was implemented in order to generate signals necessary for objective evaluation of spike sorting methods.

- An experimental verification showed that approx. 20% of neurons with activity related to eye movements were identified in basal ganglia. This is the first study to investigate activity of individual basal ganglia neurons related to eye movements in human subjects. These results were published (Sieger et al. 2013b) in PLoS ONE (2012 IF 3.73).
- An experimental verification showed that 17% of neurons with activity related to processing emotional stimuli or responding to different types of emotional stimuli were found in basal ganglia. This is the first study proving existence of individual neurons in the human STN that are involved in higher-level representation of emotions. These results were published (Sieger et al. 2015b) in Proceedings of the National Academy of Sciences (2014 IF 9.67).
- Several new relationships were found among variables describing severity of Parkinson's disease symptoms and statistical characteristics of microelectrode records and individual neuron firing patterns. A publication presenting these results is currently under preparation.

5.2 List of Candidate's Publications Related to the Thesis

5.2.1 Publications in Impacted Journals

- Wild, J., Z. Prekopcsak, T. Sieger, D. Novák, and R. Jech (2012a). “Performance Comparison of Extracellular Spike Sorting Algorithms for Single-Channel Recordings”. English. In: *Journal of Neuroscience Methods* 203.2, pp. 369–376. ISSN: 0165-0270. URL: <http://www.sciencedirect.com/science/article/pii/S0165027011006133>.

Author's participation: 60%, WoS 14 citations.

- Sieger, T., C. Bonnet, T. Serranová, J. Wild, D. Novák, F. Růžička, D. Urgošík, E. Růžička, B. Gaymard, and R. Jech (2013a). “Basal Ganglia Neuronal Activity during Scanning Eye Movements in Parkinson's Disease”. English. In: *PLoS ONE* 8.11, pp. 1–11. ISSN: 1932-6203. URL: <http://www.plosone.org/article/info%3Adoi%2F10.1371%2Fjournal.pone.0078581>.

Author's participation: 5%, WoS 1 citation.

- Macaš, M., L. Lhotská, E. Bakštein, D. Novák, J. Wild, P. Vostatek, T. Sieger, and R. Jech (2012). “Wrapper Feature Selection for Small Sample Size Data Driven by Complete Error Estimates”. English. In: *Computer Methods and Programs in Biomedicine* 108.1, pp. 138–150. ISSN: 0169-2607. URL: <http://www.sciencedirect.com/science/article/pii/S0169260712000582>.

Author's participation: 3%, WoS 4 citations.

- Sieger, T., T. Serranová, F. Růžička, P. Vostatek, J. Wild, D. Šťastná, C. Bonnet, D. Novák, E. Růžička, D. Urgošík, et al. (2015a). “Distinct populations of neurons respond to emotional valence and arousal in the human subthalamic nucleus”. English. In: *Proceedings of the National academy of sciences of the United States of America* 112.10, pp. 3116–3121. ISSN: 0027-8424. URL: <http://www.pnas.org/cgi/doi/10.1073/pnas.1410709112>.

Author's participation: 1%, WoS 1 citation.

5.2.2 Other Publications

- Wild, J., D. Novák, E. Bakštein, and R. Jech (2010a). “Automatic Nuclei Detection During Parkinson’s Stereotactic Neurosurgery”. English. In: *Analysis of Biomedical Signals and Images, BIOSIGNAL 2010, Proceedings*. Brno: Brno University of Technology, pp. 48–49. ISBN: 978-80-214-4106-4. URL: <http://www.biosignal.cz/bs2010/papers/1108.pdf>.
Author’s participation: 85%.
- Wild, J., D. Novák, T. Sieger, Z. Prekopsčsák, P. Vostatek, and R. Jech (2010b). “Detekční algoritmy pro klasifikaci neuronální aktivity”. In: *57. Společný sjezd České a Slovenské společnosti pro klinickou neurofyzilogii*. Praha: MH Consulting, p. 52.
Author’s participation: 55%.
- Wild, J., T. Sieger, D. Novák, and R. Jech (2009). “Spike Sorting Algorithms Comparison”. English. In: *Neuroinformatics 2009 - Program and Abstracts*. Lausanne: Frontiers, pp. 53–54.
Author’s participation: 50%.
- Novák, D., J. Wild, T. Sieger, and R. Jech (2009). “Identifying Number of Neurons in Extracellular Recording”. English. In: *Proceedings of the 4th International IEEE EMBS Conference on Neural Engineering*. Piscataway: IEEE, pp. 742–745. ISBN: 978-1-4244-2073-5.
Author’s participation: 20%.
- Vostatek, P., D. Novák, T. Rychnovský, and J. Wild (2010). “Diaphragm Postural Function Analysis Using Magnetic Resonance”. English. In: *10th International Conference on Information Technology and Applications in Biomedicine*. Crete: IEEE Control Syst Soc, p. 99. ISBN: 978-1-4244-6560-6.
Author’s participation: 10%.
- Jech, R., T. Sieger, F. Růžička, D. Urgošík, C. Bonnet, P. Vostatek, J. Wild, D. Šťastná, D. Novák, E. Růžička, et al. (2014). “18. Beyond Skeletomotor Function of Human Basal Ganglia: Oculomotor, Visual and Affective Neurons”. English. In: *Clinical Neurophysiology* 125.5, e30. ISSN: 1388-2457. URL: <http://www.sciencedirect.com/science/article/pii/S1388245713012923>.
Author’s participation: 9%.

- Novák, D., F. Albert, E. Cirugueda-Roldán, T. Sieger, E. Bakštein, J. Wild, D. Cuesta, and R. Jech (2012). “Discrimination of Deep Brain Nuclei using Regularity Measures”. In: *Proceedings of the 34th Annual International Conference of the IEEE Engineering in Medicine and Biology Society - Abstract Book*, p. 493. ISBN: 978-1-4244-4120-4.
Author’s participation: 5%.
- Sieger, T., C. Bonnet, T. Serranová, J. Wild, D. Novák, F. Růžička, D. Uργοšík, and R. Jech (2011). “Neuronal Activity of the Basal Ganglia and Subthalamus in Relation to Eye Movement in Parkinson’s Disease”. English. In: *Abstracts of the 14th European Congress of Clinical Neurophysiology and the 4th International Conference on Transcranial Magnetic and Direct Current Stimulation, Clinical Neurophysiology*. Dublin: Elsevier Ireland Ltd., s89–s90. URL: <http://www.sciencedirect.com/science/journal/13882457/122/supp/S1>.
Author’s participation: 5%.
- Sieger, T., J. Wild, D. Novák, R. Jech, C. Bonnet, T. Seranová, F. Růžička, and D. Uργοšík (2010). “Neuronální aktivita bazálních ganglií vázaná na oční pohyby u pacientů s parkinsonovou nemocí”. In: *57. Společný sjezd České a Slovenské společnosti pro klinickou neurofyzilogii*. Praha: MH Consulting, p. 11.
Author’s participation: 5%.

Prague, 29.8.2015

References

- Adamos, D., E. Kosmidis, and K. Theophilidis (2008). “Performance evaluation of PCA-based spike sorting algorithms”. In: *Comput Meth Prog Bio* 91, pp. 232–44.
- Adamos, D., N. Laskaris, E. Kosmidise, and G. Theophilidis (2010). “NASS: An empirical approach to spike sorting with overlap resolution based on a hybrid noise-assisted methodology”. In: *J Neurosci Meth* 190.1, pp. 129–42.
- Adolphs, R. (2002). “Neural systems for recognizing emotion”. In: *Current Opinion in Neurobiology* 12.2, pp. 169–177. DOI: 10.1016/s0959-4388(02)00301-x.
- Alexander, G. E., M. D. Crutcher, and M. R. DeLong (1991). “Chapter 6 Basal ganglia-thalamocortical circuits: Parallel substrates for motor, oculomotor, prefrontal and limbic functions”. In: *Progress in Brain Research*. Elsevier BV, pp. 119–146. DOI: 10.1016/s0079-6123(08)62678-3.
- Antoniades, C. A., P. Buttery, J. J. FitzGerald, R. A. Barker, R. H. S. Carpenter, and C. Watts (2012). “Deep Brain Stimulation: Eye Movements Reveal Anomalous Effects of Electrode Placement and Stimulation”. In: *PLoS ONE* 7.3. Ed. by I. Sugihara, e32830. DOI: 10.1371/journal.pone.0032830.
- Araujo, C., E. Kowler, and M. Pavel (2001). “Eye movements during visual search: the costs of choosing the optimal path”. In: *Vision Research* 41.25-26, pp. 3613–3625. DOI: 10.1016/s0042-6989(01)00196-1.
- Baltuch, G. H. and M. B. Stern (2007). *Deep brain stimulation for parkinson’s disease*. Parkinson’s Disease Foundation.
- Basso, M. A., J. J. Pokorny, and P. Liu (2005). “Activity of substantia nigra pars reticulata neurons during smooth pursuit eye movements in monkeys”. In: *European Journal of Neuroscience* 22.2, pp. 448–464. DOI: 10.1111/j.1460-9568.2005.04215.x.
- Bergman, H., T. Wichmann, and M. R. DeLong (1990). “Reversal of experimental parkinsonism by lesions of the subthalamic nucleus”. In: *Science* 249.4975, pp. 1436–1438.
- Braak, H., K. D. Tredici, H. Bratzke, J. Hamm-Clement, and D. Sandmann-Keil (2002). “Staging of the intracerebral inclusion body pathology associated with idiopathic

- Parkinsons disease (preclinical and clinical stages)". In: *Journal of Neurology* 249.0, pp. 1–1. DOI: 10.1007/s00415-002-1301-4.
- Bradley, M. M., M. Codispoti, and P. J. Lang (2006). "A multi-process account of startle modulation during affective perception". In: *Psychophysiology* 43.5, pp. 486–497. DOI: 10.1111/j.1469-8986.2006.00412.x.
- Brown, P and D Williams (2005). "Basal ganglia local field potential activity: Character and functional significance in the human". In: *Clinical Neurophysiology* 116.11, pp. 2510–2519. DOI: 10.1016/j.clinph.2005.05.009.
- Brucke, C. et al. (2007). "The subthalamic region is activated during valence-related emotional processing in patients with Parkinsons disease". In: *European Journal of Neuroscience* 26.3, pp. 767–774. DOI: 10.1111/j.1460-9568.2007.05683.x.
- Buhmann, C., S. Kraft, K. Hinkelmann, S. Krause, C. Gerloff, and W. H. Zangemeister (2015). "Visual Attention and Saccadic Oculomotor Control in Parkinson's Disease". In: *EUROPEAN NEUROLOGY* 73.5-6, 283–293. ISSN: 0014-3022. DOI: {10.1159/000381335}.
- Buzsaki, G. (2004). "Large-scale recording of neuronal ensembles". In: *Nature Neuroscience* 7, No. 5, pp. 446–451.
- Cacioppo, J. T., R. E. Petty, M. E. Losch, and H. S. Kim (1986). "Electromyographic activity over facial muscle regions can differentiate the valence and intensity of affective reactions." In: *Journal of Personality and Social Psychology* 50.2, pp. 260–268. DOI: 10.1037//0022-3514.50.2.260.
- Castrioto, A., E. Lhomme, E. Moro, and P. Krack (2014). "Mood and behavioural effects of subthalamic stimulation in Parkinsons disease". In: *The Lancet Neurology* 13.3, pp. 287–305. DOI: 10.1016/s1474-4422(13)70294-1.
- Cheeseman, P. and J. Stutz (1996). *Bayesian classification (autoclass): theory and results*. AAAI Press, MIT Press.
- Contarino, M. F., L. J. Bour, M. Bot, P. van den Munckhof, J. D. Speelman, P. R. Schuurman, and R. M. de Bie (2012). "Tremor-specific neuronal oscillation pattern in dorsal subthalamic nucleus of parkinsonian patients". In: *Brain stimulation* 5.3, pp. 305–314.
- Degos, B., J.-M. Deniau, M. Chavez, and N. Maurice (2008). "Chronic but not Acute Dopaminergic Transmission Interruption Promotes a Progressive Increase in Cortical Beta Frequency Synchronization: Relationships to Vigilance State and Akinesia". In: *Cerebral Cortex* 19.7, pp. 1616–1630. DOI: 10.1093/cercor/bhn199.

- Delescluse, M. and C. Pouzat (2006). “Efficient spike-sorting of multi-state neurons using inter-spike intervals information.” In: *J Neurosci Meth* 150.1, pp. 16–29.
- Ding, W. and J. Yuan (2008). “Spike sorting based on multi-class support vector machine with superposition resolution”. In: *Med Bio Eng Comput* 46, pp. 139–45.
- Ebrahimi, M., P. Aghagolzadeh, N. Shamabadi, A. Tahmasebi, M. Alsharifi, D. L. Adelson, F. Hemmatzadeh, and E. Ebrahimie (2014). “Understanding the Underlying Mechanism of HA-Subtyping in the Level of Physic-Chemical Characteristics of Protein”. In: *PLOS ONE* 9.5. ISSN: 1932-6203. DOI: {10.1371/journal.pone.0096984}.
- Eitan, R., R. R. Shamir, E. Linetsky, O. Rosenbluh, S. Moshel, T. Ben-Hur, H. Bergman, and Z. Israel (2013). “Asymmetric right/left encoding of emotions in the human subthalamic nucleus”. In: *Front. Syst. Neurosci.* 7. DOI: 10.3389/fnsys.2013.00069.
- Espinosa-Parrilla, J.-F., C. Baunez, and P. Apicella (2015). “Modulation of neuronal activity by reward identity in the monkey subthalamic nucleus”. In: *EUROPEAN JOURNAL OF NEUROSCIENCE* 42.1, 1705–1717. ISSN: 0953-816X. DOI: {10.1111/ejn.12938}.
- Faure, A., S. M. Reynolds, J. M. Richard, and K. C. Berridge (2008). “Mesolimbic Dopamine in Desire and Dread: Enabling Motivation to Be Generated by Localized Glutamate Disruptions in Nucleus Accumbens”. In: *Journal of Neuroscience* 28.28, pp. 7184–7192. DOI: 10.1523/jneurosci.4961-07.2008.
- Fawcett, A. P., J. O. Dostrovsky, A. M. Lozano, and W. D. Hutchison (2004). “Eye movement-related responses of neurons in human subthalamic nucleus”. In: *Exp Brain Res* 162.3, pp. 357–365. DOI: 10.1007/s00221-004-2184-7.
- Fawcett, A. P., D. Cunic, C. Hamani, M. Hodaie, A. M. Lozano, R. Chen, and W. D. Hutchison (2007). “Saccade-related potentials recorded from human subthalamic nucleus”. In: *Clinical Neurophysiology* 118.1, pp. 155–163. DOI: 10.1016/j.clinph.2006.09.016.
- Fawcett, A. P., E. G. Gonzalez, E. Moro, M. J. Steinbach, A. M. Lozano, and W. D. Hutchison (2009). “Subthalamic Nucleus Deep Brain Stimulation Improves Saccades in Parkinsons Disease”. In: *Neuromodulation: Technology at the Neural Interface* 13.1, pp. 17–25. DOI: 10.1111/j.1525-1403.2009.00246.x.
- Fee, M. S., P. P. Mitra, and D. Kleinfeld (1996). “Automatic sorting of multiple unit neuronal signals in the presence of anisotropic and non-gaussian variability”. In: *J Neurosci Meth* 69.2, pp. 175–88.

- Fee, M. S., P. P. Mitra, and D. Kleinfeld (1997). “Erratum: Automatic sorting of multiple unit neuronal signals in the presence of anisotropic and non-gaussian variability”. In: *J Neurosci Meth* 71.2, p. 233.
- Franke, F., M. Natora, C. Boucsein, M. H. J. Munk, and K. Obermayer (2009). “An online spike detection and spike classification algorithm capable of instantaneous resolution of overlapping spikes.” In: *J Comput Neurosci* 29, pp. 127–48.
- Fruhholz, S. and D. Grandjean (2012). “Towards a fronto-temporal neural network for the decoding of angry vocal expressions”. In: *NeuroImage* 62.3, pp. 1658–1666. DOI: 10.1016/j.neuroimage.2012.06.015.
- Gasthaus, J. (2008). “Spike Sorting Using Time-Varying Dirichlet Process Mixture Models”. MA thesis. University College London.
- Gatev, P., O. Darbin, and T. Wichmann (2006). “Oscillations in the basal ganglia under normal conditions and in movement disorders”. In: *Movement disorders* 21.10, pp. 1566–1577.
- Gerstein, G. L. and W. Clark (1964). “Simultaneous studies of firing patterns in several neurons”. In: *Science* 143.20, pp. 1325–27.
- Ghashghaei, H., C. Hilgetag, and H. Barbas (2007). “Sequence of information processing for emotions based on the anatomic dialogue between prefrontal cortex and amygdala”. In: *NeuroImage* 34.3, pp. 905–923. DOI: 10.1016/j.neuroimage.2006.09.046.
- Gibson, S., J. Judy, and D. Markovic (2008). “Comparison of spike-sorting algorithms for future hardware implementation”. In: *Engineering in Medicine and Biology Society, 2008. EMBS 2008. 30th Annual International Conference of the IEEE*. IEEE, pp. 5015–20.
- Gibson, S., J. Judy, and D. Markovic (2010). “Technology-Aware Algorithm Design for Neural Spike Detection, Feature Extraction, and Dimensionality Reduction”. In: *IEEE Trans Neural Syst Rehabil Eng* 18.5, pp. 469–78. ISSN: 1534-4320. DOI: 10.1109/TNSRE.2010.2051683.
- Guillory, S. A. and K. A. Bujarski (2014). “Exploring emotions using invasive methods: review of 60 years of human intracranial electrophysiology”. In: *Social Cognitive and Affective Neuroscience* 9.12, pp. 1880–1889. DOI: 10.1093/scan/nsu002.
- Gulie, S. (2007a). *A Shock to the System*. online; <http://www.spectrum.ieee.org/oct07/5669>.
- Gulie, S. (2007b). *Deep-Brain Stimulators for Parkinson’s Disease Increase Impulsive Decision Making*. online; http://www.wired.com/wired/archive/15.03/brainsurgery_pr.html.

- Hajek, P. and K. Michalak (2013). “Feature selection in corporate credit rating prediction”. In: *KNOWLEDGE-BASED SYSTEMS* 51, 72–84. ISSN: 0950-7051. DOI: {10.1016/j.knosys.2013.07.008}.
- Hamann, S (2004). “Individual differences in emotion processing”. In: *Current Opinion in Neurobiology* 14.2, pp. 233–238. DOI: 10.1016/j.conb.2004.03.010.
- Hammond, C., H. Bergman, and P. Brown (2007). “Pathological synchronization in Parkinson’s disease: networks, models and treatments”. In: *Trends in neurosciences* 30.7, pp. 357–364.
- Harris, K. D. (2000). “Accuracy of tetrode spike separation as determined by simultaneous intracellular and extracellular measurements”. In: *J Neurophysiol* 84.1, pp. 401–14.
- Herbst, J., S. Gammeter, D. Ferrero, and R. Hahnloser (2008). “Spike sorting with hidden Markov models”. In: *J Neurosci Meth* 174.1, pp. 126–34. ISSN: 0165-0270.
- Hodgson, T (2002). “Abnormal gaze strategies during problem solving in Parkinsons disease”. In: *Neuropsychologia* 40.4, pp. 411–422. DOI: 10.1016/s0028-3932(01)00099-9.
- Hoffman, P. and G. Grinstein (1997). *Visualizations for high dimensional data mining - table visualizations*.
- Huebl, J., T. Schoenecker, S. Siegert, C. Brucke, G.-H. Schneider, A. Kupsch, K. Yarrow, and A. A. Kuhn (2011). “Modulation of subthalamic alpha activity to emotional stimuli correlates with depressive symptoms in Parkinsons disease¹”. In: *Mov. Disord.* 26.3, pp. 477–483. DOI: 10.1002/mds.23515.
- Huebl, J., B. Spitzer, C. Brucke, T. Schonecker, A. Kupsch, F. Alesch, G.-H. Schneider, and A. A. Kuhn (2014). “Oscillatory subthalamic nucleus activity is modulated by dopamine during emotional processing in Parkinsons disease”. In: *Cortex* 60, pp. 69–81. DOI: 10.1016/j.cortex.2014.02.019.
- Hulata, E., R. Segev, and E. Ben-Jacob (2002). “A method for spike sorting and detection based on wavelet packets and Shannons mutual information”. In: *J Neurosci Meth* 117, pp. 1–12.
- Humphries, M. D. and T. J. Prescott (2010). “The ventral basal ganglia, a selection mechanism at the crossroads of space, strategy, and reward.” In: *Progress in Neurobiology* 90.4, pp. 385–417. DOI: 10.1016/j.pneurobio.2009.11.003.
- Hutchison, W., R. Allan, H. Opitz, R. Levy, J. Dostrovsky, A. Lang, and A. Lozano (1998a). “Neurophysiological identification of the subthalamic nucleus in surgery for Parkinson’s disease”. In: *Annals of Neurology* 44, pp. 622–628.

- Hutchison, W., R. Allan, H. Opitz, R. Levy, J. Dostrovsky, A. Lang, and A. Lozano (1998b). “Neurophysiological identification of the subthalamic nucleus in surgery for Parkinson’s disease”. In: *Annals of Neurology* 44, pp. 622–628.
- Isoda, M. and O. Hikosaka (2008). “Role for Subthalamic Nucleus Neurons in Switching from Automatic to Controlled Eye Movement”. In: *Journal of Neuroscience* 28.28, pp. 7209–7218. DOI: 10.1523/jneurosci.0487-08.2008.
- Jahanshahi, M. and C. D. Marsden (2000). *Parkinson’s Disease: A Self-Help Guide*. Demos Medical Press.
- Jahanshahi, M., I. H. Jenkins, R. G. Brown, C. D. Marsden, R. E. Passingham, and D. J. Brooks (1995). “Self-initiated versus externally triggered movements”. In: *Brain* 118.4, pp. 913–933. DOI: 10.1093/brain/118.4.913.
- Jech, R., E. Ruzicka, D. Urgosik, T. Serranova, M. Volfova, O. Novakova, J. Roth, P. Dusek, and P. Mecir (2006). “Deep brain stimulation of the subthalamic nucleus affects resting EEG and visual evoked potentials in Parkinsons disease”. In: *Clinical Neurophysiology* 117.5, pp. 1017–1028. DOI: 10.1016/j.clinph.2006.01.009.
- Jenkinson, N. and P. Brown (2011). “New insights into the relationship between dopamine, beta oscillations and motor function”. In: *Trends in Neurosciences* 34.12, pp. 611–618. DOI: 10.1016/j.tins.2011.09.003.
- Joshua, M., S. Elias, O. Levine, and H. Bergmana (2007). “Quantifying the isolation quality of extracellularly recorded action potentials”. In: *J Neurosci Meth* 163, pp. 267–82.
- Karabadiji, N. E. I., H. Seridi, I. Khelf, N. Azizi, and R. Boulkroune (2014). “Improved decision tree construction based on attribute selection and data sampling for fault diagnosis in rotating machines”. In: *ENGINEERING APPLICATIONS OF ARTIFICIAL INTELLIGENCE* 35, 71–83. ISSN: 0952-1976. DOI: {10.1016/j.engappai.2014.06.010}.
- Karama, S., J. Armony, and M. Beauregard (2011). “Film Excerpts Shown to Specifically Elicit Various Affects Lead to Overlapping Activation Foci in a Large Set of Symmetrical Brain Regions in Males”. In: *PLoS ONE* 6.7. Ed. by J. Lauwereyns, e22343. DOI: 10.1371/journal.pone.0022343.
- Kawasaki, H., R. Adolphs, H. Oya, C. Kovach, H. Damasio, O. Kaufman, and M. Howard (2005). “Analysis of Single-Unit Responses to Emotional Scenes in Human Ventromedial Prefrontal Cortex”. In: *Journal of Cognitive Neuroscience* 17.10, pp. 1509–1518. DOI: 10.1162/089892905774597182.

- Kretzberg, J., T. Coors, and J. Furche (2009). “Comparison of valley seeking and T-distributed EM algorithm for spike sorting”. In: *BMC Neurosci* 10.1, p. 47. ISSN: 1471-2202. DOI: 10.1186/1471-2202-10-S1-P47. URL: <http://www.biomedcentral.com/1471-2202/10/S1/P47>.
- Kringelbach, M., N. Jenkinson, S. Owen, and T. Aziz (2007). “Translational principles of deep brain stimulation”. In: *National Reviews Neuroscience* 8, no. 8, pp. 623–635.
- Kuhbandner, C. and M. Zehetleitner (2011). “Dissociable Effects of Valence and Arousal in Adaptive Executive Control”. In: *PLoS ONE* 6.12. Ed. by A. V. Garcia, e29287. DOI: 10.1371/journal.pone.0029287.
- Kuhn, A. A., M. I. Hariz, P. Silberstein, S. Tisch, A. Kupsch, G. H. Schneider, P. Limousin-Dowsey, K. Yarrow, and P. Brown (2005). “Activation of the subthalamic region during emotional processing in Parkinson disease”. In: *Neurology* 65.5, pp. 707–713. DOI: 10.1212/01.wnl.0000174438.78399.bc.
- Kühn, A. A., T. Trottenberg, A. Kivi, A. Kupsch, G.-H. Schneider, and P. Brown (2005). “The relationship between local field potential and neuronal discharge in the subthalamic nucleus of patients with Parkinson’s disease”. In: *Experimental neurology* 194.1, pp. 212–220.
- Kühn, A. A. et al. (2008). “High-frequency stimulation of the subthalamic nucleus suppresses oscillatory β activity in patients with Parkinson’s disease in parallel with improvement in motor performance”. In: *The Journal of neuroscience* 28.24, pp. 6165–6173.
- Lang, P. J., M. M. Bradley, and B. N. Cuthbert (1998). “Emotion, motivation, and anxiety: brain mechanisms and psychophysiology”. In: *Biological Psychiatry* 44.12, pp. 1248–1263. DOI: 10.1016/s0006-3223(98)00275-3.
- Lang, P., M. Bradley, and B. Cuthbert (1999). *International affective picture system (IAPS): Technical manual and affective ratings*. Gainesville: University of Florida, Center for Research in Psychophysiology.
- Laxton, A. W., J. S. Neimat, K. D. Davis, T. Womelsdorf, W. D. Hutchison, J. O. Dostrovsky, C. Hamani, H. S. Mayberg, and A. M. Lozano (2013). “Neuronal Coding of Implicit Emotion Categories in the Subcallosal Cortex in Patients with Depression”. In: *Biological Psychiatry* 74.10, pp. 714–719. DOI: 10.1016/j.biopsych.2013.03.029.
- Lewicki, M. (1998). “A review of methods for spike sorting: the detection and classification of neural action potentials”. In: *Network-Comp Neural* 9.4, pp. 53–78. ISSN: 0954-898X.

- Little, S., A. Pogosyan, A. Kuhn, and P. Brown (2012). “Beta band stability over time correlates with Parkinsonian rigidity and bradykinesia”. In: *Experimental Neurology* 236.2, pp. 383–388. ISSN: 0014-4886. DOI: <http://dx.doi.org/10.1016/j.expneurol.2012.04.024>. URL: <http://www.sciencedirect.com/science/article/pii/S0014488612001963>.
- Matsumura, M., J. Kojima, T. W. Gardiner, and O. Hikosaka (1991). “Visual and oculomotor functions of the monkey subthalamic nucleus”. In: *Neuroscience Research Supplements* 14, S78. DOI: 10.1016/s0921-8696(06)80223-9.
- McLean, R. A., W. L. Sanders, and W. W. Stroup (1991). “A Unified Approach to Mixed Linear Models”. English. In: *The American Statistician* 45.1, pp. 54–64. ISSN: 00031305. URL: <http://www.jstor.org/stable/2685241>.
- Morel, A. (2007). *Stereotactic Atlas of the Human Thalamus and Basal Ganglia*. Informa Healthcare. DOI: 10.3109/9781420016796.
- Moshki, M., P. Kabiri, and A. Mohebalhojeh (2015). “Scalable Feature Selection in High-Dimensional Data Based on GRASP”. In: *APPLIED ARTIFICIAL INTELLIGENCE* 29.3, 283–296. ISSN: 0883-9514. DOI: {10.1080/08839514.2015.1004616}.
- NINDS Office of Communications and Public Liaison (2006). *Parkinson’s disease: Hope through research*. NINDS Office of Communications and Public Liaison.
- Noton, D. and L. Stark (1971). “Scanpaths in Eye Movements during Pattern Perception”. In: *Science* 171.3968, pp. 308–311. DOI: 10.1126/science.171.3968.308.
- Okun, M. S. (2012). “Deep-Brain Stimulation for Parkinsons Disease”. In: *New England Journal of Medicine* 367.16, pp. 1529–1538. DOI: 10.1056/nejmct1208070.
- Peron, J., S. Fruhholz, M. Verin, and D. Grandjean (2013). “Subthalamic nucleus: A key structure for emotional component synchronization in humans”. In: *Neuroscience & Biobehavioral Reviews* 37.3, pp. 358–373. DOI: 10.1016/j.neubiorev.2013.01.001.
- Pinkhardt, E. H., R. Jurgens, D. Lule, J. Heimrath, A. C. Ludolph, W. Becker, and J. Kassubek (2012). “Eye movement impairments in Parkinsons disease: possible role of extradopaminergic mechanisms”. In: *BMC Neurology* 12.1, p. 5. DOI: 10.1186/1471-2377-12-5.
- Pollak, P., A.-L. Benabid, P. Limousin, A. Benazzouz, D. Hoffmann, J.-F. LeBas, and J. Perret (1996). “Subthalamic nucleus stimulation alleviates akinesia and rigidity in parkinsonian patients”. In: *Parkinson’s Disease* 69, pp. 591–594.
- Quiroga, R. Q., Z. Nadasdy, and Y. Ben-Shaul (2004). “Unsupervised spike detection and sorting with wavelets and superparamagnetic clustering”. In: *Neural Comput* 16.8, pp. 1661–87.

- R Core Team (2015). *R: A Language and Environment for Statistical Computing*. R Foundation for Statistical Computing. Vienna, Austria. URL: <http://www.R-project.org/>.
- Roy, M., D. Shohamy, and T. D. Wager (2012). “Ventromedial prefrontal-subcortical systems and the generation of affective meaning”. In: *Trends in Cognitive Sciences* 16.3, pp. 147–156. DOI: 10.1016/j.tics.2012.01.005.
- Russell, J. A. (2003). “Core affect and the psychological construction of emotion.” In: *Psychological Review* 110.1, pp. 145–172. DOI: 10.1037//0033-295x.110.1.145.
- Rutishauser, U. (2006). “Online detection and sorting of extracellularly recorded action potentials in human medial temporal lobe recordings, in vivo.” In: *J Neurosci Meth* 154, pp. 204–24.
- Sahani, M. (1999). “Latent variable models for neural data analysis”. PhD thesis. Pasadena, California: California Institute of Technology.
- Salganicoff, M., M. Sarna, L. Sax, and G. L. Gerstein (1998). “Unsupervised waveform classification for multineuron recordings: a real-time, software-based system”. In: *J Neurosci Meth* 25.3, pp. 181–7.
- Sauleau, P., P. Pollak, P. Krack, J.-H. Courjon, A. Vighetto, A.-L. Benabid, D. Pelisson, and C. Tilikete (2008). “Subthalamic stimulation improves orienting gaze movements in Parkinson’s disease”. In: *Clinical Neurophysiology* 119.8, pp. 1857–1863. DOI: 10.1016/j.clinph.2008.04.013.
- Schmitzer-Torbert, N., J. Jackson, D. Henze, K. Harrisc, and A. Redish (2005). “Quantitative measures of cluster quality for use in extracellular recordings”. In: *Neuroscience* 131 (1), pp. 1–11.
- Schneider, F., U. Habel, J. Volkmann, S. Regel, J. Kornischka, V. Sturm, and H.-J. Freund (2003). “Deep Brain Stimulation of the Subthalamic Nucleus Enhances Emotional Processing in Parkinson Disease”. In: *Arch Gen Psychiatry* 60.3, p. 296. DOI: 10.1001/archpsyc.60.3.296.
- Schoffelen, J.-M., R. Oostenveld, and P. Fries (2005). “Neuronal coherence as a mechanism of effective corticospinal interaction”. In: *Science* 308.5718, pp. 111–113.
- Selemon, L. D. and P. S. Goldman-Rakic (1990). “Topographic intermingling of striatonigral and striatopallidal neurons in the rhesus monkey”. In: *The Journal of Comparative Neurology* 297.3, pp. 359–376. DOI: 10.1002/cne.902970304.
- Sharott, A. et al. (2014). “Activity parameters of subthalamic nucleus neurons selectively predict motor symptom severity in Parkinson’s disease”. In: *The Journal of Neuroscience* 34.18, pp. 6273–6285.

- Shin, S. and M. A. Sommer (2010). “Activity of Neurons in Monkey Globus Pallidus During Oculomotor Behavior Compared With That in Substantia Nigra Pars Reticulata”. In: *Journal of Neurophysiology* 103.4, pp. 1874–1887. DOI: 10.1152/jn.00101.2009.
- Shires, J., S. Joshi, and M. A. Basso (2010). “Shedding new light on the role of the basal ganglia-superior colliculus pathway in eye movements”. In: *Current Opinion in Neurobiology* 20.6, pp. 717–725. DOI: 10.1016/j.conb.2010.08.008.
- Shoham, S., M. R. Fellows, and R. A. Normann (2003). “Robust, automatic spike sorting using mixtures of multivariate T-distributions”. In: *J Neurosci Meth* 127.2, pp. 111–22.
- Sieger, T. et al. (2013b). “Basal Ganglia Neuronal Activity during Scanning Eye Movements in Parkinson’s Disease”. In: *PLoS ONE* 8.11. Ed. by B. Hou, e78581. DOI: 10.1371/journal.pone.0078581.
- Sieger, T. et al. (2015b). “Distinct populations of neurons respond to emotional valence and arousal in the human subthalamic nucleus”. In: *Proceedings of the National Academy of Sciences* 112.10, pp. 3116–3121.
- Simpson, D. M., A. F. C. Infantosi, and D. A. B. Rosas (2001). “Estimation and significance testing of cross-correlation between cerebral blood flow velocity and background electro-encephalograph activity in signals with missing samples”. In: *Medical & Biological Engineering & Computing* 39.4, pp. 428–433. DOI: 10.1007/bf02345364.
- Slavin, K., K. Thulborn, C. Wess, and H. Nersesyan (2007). “Direct visualization of the human subthalamic nucleus with 3t mr imaging”. In: *American Journal of Neuroradiology* 27, no. 1, pp. 80–84.
- Smith, S. W. (1999). *The Scientist and Engineer’s Guide to Digital Signal Processing*. San Diego, California: California Technical Publishing.
- Tabbal, S. D., M. Ushe, J. W. Mink, F. J. Revilla, A. R. Wernle, M. Hong, M. Karimi, and J. S. Perlmutter (2008). “Unilateral subthalamic nucleus stimulation has a measurable ipsilateral effect on rigidity and bradykinesia in Parkinson disease”. In: *Experimental neurology* 211.1, pp. 234–242.
- Takahashi, S., Y. Anzai, and Y. Sakurai. (2003a). “A new approach to spike sorting for multi-neuronal activities recorded with a tetrode - how ICA can be practical”. In: *Neurosci Res* 46.3, pp. 265–72.
- Takahashi, S., Y. Anzai, and Y. Sakurai. (2003b). “Automatic sorting for multineuronal activity recorded with tetrodes in the presence of overlapping spikes”. In: *J Neurophysiol* 89.4, pp. 2245–58.

- Tamietto, M. and B. de Gelder (2010). “Neural bases of the non-conscious perception of emotional signals”. In: *Nature Reviews Neuroscience* 11.10, pp. 697–709. DOI: 10.1038/nrn2889.
- Tankus, A., Y. Yeshurun, and I. Fried (2009). “An automatic measure for classifying clusters of suspected spikes into single cells versus multiunits”. In: *J Neural Eng* 6.5, p. 056001.
- Toh, W. L., S. L. Rossell, and D. J. Castle (2011). “Current visual scanpath research: a review of investigations into the psychotic, anxiety, and mood disorders”. In: *Comprehensive Psychiatry* 52.6, pp. 567–579. DOI: 10.1016/j.comppsy.2010.12.005.
- Trukenbrod, H. A. and R. Engbert (2012). “Eye movements in a sequential scanning task: Evidence for distributed processing”. In: *Journal of Vision* 12.1, pp. 5–5. DOI: 10.1167/12.1.5.
- Tsunoda, M., M. Kurachi, S. Yuasa, Y. Kadono, M. Matsui, and A. Shimizu (1992). “Scanning eye movements in schizophrenic patients”. In: *Schizophrenia Research* 7.2, pp. 159–168. DOI: 10.1016/0920-9964(92)90046-8.
- Vinh, N., J. Epps, and J. Bailey (2009). “Information theoretic measures for clusterings comparison: is a correction for chance necessary?” In: *Proceedings of the 26th Annual International Conference on Machine Learning*. ACM, pp. 1073–80.
- Vinh, N., J. Epps, and J. Bailey (2010). “Information Theoretic Measures for Clusterings Comparison: Variants, Properties, Normalization and Correction for Chance”. In: *JMLR* 11, pp. 2837–54.
- Voon, V., C. Kubu, P. Krack, J.-L. Houeto, and A. I. Tröster (2006). “Deep brain stimulation: Neuropsychological and neuropsychiatric issues”. In: *Movement Disorders* 21.S14, S305–S327. DOI: 10.1002/mds.20963.
- Vrana, S. R., E. L. Spence, and P. J. Lang (1988). “The startle probe response: A new measure of emotion?” In: *Journal of Abnormal Psychology* 97.4, pp. 487–491. DOI: 10.1037//0021-843x.97.4.487.
- Wang, G., Y. Zhou, A. Chen, P. Zhang, and P. Liang (2006). “A robust method for spike sorting with automatic overlap decomposition”. In: *IEEE T Bio-Med Eng* 53.6, pp. 1195–98. ISSN: 0018-9294.
- Wang, S., O. Tudusciuc, A. N. Mamelak, I. B. Ross, R. Adolphs, and U. Rutishauser (2014). “Neurons in the human amygdala selective for perceived emotion”. In: *Proceedings of the National Academy of Sciences* 111.30, E3110–E3119. DOI: 10.1073/pnas.1323342111.

- Warrens, M. (2008). “On the equivalence of Cohen’s kappa and the Hubert-Arabie adjusted Rand index”. In: *J Classif* 25.2, pp. 177–83. ISSN: 0176-4268.
- Wartburg, R. von, P. Wurtz, T. Pflugshaupt, and T. Nyffeler (2007). “Size matters: Saccades during scene perception”. In: *Perception* 36.3, pp. 355–365. DOI: 10.1068/p5552.
- Weinberger, M., W. D. Hutchison, A. M. Lozano, M. Hodaie, and J. O. Dostrovsky (2009). “Increased Gamma Oscillatory Activity in the Subthalamic Nucleus During Tremor in Parkinson’s Disease Patients”. In: *Journal of Neurophysiology* 101.2, pp. 789–802. ISSN: 0022-3077. DOI: 10.1152/jn.90837.2008.
- Weinberger, M., N. Mahant, W. D. Hutchison, A. M. Lozano, E. Moro, M. Hodaie, A. E. Lang, and J. O. Dostrovsky (2006). “Beta Oscillatory Activity in the Subthalamic Nucleus and Its Relation to Dopaminergic Response in Parkinson’s Disease”. In: *Journal of Neurophysiology* 96.6, pp. 3248–3256. ISSN: 0022-3077. DOI: 10.1152/jn.00697.2006.
- Welter, M., J. Houeto, and A. Bonnet (2004). “Effects of high-frequency stimulation on subthalamic neuronal activity in parkinsonian patients”. In: *Archives of Neurology* 61.1, pp. 89–96. DOI: 10.1001/archneur.61.1.89. eprint: /data/Journals/NEUR/13722/NOC30162.pdf. URL: +http://dx.doi.org/10.1001/archneur.61.1.89.
- Wiese, H., P. Stude, K. Nebel, A. de Greiff, M. Forsting, H. C. Diener, and M. Keidel (2004). “Movement preparation in self-initiated versus externally triggered movements: an event-related fMRI-study”. In: *Neuroscience Letters* 371.2-3, pp. 220–225. DOI: 10.1016/j.neulet.2004.08.078.
- Wild, J., Z. Prekopcsak, T. Sieger, D. Novak, and R. Jech (2012b). “Performance comparison of extracellular spike sorting algorithms for single-channel recordings”. In: *Journal of Neuroscience Methods* 203.2, pp. 369–376. DOI: 10.1016/j.jneumeth.2011.10.013.
- Winston, J. S. (2005). “Integrated Neural Representations of Odor Intensity and Affective Valence in Human Amygdala”. In: *Journal of Neuroscience* 25.39, pp. 8903–8907. DOI: 10.1523/jneurosci.1569-05.2005.
- Winter, C., C. Lemke, R. Sohr, W. Meissner, D. Harnack, G. Juckel, R. Morgenstern, and A. Kupsch (2007). “High frequency stimulation of the subthalamic nucleus modulates neurotransmission in limbic brain regions of the rat”. In: *Exp Brain Res* 185.3, pp. 497–507. DOI: 10.1007/s00221-007-1171-1.

Appendix A

List of Candidate’s Publications Citations

Wild, J., Z. Prekopcsak, T. Sieger, D. Novak, and R. Jech (2012b). “Performance comparison of extracellular spike sorting algorithms for single-channel recordings”. In: *Journal of Neuroscience Methods* 203.2, pp. 369–376. DOI: 10.1016/j.jneumeth.2011.10.013.

- Bongard, M., D. Micol, and E. Fernandez (2014). “NEV2lkit: A NEW OPEN SOURCE TOOL FOR HANDLING NEURONAL EVENT FILES FROM MULTI-ELECTRODE RECORDINGS”. in: *INTERNATIONAL JOURNAL OF NEURAL SYSTEMS* 24.4. ISSN: 0129-0657. DOI: {10.1142/S0129065714500099}.
- Deng, X., D. F. Liu, K. Kay, L. M. Frank, and U. T. Eden (2015). “Clusterless Decoding of Position from Multiunit Activity Using a Marked Point Process Filter”. In: *NEURAL COMPUTATION* 27.7, 1438–1460. ISSN: 0899-7667. DOI: {10.1162/NECO_a_00744}.
- Friedman, A., M. D. Keselman, L. G. Gibb, and A. M. Graybiel (2015). “A multistage mathematical approach to automated clustering of high-dimensional noisy data”. In: *PROCEEDINGS OF THE NATIONAL ACADEMY OF SCIENCES OF THE UNITED STATES OF AMERICA* 112.14, 4477–4482. ISSN: 0027-8424. DOI: {10.1073/pnas.1503940112}.
- Furno, L., J. Rigosa, A. Panarese, and S. Micera (2013). “Assessing Spike Sorting contribution to neural implant reliability”. In: *2013 6TH INTERNATIONAL IEEE/EMBS CONFERENCE ON NEURAL ENGINEERING (NER)*. International

IEEE EMBS Conference on Neural Engineering. 6th International IEEE EMBS Conference on Neural Engineering (NER), San Diego, CA, NOV 06-08, 2013. IEEE EMBS; Battelle; Brain Vis LLC; Cortech Solut; Univ Minnesota, IGERT Program, Syst Neuroengineering; IOP Publishing; Ripple; Univ Minnesota, Inst Engn Med; Plexon, 1421–1424. ISBN: 978-1-4673-1969-0.

- Haggag, S., S. Mohamed, A. Bhatti, H. Haggag, and S. Nahavandi (2014). “Neuron’s Spikes Noise Level Classification Using Hidden Markov Models”. In: *NEURAL INFORMATION PROCESSING, ICONIP 2014, PT III*. ed. by Loo, CK and Yap, KS and Wong, KW and Teoh, A and Huang, K. Vol. 8836. Lecture Notes in Computer Science. 21st International Conference on Neural Information Processing (ICONIP), Kuching, MALAYSIA, NOV 03-06, 2014, 501–508. ISBN: 978-3-319-12643-2; 978-3-319-12642-5.
- Hwang, W.-J., S.-H. Wang, and Y.-T. Hsu (2014). “Spike Detection Based on Normalized Correlation with Automatic Template Generation”. In: *SENSORS* 14.6, 11049–11069. ISSN: 1424-8220. DOI: {10.3390/s140611049}.
- Masse, N. Y., B. Jarosiewicz, J. D. Simeral, D. Bacher, S. D. Stavisky, S. S. Cash, E. M. Oakley, E. Berhanu, E. Eskandar, G. Friehs, et al. (2014). “Non-causal spike filtering improves decoding of movement intention for intracortical BCIs”. In: *JOURNAL OF NEUROSCIENCE METHODS* 236, 58–67. ISSN: 0165-0270. DOI: {10.1016/j.jneumeth.2014.08.004}.
- Masse, N. Y., B. Jarosiewicz, J. D. Simeral, D. Bacher, S. D. Stavisky, S. S. Cash, E. M. Oakley, E. Berhanu, E. Eskandar, G. Friehs, et al. (2015). “Reprint of “Non-causal spike filtering improves decoding of movement intention for intracortical BCIs””. In: *JOURNAL OF NEUROSCIENCE METHODS* 244.SI, 94–103. ISSN: 0165-0270. DOI: {10.1016/j.jneumeth.2015.02.001}.
- Nguyen, T., A. Bhatti, A. Khosravi, S. Haggag, D. Creighton, and S. Nahavandi (2015). “Automatic spike sorting by unsupervised clustering with diffusion maps and silhouettes”. In: *NEUROCOMPUTING* 153, 199–210. ISSN: 0925-2312. DOI: {10.1016/j.neucom.2014.11.036}.
- Nguyen, T., A. Khosravi, D. Creighton, and S. Nahavandi (2014). “Spike sorting using locality preserving projection with gap statistics and landmark-based spectral

clustering”. In: *JOURNAL OF NEUROSCIENCE METHODS* 238, 43–53. ISSN: 0165-0270. DOI: {10.1016/j.jneumeth.2014.09.011}.

- Paraskevopoulou, S. E., D. Wu, A. Eftekhar, and T. G. Constandinou (2014). “Hierarchical Adaptive Means (HAM) clustering for hardware-efficient, unsupervised and real-time spike sorting”. In: *JOURNAL OF NEUROSCIENCE METHODS* 235, 145–156. ISSN: 0165-0270. DOI: {10.1016/j.jneumeth.2014.07.004}.
- Siegle, J. H., G. J. Hale, J. P. Newman, and J. Voigts (2015). “Neural ensemble communities: open-source approaches to hardware for large-scale electrophysiology”. In: *CURRENT OPINION IN NEUROBIOLOGY* 32, 53–59. ISSN: 0959-4388. DOI: {10.1016/j.conb.2014.11.004}.
- Valdez, A. B., M. H. Papesch, D. M. Treiman, K. A. Smith, S. D. Goldinger, and P. N. Steinmetz (2015). “Distributed Representation of Visual Objects by Single Neurons in the Human Brain”. In: *JOURNAL OF NEUROSCIENCE* 35.13, 5180–5186. ISSN: 0270-6474. DOI: {10.1523/JNEUROSCI.1958-14.2015}.
- Van Dijck, G. and M. M. Van Hulle (2014). “Review of machine learning and signal processing techniques for automated electrode selection in high-density microelectrode arrays”. In: *BIOMEDICAL ENGINEERING-BIOMEDIZINISCHE TECHNIK* 59.4, SI, 323–333. ISSN: 0013-5585. DOI: {10.1515/bmt-2013-0037}.

Sieger, T., C. Bonnet, T. Serranova, J. Wild, D. Novak, F. Ruzicka, D. Urgosik, E. Ruzicka, B. Gaymard, and R. Jech (2013b). “Basal Ganglia Neuronal Activity during Scanning Eye Movements in Parkinson’s Disease”. In: *PLoS ONE* 8.11. Ed. by B. Hou, e78581. DOI: 10.1371/journal.pone.0078581.

- Buhmann, C., S. Kraft, K. Hinkelmann, S. Krause, C. Gerloff, and W. H. Zangemeister (2015). “Visual Attention and Saccadic Oculomotor Control in Parkinson’s Disease”. In: *EUROPEAN NEUROLOGY* 73.5-6, 283–293. ISSN: 0014-3022. DOI: {10.1159/000381335}.

Sieger, T., T. Serranova, F. Ruzicka, P. Vostatek, J. Wild, D. Stastna, C. Bonnet, D. Novak, E. Ruzicka, and D. Urgosik (2015b). “Distinct populations of neurons respond to emotional valence and arousal in the human subthalamic nucleus”. In: *Proceedings of the National Academy of Sciences* 112.10, pp. 3116–3121.

- Espinosa-Parrilla, J.-F., C. Baunez, and P. Apicella (2015). “Modulation of neuronal activity by reward identity in the monkey subthalamic nucleus”. In: *EUROPEAN JOURNAL OF NEUROSCIENCE* 42.1, 1705–1717. ISSN: 0953-816X. DOI: {10.1111/ejn.12938}.

Macaš, M., L. Lhotská, E. Bakštein, D. Novák, J. Wild, P. Vostatek, T. Sieger, and R. Jech (2012). “Wrapper Feature Selection for Small Sample Size Data Driven by Complete Error Estimates”. English. In: *Computer Methods and Programs in Biomedicine* 108.1, pp. 138–150. ISSN: 0169-2607. URL: <http://www.sciencedirect.com/science/article/pii/S0169260712000582>.

- Ebrahimi, M., P. Aghagolzadeh, N. Shamabadi, A. Tahmasebi, M. Alsharifi, D. L. Adelson, F. Hemmatzadeh, and E. Ebrahimie (2014). “Understanding the Underlying Mechanism of HA-Subtyping in the Level of Physic-Chemical Characteristics of Protein”. In: *PLOS ONE* 9.5. ISSN: 1932-6203. DOI: {10.1371/journal.pone.0096984}.
- Hajek, P. and K. Michalak (2013). “Feature selection in corporate credit rating prediction”. In: *KNOWLEDGE-BASED SYSTEMS* 51, 72–84. ISSN: 0950-7051. DOI: {10.1016/j.knosys.2013.07.008}.
- Karabadji, N. E. I., H. Seridi, I. Khelf, N. Azizi, and R. Boulkroune (2014). “Improved decision tree construction based on attribute selection and data sampling for fault diagnosis in rotating machines”. In: *ENGINEERING APPLICATIONS OF ARTIFICIAL INTELLIGENCE* 35, 71–83. ISSN: 0952-1976. DOI: {10.1016/j.engappai.2014.06.010}.
- Moshki, M., P. Kabiri, and A. Mohebalhojeh (2015). “Scalable Feature Selection in High-Dimensional Data Based on GRASP”. in: *APPLIED ARTIFICIAL INTELLIGENCE* 29.3, 283–296. ISSN: 0883-9514. DOI: {10.1080/08839514.2015.1004616}.